Development and Characterization of Instrumentation for Future Extraterrestrial Soil Analyses: Investigation of Terrestrial Soil and Extraterrestrial Soil Analogues by Electrochemical Sensors and Ion Chromatography

A dissertation

submitted by

Kyle M. McElhoney

In partial fulfillment of the requirements
for the degree of

Doctor of Philosophy

in

Chemistry

TUFTS UNIVERSITY

August 2013

Adviser: Samuel P. Kounaves

Abstract

The research presented herein discusses the analysis of Martian soil from the Phoenix mission and the development of a new instrument to further our understanding of remote terrestrial and extraterrestrial environments. The focus of the Phoenix analysis work was placed on the quantification of the soluble sulfate in the Phoenix samples and the determination of perchlorate parent salts using modelling software, soil simulants, ion-selective electrodes and ion chromatography. The implications of these analyses, especially the presence of $CaClO_4$, indicate an arid Martian environment at the Phoenix landing site.

Building on the successful Phoenix mission, as well as other un-flown instruments including the Robotic Chemical Analysis Laboratory, a new instrument was conceived, designed, and fabricated. The new instrument, the *In-situ* Chemical Analysis Laboratory and Sensor Array, increased the sampling capabilities compared with Phoenix by decreasing the size of the sample analysis unit while incorporating an increased number of sensors per unit. The scalable instrument can accommodate 4-100 units upon mass fabrication. Each sample analysis unit can house a maximum of 42 ion-selective electrodes, 3 reference electrodes, whilst reserving one wall for other electrochemical sensors. The increased sensor redundancy will allow for a more accurate and precise measurement of the soluble species present in the sample. The increased number of sensors was achieved by miniaturizing and optimizing the sensor design and materials. The final design, which utilized silver epoxy and porous carbon with an ion-selective membrane,

yielded miniaturized sensors with similar sensitivity and stability while also increasing the overall lifetime.

An investigation into soil leaching parameters was also performed to investigate the effects of miniaturizing the sample analysis unit from accommodating 25 mL to less than 10 mL leaching solution. Ion chromatography showed that the greatest increase on the soluble species present in the leachate occurred as the leach ratio (g leach solution:g soil) and leach time increased for Antarctic soil samples. The low levels of calcium and magnesium resulted in the opposite trend, where the concentration was decreased as the leach ratio and time increased, due to the presence of carbonates in the leaching solution and soil sample.

Acknowledgements

I would like to thank my adviser, Samuel Kounaves, for his endless support and encouragement during my graduate career. I am eternally grateful for the opportunity to perform research in his group and learn from him as both a researcher and educator. I would also like to thank the members of my graduate committee, Arthur Utz and Charlie Sykes, for their support and advisement throughout study topics, original proposals and my thesis. I also extend thanks to my external committee member, Joseph Bauer, for serving on my committee.

My thanks are extended unconditionally to my fellow group members, past and present, especially Glen O'Neil, as well as Shannon Stroble, Jody Maisano, Brandi Carrier, Trish Hredzak, Andrew Weber, Victoria Hansen, Kaitlin Folds, Elizabeth Oberlin, Kalina Gospodinova, Jason Kapit, Rachel Anderson, Leonard Ashu, Patric Gibbons, Quincy Moore, Andrew Morgenthaler, Jen Shusterman, and Justin Wage. I also thank our visiting researcher, Nikos Chaniotakis, for his guidance and experience pertaining to ISEs. My thanks are also extended to my fellow graduate students, especially those I have shared many years with including: Patrick Antle, Celeo Guifarro, Albert G. Kennedy, Amanda Kowalsick, Tim Lawton, Cary Lipovsky, Taryn Palluccio, and Eric Peterson, as well as many other graduate students that shared their experiences with me and that I have shared my experiences with. Special thanks to April Jewell, Steven Shafer, Maël Manesse and Zach Smith for their careful reading of various manuscripts, reports and other materials including this dissertation. Thank you to all members of the faculty and staff for their constant help and support throughout the years.

My thanks also extend to the many collaborators including those at Draper Laboratory for their work on CHEMSENS and RCAL: Joseph Bauer, Dan Traviglia, Dan Harjes, Jim Bickford, Shawn Murphy, and their various coworkers. I also want to extend my thanks to those at NASA's Jet Propulsion Laboratory at the California Institute of Technology for their support with RCAL including: Max Coleman, Randall Mielke, Michael Garrett, Hrand Aghazarian, Allen Sirota, Terrance Huntsberger, Hung Tran, among many others.

Last, but not least, I would like to thank my family for their continued love and support over the last five years. Thank you Mom, Dad, Joe, Spenser, Grandma, as well as the rest of my extended family and friends. I know that I have been in school for longer than you could have ever imagined, but thanks for sticking by my side and continually asking when I am going to finish. I could not have done this without you.

Table of Contents

List of Tables

List of Figures

List of Abbreviations

ADV	Antarctic Dry Valleys
AM-SC-ISE	Asymmetric Membrane Solid-Contact ISE
ASV	Anodic Stripping Voltammetry
CHEMSENS	*In-situ* Chemical Analysis Laboratory and Sensor Array
CP	Chronopotentiometry
CTZ	Coastal Thaw Zone (see ADV)
CV	Cyclic Voltammetry
CW-ISE	Coated Wire Ion-selective Electrodes
DOS	Bis(2-ethylhexyl) sebacate
EETA 79001	Elephant Moraine Meteorite Cut A 79001
FIM	Fixed Interference Method
GC	Gas Chromatography/Chromatograph
GUI	Graphical User Interface
GWB	Geochemist's Workbench
IC	Ion Chromatography
ID	Inner Diameter
ISE(s)	Ion-selective Electrode(s)
ISM	Ion-selective Membrane
JPL	Jet Propulsion Laboratory, California Institute of Technology, Pasadena, CA
KTFPB	Potassium tetrakis[3,5-bis(trifluoromethyl)phenyl]borate
MARDI	Mars Decent Imager (Phoenix)
MECA	Microscopy, Electrochemistry and Conductivity Analyzer (Phoenix)
MER	Mars Exploration Rovers
MET	Meteorological Station (Phoenix)
MS	Mass Spectrometry/Spectrometer
MSL	Mars Science Laboratory
NaTFPB	Sodium tetrakis[3,5-bis(trifluoromethyl)phenyl]borate
OD	Outer Diameter
o-NPOE	2-nitrophenyl octyl ether
ORP	Oxidation-reduction Potential
pHEMA	Polymeric Hydrogel (poly(2-hydroxyethyl methacrylate)
PVC	Poly(vinyl chloride)
RA	Robotic Arm
RCAL	Robotic Chemical Analysis Laboratory
RR	Rosy Red Soil Sample (Phoenix)
SAU	Sample Analysis Unit
SC-ISE	Solid-contact Ion-selective Electrode

SE	Silver Epoxy
SE-SC-ISE	Silver Epoxy Solid-Contact ISE
SM	Symmetric Membrane
SM-ISE	Symmetric Membrane ISE
SM-SC-ISE	Symmetric Membrane Solid-Contact ISE
SRR2K	Sample Return Rover 2K
SSI	Surface Stereo Imager (Phoenix)
SSM	Separate Solutions Method
SUZ	Stable Upland Zone (see ADV)
TB (2)	WCL Test-bed #2
TEGA	Thermal and Evolved Gas Analyzer
TS (20)	WCL Test Solution (Calibration Solution) 20
TV	Taylor Valley, Antarctica
WCL	Wet Chemistry Laboratory (Phoenix)

Development and Characterization of Instrumentation for Future Extraterrestrial Soil Analyses: Investigation of Terrestrial Soil and Extraterrestrial Soil Analogues by Electrochemical Sensors and Ion Chromatography

1. Background and Theory

1.1. Mars Exploration 1976-2008

There have been several successful landed missions to Mars prior to the landing of the Phoenix Mars Scout lander in 2008. The first missions to land on Mars were the Viking 1 & 2 landers in 1976, followed by Pathfinder base station and the Sojourner rover in 1997, and the Mars Exploration Rovers (MER) Spirit and Opportunity in 2004 (*1*). The scientific goals of the first landers, Viking 1 & 2, were to determine if life and organics were present on the Martian surface through a series of biological and chemical experiments. The primary analytical instrument on board was a gas chromatograph-mass spectrometer (GC-MS). Results from the GC-MS showed that no organics were present on the surface. However, the protocol included the pyrolysis of the sample and since a strong oxidizer was detected any possible organics were combusted before reaching the MS (*2–4*). Twenty years later, the primary goal of the Pathfinder mission was to demonstrate the ability to deliver a rover, Sojourner, to the Martian surface. The mission was a success and over 16,000 images were returned from this mission, resulting in some of our current knowledge regarding the geology of the planet (*5–7*). Spirit and Opportunity (MER) added to our knowledge regarding the geology and atmosphere of the planet, including the determination that Gusev crater was mainly basaltic by Spirit (*8–12*). The MER mission defined four main science objectives that future Mars exploration projects would utilize: (1) determine whether life was present on Mars; (2) characterize the climate of Mars; (3) characterize the geology of Mars; and (4) characterize the surface for potential human exploration (*13*). These science

objectives were at the core of the Phoenix mission, as well as the current Mars Science Laboratory (MSL) Curiosity rover. For the purposes of this work, a focus will be placed on the Phoenix lander (henceforth referred to as Phoenix), as this was the payload that included instrumentation developed here, at Tufts University in the Kounaves research group.

1.2. Phoenix Rising (and Landing)

The Phoenix Mars Scout Lander launched in August of 2007, and landed on Mars on 25 May 2008 (*14*, *15*). Onboard Phoenix were several scientific instruments focused on defining Mars in terms of the aforementioned science objectives. The instruments can be divided into three categories: (1) imaging; (2) characterizing the climate; as well as (3) the chemistry/geology. The imaging instrumentation included the robotic arm (RA) and camera, the Surface Stereo Imager (SSI), and the Mars Decent Imager (MARDI) (*16*–*18*). The instrument to characterize the climate of Mars was the Meteorological Station (MET) (*19*, *20*) while the chemical and geological instruments were the Thermal and Evolved Gas Analyzer (TEGA) (*21*) and the Microscopy, Electrochemistry, and Conductivity Analyzer (MECA) suite of instruments (*22*, *23*). Four Wet Chemistry Laboratory (WCL) units were included in the MECA suite of instruments, each WCL being one-time use (*23*). A view of the WCL units as seen by the camera located on the RA can be seen in Figure 1.1. Each WCL unit consisted of an actuator assembly and a beaker where the electrochemical sensors were housed, shown assembled in Figure 1.2.

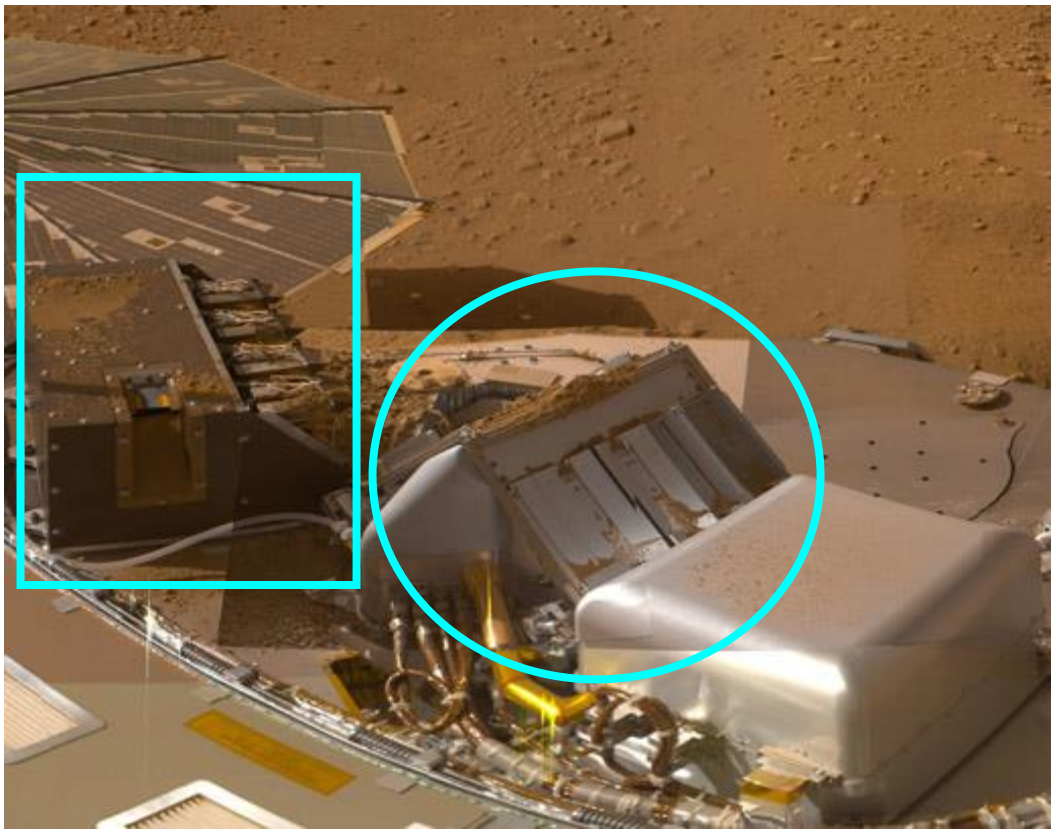

Figure 1.1. Instrumentation aboard Phoenix, including WCL (square) and TEGA (circle). Image taken by camera located on RA. Image credit: NASA/JPL-Caltech/University of Arizone/Texas A&M University.

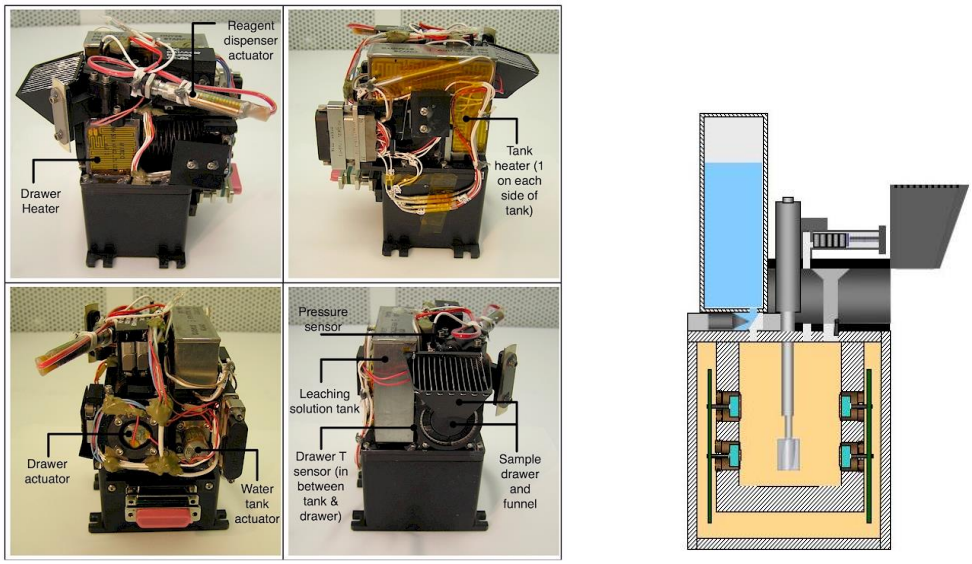

Figure 1.2. Views of the WCL units assembled (left) and a mockup of a side view (right) showing the beaker lined with sensors. Image credit, left: (*23*).

Each WCL beaker contained 23 electrochemical sensors, including 15 ion-selective electrodes (ISEs). Each ISE present detected a primary soluble ion, and the anions and cations investigated were: Cl^-, Br^-, I^-, NO_3^-/ClO_4^-, Na^+, K^+, NH_4^+, H^+ (pH), Li^+ (serving as the reference electrode), Mg^{2+}, Ca^{2+}, and Ba^{2+} (titrimetric determination of SO_4^{2-}). Of the above listed species, ISEs were duplicated for Cl^-, pH and Li^+, yielding the total of 15 ISEs. These electrodes were duplicated because of the importance of the determination of the pH of Martian soil as well as the reference electrode (Li^+/Cl^-). The remaining eight electrochemical sensors were electrodes for chronopotentiometry (CP), cyclic voltammetry (CV), oxidation-reduction potential (ORP), anodic stripping voltammetry (ASV), conductivity and an iridium oxide electrode for verification of pH. A discussion of the Phoenix results can be found in the literature (*24–30*) but a brief summary of the major results with an expanded discussion of the work performed over the last few years will be presented in the subsequent chapter. Before discussing the results from the ISEs, the theory and background of these powerful analytical devices will be presented.

1.3. Ion-Selective Electrodes

1.3.1. Theory and Background

Ion-selective electrodes (ISEs) are powerful analytical devices that quantify the amount of various ionic species in a desired sample. The applications of ISEs are vast and boundless including environmental monitoring and the analysis of ionic species in urine and blood. As stated in the previous section, ISEs can also be used

to determine the characteristics of extraterrestrial soils. In general, ISEs are easy to fabricate and use, inexpensive (compared to traditional analytical instrumentation), provide a non-destructive analysis and are available for a variety of ionic species, including: inorganic cations, anions, transition metals, organics, and acids/bases. The core of the work presented here is the study of ISEs for future instrument suites for remote and autonomous measurements. Therefore, presented below is a discussion of the theory and background of ISEs.

1.3.1.1 Potentiometry and Potentiometric Sensors

In potentiometry a potential is measured between two electrodes, elucidating the composition of a sample (*31*). The current flow between these two electrodes should be kept constant (ideally zero). Potentiometry has been used for sample determination and characterization for many decades, but the developments regarding the most common potentiometric devices, ISEs, have resulted in an increase in their use across many fields of science. There are three main components that make up a potentiometric measurement: (1) a working electrode (an ISE); (2) a reference electrode; and (3) a device capable of measuring potential change. These devices can range from the common pH/millivolt meters that are prevalent in many labs around the world, to more complex systems that can accommodate many ISEs at once (with varying number of required reference electrodes). A typical set-up can be seen in Figure 1.3. The purpose of the reference electrode, seen on the left, is to exhibit a constant potential regardless of changes in the analyte solution. This ensures that any changes in potential are due to the detection of (ideally) a specific ionic species by the ISE. A typical (commercial,

liquid junction) ISE is composed of an internal reference element (shown above as Ag|AgCl) with an internal electrolyte solution of known, constant activity and an ion-selective membrane (ISM) all encased in a housing.

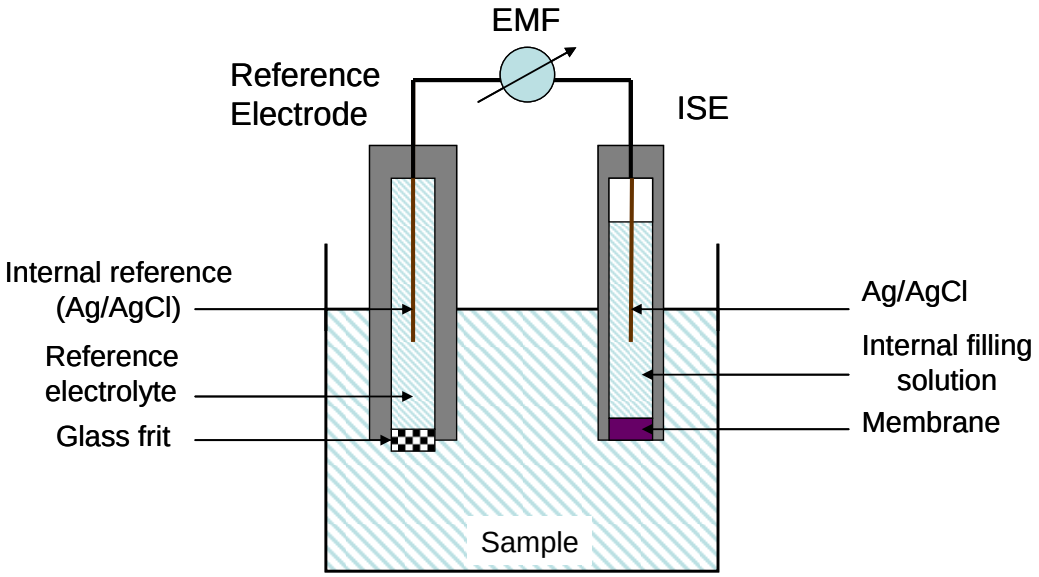

Figure 1.3. Typical experimental set-up used for potentiometry. Adapted from (*31*).

The detection of ionic species occurs by electroactive components that are present in an ISM. Membranes are permselective, water insoluble and mechanically stable. Commonly, ISMs are polymeric in nature and can be plasticized using different organic solvents. The main electroactive species present is an ionophore, or other selectively binding material, specific to the binding of the target ion into the membrane or facilitating ion exchange into the membrane. Ideally, the ionophore only targets the specific ion of interest, ignoring the other species present in the background matrix. This usually is not the case as there are other ions that can be targeted, and this will be discussed further in Section 1.3.1.4. Commercial ISEs contain an internal solution of constant activity present behind the ISM (the

back, non-sensing, side of the ISM). This reservoir of constant activity provides a stable potential for the internal reference element (depicted here as Ag/AgCl).

The binding or uptake of an ion causes a gradient of activity within the ISM, which translates to a change in potential. This change in potential is quantifiable and is measured against a reference electrode, which ideally remains constant regardless of the sample and matrix composition. Before expanding on the free energy-potential relationship it is important to understand the relationship between concentration and activity. The activity of an ion *i* in a solution (a_i), defined as the thermodynamic effective concentration, is determined by:

$$a_i = \gamma_i C_i$$

where γ_i and C_i are the activity coefficient and concentration of the ion *i* respectively. The activity coefficient is determined by the Debye-Huckel equation given below as:

$$\log \gamma_i = \frac{-0.51\, z_i^2 \sqrt{\mu}}{1 + \sqrt{\mu}}$$

where *z* is the charge of the target ion *i*, and μ is the ionic strength of the solution.

Thermodynamics state that this gradient of activity present in the ISM produces a gradient of free energy (ΔG), given by the equation:

$$\Delta G = -RT \ln \left(\frac{a_{i,\,\text{sample}}}{a_{i,\ \text{int. soln.}}} \right)$$

where *R* is the universal gas constant (8.314 J K^{-1} mol^{-1}), *T* is the temperature (K), and a_i is the activity of the sample and internal solution for the target species *i*. The potential (*E*, also referred to as the electromotive force, emf) is related to the gradient of free energy by:

$$\Delta G = -nFE$$

where *n* is the charge of the target ion and *F* is Faraday's constant (96,485 J). The combination of the previous two equations yields:

$$E = \frac{RT}{nF} \ln \left(\frac{a_{i,\,\text{sample}}}{a_{i,\ \text{int. soln.}}} \right)$$

The determination of the activity of the target ion, *i*, consists of several potential contributions. An electrochemical cell, given below:

$$\underset{E_1}{\text{Ag|AgCl}} \mid \underset{E_2}{\text{Ref. Internal Solution}} \parallel \underset{E_J}{\text{Sample}} \mid \underset{E_M}{\text{ISM}} \mid \underset{E_3}{\text{ISE Inner Solution}} \mid \underset{E_4}{\text{AgCl|Ag}}$$

begins to elucidate where potential contributions occur, where E_J is the junction potential, E_M is the membrane potential and $E_{1\text{-}4}$ are various potential contributions that are sample independent. A summary of these contributions is given as:

$$emf = E_{const} + E_J + E_M$$

where all sample independent potential contributions have been summed to form the term E_{const}. As indicated by the electrochemical cell, the junction potential arises from migration of ions between the electrolyte and sample solutions due to the differences in activity between the two solutions. The magnitude of E_J can be minimized by selecting a reference electrolyte of high activity and of similar mobility to the target ion. If the value of E_J cannot be kept small and constant, then it can be determined by the Henderson equation.

The combination of the previous two equations yields an equation for the determination of the activity of the ionic species in solution:

$$E_{const} + E_J + E_M = \frac{RT}{nF} \ln \left(\frac{a_{i,\,\text{sample}}}{a_{i,\ \text{int. soln.}}} \right)$$

This equation can be further simplified by combining the E_J and E_{const} as well as dropping $a_{i,\ int\ soln}$ (assuming it remains constant throughout the measurement) which yields the Nernst equation:

$$E = E^o \pm 0.05916\ \text{V}\left(\frac{RT}{nF}\right)\log(a_i)$$

where E^o is the combination of E_J and E_{const} and the a factor of 2.303 was used to calculate 0.05916 V upon the conversion of ln into log.

A plot of the potential versus the logarithm of activity ideally yields a linear relationship with a slope of 59.16/*n* mV/decade. For every ten-fold change in the concentration of a_i, there is a 59.16/*n* mV change in potential (dependent on the charge and magnitude of the target ion). An electrode that exhibits this slope behavior is said to be "Nernstian". An idealized calibration plot is shown in Figure 1.4.

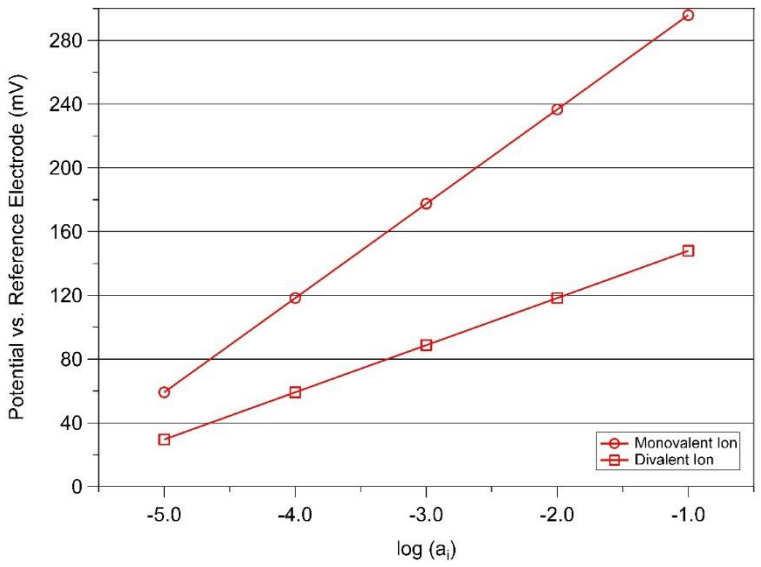

Figure 1.4. Ideal potential response of a Nernstian electrode. The monovalent ion (○) exhibits a Nernstian slope of 59.16 mV/decade, while the divalent ion (□) exhibits a Nernstian slope of 29.58 mV/decade.

1.3.1.2 ISE Fabrication and Characteristics

As previously mentioned, an ISE is fabricated with three main parts: (1) an internal reference element; (2) an internal reference solution (or solid support that replaces the aqueous phase); and (3) an ISM. Electrodes can vary in size (diameter and length) and have changed drastically in the past few decades. Commercially available ISEs, similar to those in Figure 1.3, are typically on the order of lengths > 10 cm and diameters > 1 cm. The accommodation of a single ISE and reference in a beaker with a sample analyte is easy in the laboratory setting, but the introduction of multiple ISEs (and possibly multiple references) poses a challenge, especially when using portable instrumentation in the field or when there is a limited amount of sample. For this reason, many advances have been achieved in the miniaturization of ISEs. Although there are many advantages associated with miniaturized ISEs, there are also complications that arise.

The replacement of the internal solution upon the miniaturization of ISEs poses the largest obstacle during the fabrication process. In most commercially available ISEs, the internal solution can be refilled to ensure proper function. Upon miniaturization, smaller volumes evaporate quicker and require more frequent replacement. A possible remedy to this problem is to replace this solution with a solid support, yielding what is known as solid-contact ISEs (SC-ISEs) (*32*). The solid support must function in a similar manner as the internal solution, in that it still needs to serve as a reservoir for the internal reference element, which yields a stable, constant potential. Many authors have used various supports to solve this problem including conducting polymers (*33–41*), porous carbon (*42*, *43*), and more

recently carbon nanomaterials (*44–49*). The replacement of the internal solution with a smaller solid support is an important first step into the fabrication of miniaturized ISEs, but the process itself poses as a large obstacle in and of itself. Smaller housings can provide little room for the adhesion of the ISM, the smaller surface area of the ISM can result in a quicker leaching of the electroactive components, and also increase the electrical resistance of the measurement. These problems manifest themselves by affecting the potential of the ISE (sensor sensitivity, stability, selectivity and lifetime).

1.3.1.3 Stability and Detection Limits

One of the main reasons ISEs are widely used is their ability to detect a target ion across a broad range of activities. The detection limit is dependent of each individual sensor and is determined as a function of the calibration curve. The ISE will have a linear detection range and will eventually approach a lower limit, the limit of detection. A representation of this is seen in Figure 1.5, where the intersection of the two best fit lines of the linear detection range and the non-linear range yields the detection limit of the electrode.

Ideally each electrode would also produce a constant and precise measurement each time it is used. As this is not the case, the stability of a sensor is another important characteristic. Stability is defined as the repeatable response of the electrode at a fixed activity of analyte (target ion). For instance, later work will investigate the stability of fabricated K^+ ISEs, where the values obtained all occurred at an activity ~10^{-3} M K^+. The need for a stable sensor is especially

important when conducting remote and autonomous measurements, where sensors cannot be replaced at-will or recalibrated. A reproducible response to known analytes and mixtures will ensure the electrode is properly functioning, for instance, on Earth and Mars alike. The ISEs' potential stability is affected by the leaching of electroactive components from the ISM, uptake of water by the ISM, and development of a water layer between the ISM and solid-contact, among other factors.

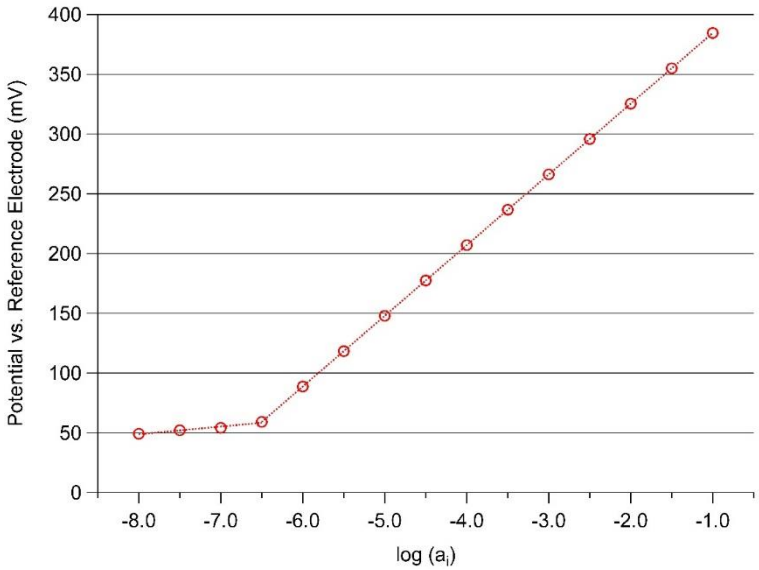

Figure 1.5. Calibration of an idealized monovalent ion for the determination of the detection limit. The electrode response is linear between -8.0 and -6.5, and -6.5 and -1.0. The intersection of these lines represents the detection limit, seen her as -6.5 or an activity of $10^{-6.5}$ M.

1.3.1.4 Selectivity

Ideally, an ISE should be *specific* towards the detection of a target ion. In reality, each ISE is *selective* towards a target ion, where the target ion lies on a spectrum of selectivity for various ionic species. For instance, a commercially available K^+ ISE also detects certain amounts of Li^+, Na^+, Rb^+, Cs^+, NH_4^+, Ca^{2+} and Mg^{2+} (*50*).

The Nikolskii-Eisenman equation shows the effect of interfering ions on the potential:

$$E = E^o \pm 0.05916\ \text{V}\left(\frac{RT}{nF}\right)\log(a_i + k_{ij}a_j^{z_i/z_j})$$

where k_{ij} is the selectivity coefficient versus the interferent j, a_j is the activity of the interfering ion and z is the charge of the target ion (z_i) and interfering ion (z_j). Selectivity coefficients are usually given in the form of a logarithm, where if $k >> 1$ then the electrode is more selective towards the interfering ion, but usually $k < 1$ meaning that it is more selective towards the target ion than the interfering species. For example, for the K^+ electrode discussed above to produce the same response as K^+, the affinity of the ISM for Na^+ would have to be 2,300 times that of K^+. The technical specifications also list the selectivity coefficients for each species, listed in Table 1.1. Therefore, the electrode is much more selective towards potassium than sodium.

Table 1.1. Selectivity coefficients of a commercial potassium ISE from Nico 2000. Adapted from (*50*).

Interfering Species	Selectivity Coefficient, $\log(k_{K,j})$
Rb^+	0.30
Cs^+	-0.40
NH_4^+	-2.00
Na^+	-3.40
Ca^{2+}	-3.50
Mg^{2+}	-3.50
Li^+	-4.00

The two most commonly used methods to determine the selectivity of an electrode are the separate solutions method (SSM) and the fixed interference method (FIM) (*51*, *52*). In the SSM, the selectivity is determined by comparing the

response of the electrodes in two solutions: one containing the target ion only, and the other the interfering ion only (at the same concentration of the target ion in the first solution). The selectivity is then given by:

$$\log k_{i,j}^{Pot} = \frac{\left(E_j - E_i\right) z_i F}{RT \ln 10} + (1 - z_i/z_b)\log(a_i)$$

If the responses in both solutions are equal then the selectivity coefficient can be calculated by:

$$k_{i,j}^{Pot} = \frac{a_i}{a_j^{z_i/z_j}}$$

The FIM calibrates the electrode for the target ion in a constant background of an interfering ion. After plotting the potential vs. the logarithm of activity for both measurements, the detection limit indicates the value of a_i to be used above equation ($E_j = E_i$ SSM equation). Both methods rely on the Nikolskii-Eisenman equation, which serve as an approximation of the selectivity, although both falter, especially when the magnitude of charges for the target ion and interfering ion are not equal.

1.3.2 Benefit of ISEs for Martian Chemical Analysis

The availability of various ionophores and complexing agents for a variety of ionic species, the broad detection range, detection limits within what was expected to be present on Mars, sensitivity, stability, size, and robustness were just some of the reasons ISEs were selected as the analytical devices for the WCL. A maximum number of analyses is desired for any mission to gather as much information as possible about the environment being studied. For this reason, the presence of 15

ISEs in each WCL cell (along with various other electrochemical sensors) is a valuable selling point of the instrument for inclusion as part of the payload. To ensure that the ISEs could function after long pre-flight and cruise periods, the sensors underwent vigorous environmental testing (more information can be found here (*23*)).

The successful use of ISEs on Mars for the Phoenix mission after the pre-flight, cruise, landing and Martian surface conditions proved their robustness and capabilities to function. Compared with other analytical techniques and instrumentation, ISEs also provide an *in-situ* analysis of the sample in real-time. This provides valuable information regarding the solubility of the ions in the sample, i.e. are certain species immediately soluble or are there are other species that become more soluble over time. Upon equilibrium, experiments can be performed to further elucidate the chemistry of the sample instead of using a destructive method (the pyrolytic sample treatment for GC). For these reasons, ISEs were ultimately selected as the main chemical analysis instruments for the WCL cells.

1.3.3 Phoenix ISEs

The electrodes incorporated in each Phoenix WCL cell were a pseudo form of SC-ISEs, as previously mentioned in Section 1.3.1.2. The major exception was that instead of using a conducting polymer or solid support, the Phoenix ISEs utilized a polymeric hydrogel. A hydrogel is a polymer network whose main component is water but exists as a cured gel. The advantages of a hydrogel over other polymers

is the fact that it is comprised of mainly water and can be conditioned in various ionic solutions. The use of a hydrogel most closely mimics an aqueous solution without having the actual solution. Each membrane-based ISE fabricated contained a hydrogel component conditioned in the target ionic species (balanced by a counterion, usually Cl^- or NO_3^-). The hydrogel selected was poly(2-hydroxyethyl methacrylate), referred to for the rest of this study as pHEMA. The conditioning of each hydrogel provided the constant activity of background ionic species while eliminating the internal reference solution. The ISM for each ISE was placed on the hydrogel layer as seen in Figure 1.6. The ionophores used for each ISM can be found in Table 1.2. Other ISEs, mainly the halide ISEs were fabricated with a solid-pellet crystals. These ISEs will not be discussed here and further reading can be found in (*31*, *53*).

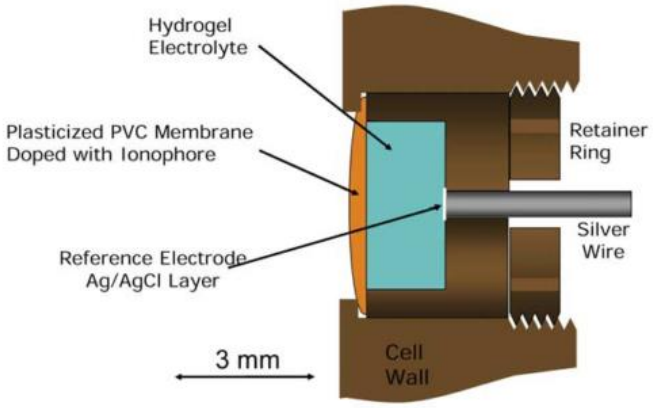

Figure 1.6. Phoenix WCL membrane-based electrodes. Image taken from (*23*).

Table 1.2. Summary of the ionophores used in the ISMs of the Phoenix membrane-based electrodes. Adapted from (*24*).

ISE	Ionophore
NH_4^+	Nonactin
Ba^{2+}	Ba Ionophore I
Ca^{2+}	ETH-1001*
Li^+	Li Ionophore VI
Mg^{2+}	ETH-7025*
NO_3^-/ClO_4^-	Ion exchanger
pH	ETH-2418*
K^+	Valinomycin
Na^+	Na Ionophore VI

*ETH: Eidgenössische Technische Hochschule, Zürich (Swiss Federal Institute of Technology, Zurich)

Of the 15 ISEs aboard Phoenix there are several that warrant individual discussion. First, the ISE originally intended to detect NO_3^-, doped with an ionic exchanger, in fact detected another ionic species. Due to the lack of selectivity of the ionic exchanger, the NO_3^- ISE functioned as a Hofmeister electrode. A shortened version of the Hofmeister series is present here as:

$$ClO_4^- > I^- > Br^- > NO_3^- > NO_2^- > HCO_3^- > Cl^-$$

where the species to the left of NO_3^- would be detected by the ionic exchanger more than NO_3^- itself (*23*). Therefore, any appreciable amount of ClO_4^- would be detected at levels much higher than NO_3^-. This was the case in the Phoenix soil samples, where it was determined that perchlorate was present (*24*, *25*). The presence of ClO_4^- was confirmed by performing similar experiments to those conducted on Phoenix here on Earth on spare WCL flight units. Further investigations regarding the Phoenix ClO_4^- are discussed in Sections 2.1 and 2.3. Next, the Ba^{2+} ISE indirectly measures the amount of soluble SO_4^{2-} via a titrimetric analysis (Section 2.2). Lastly, the Li^+ electrodes served as the reference electrodes for the remainder of the ISEs.

A lack of solid-state reference electrode technology at the time, still a problem in the field today, resulted in the use of an ISE as a reference for the WCL analyses. As discussed, the reference electrode should remain constant regardless of the sample solution (including changes to the sample solution). Lithium was chosen as the ISE for the reference due to the hypothesis that Li^+ would not be present in the Martian soil at significant levels. To ensure that the Li^+ response remained constant, the background leaching solution which contained various amounts of ionic species (see Table 2.2 in Section 2.2) also with a constant amount of Li^+ at a level of 1.0 mM. The addition of the sample should produce no change in the Li^+ levels since the concentration of Li^+ in the background is at an elevated level.

1.4 Ion Chromatography

The validation of the results obtained from ISEs was performed by another analytical technique, ion chromatography (IC). A form of liquid chromatography, IC is a separation technique that relies on the attraction/repulsion of ionic species to a charged stationary phase. Since its introduction in 1975, it has grown into a major analytical tool for the detection of ionic species at sub-ppm levels (*54–56*). The detection limits of IC are typically below that of ISEs (Phoenix LODs were on the order of 10^{-5} M), but require larger and more complex instrumentation. A typical set-up includes a high-pressure system encompassing: (1) a pump; (2) eluent(s); (3) an injection mechanism; (4) a guard and analytical column; (5) a suppressor; (6) a

conductivity detector; and (7) a data analysis system. A flow diagram of the components is shown in Figure 1.7.

Eluents are typically a strong acid or base that is compatible with the stationary phase of the analytical column, a pellicular microbead with either a cation- or an anion-exchange latex coating. Pellicular microbeads are the backbone of choice due to their high surface area, porosity and ability to maintain flow. These characteristics decrease band broadening allowing for a more precise separation.

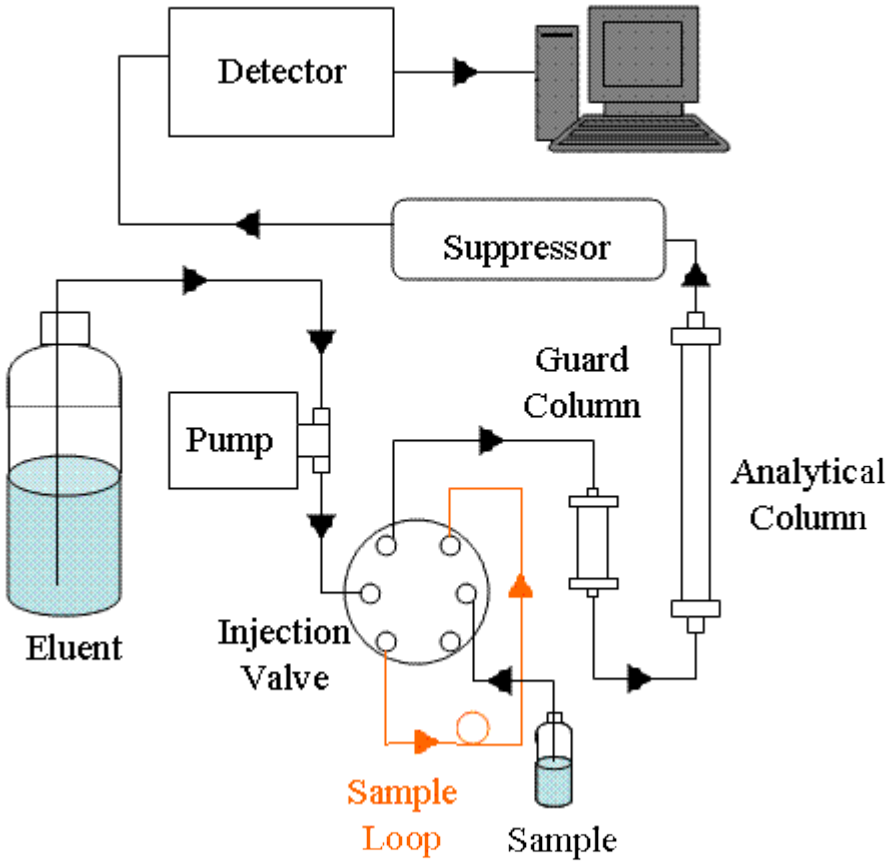

Figure 1.7. Flow diagram of a commercial IC system. Adapted from Thermo-Scientific.

The use of solvents of analytical purity as the mobile phase is of great importance to ensure the separation of analytes and to not introduce contaminants into the system, especially the analytical column. For this reason, the most common eluent systems are not prepared by the user, but instead purchased as a reagent free eluent generation cartridge, shown in Figure 1.8. In this case, the user supplies purified water that flows through a KOH (eluent) generation chamber. A concentrated reservoir of K_2HPO_4 serves as the source for K^+ ions. An externally controlled power supply connects an anode in the reservoir and a cathode in the KOH

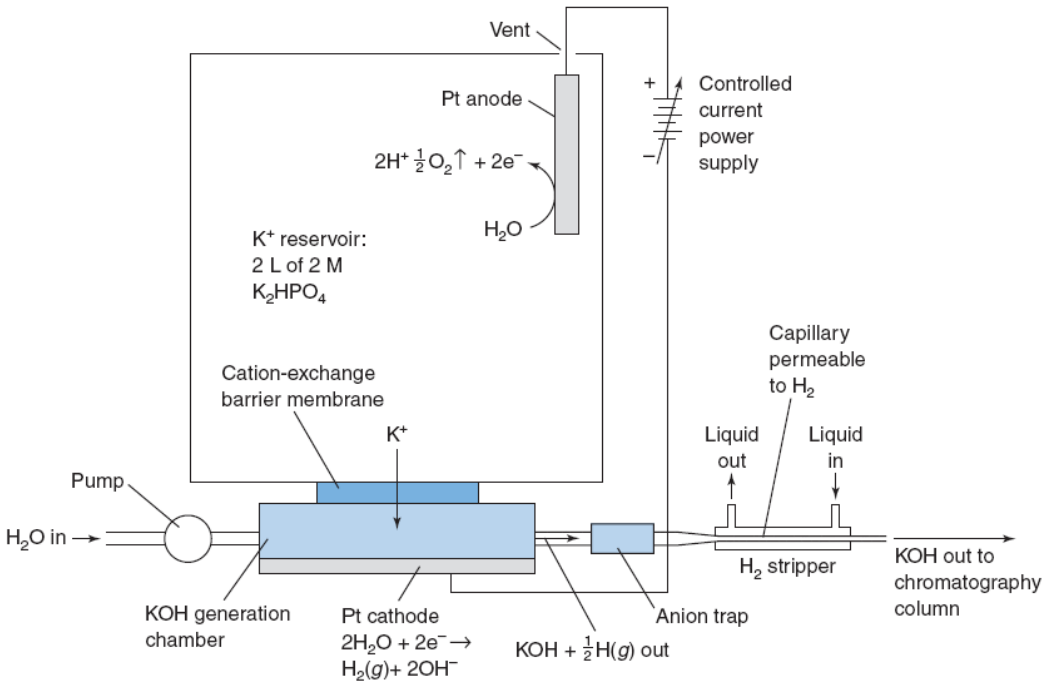

Figure 1.8. Reagent Free cartridge for use with IC. Image credit: (*57*).

generation chamber. As current is applied, the electrolysis of water oxidizes water at the anode and reduces water at the cathode. This reaction causes free K^+ to pass through a cation-exchange barrier membrane to produce KOH in the generation

chamber. The amount of KOH formed is proportional to the current applied and inversely proportional to the flow rate. The hydrogen gas generated is removed and the resulting eluent is a constant concentration of KOH.

Several detection platforms are readily available for IC, although a conductivity detector is the most common. A challenge of this type of detection is the use of the eluents previously described. The use of a strong acid or base will result in a high background conductivity, hindering the detection of ionic species at low concentrations. The original solution to this problem was to use an ion-exchange resin packed column with fibrous membranes placed before the detector (*58*). Although this experimental set-up lowered the background conductivity, it also required copious amounts of regeneration solution and introduced peak broadening and dispersion. Dionex (now a part of Thermo Scientific) introduced a self-regenerating suppression mechanism in the early 1990s (*58*). This suppressor, which is still in use today, relies on the hydrolysis of water. The use of water as the regeneration solvent is ideal, because it is already supplied by the user for the generation of the eluent. The suppressor also contains a set of semi-permeable ion-exchange membranes that are sandwiched between three sets of ion-exchange screens. The result is shown in Figure 1.9. After the analytes are separated in the analytical column they are flowed into the suppressor. For example purposes, the discussion will focus on the separation of anionic species (X^-), where given the eluent is KOH. Each anion will be present as KX at the introduction site of the suppressor due to the choice of eluent. The suppressor, which contains cation-exchange membranes, allows the movement of the K^+ ion through the membrane

and upon the electrolysis of water the analyte is now present as HX before reaching the detector (since H^+ can also move through the membrane). Meanwhile, the eluent, KOH, is being converted to H_2O. The conversion of the eluent from KOH to H_2O decreases the background conductivity, allowing the detection of small changes of analyte (X^-).

The most important component in IC, the stationary phase housed in the analytical column, is where the separation occurs. The selection of the analytical column can vary based on the desired analyte and eluent composition. As the analyte moves through the column it is competing for places on the stationary

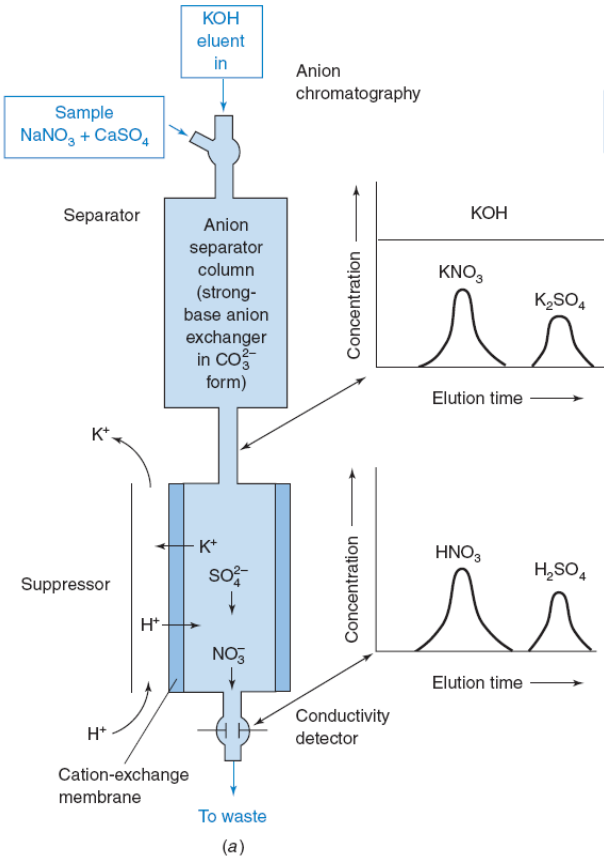

Figure 1.9. Suppression in IC and the corresponding chromatogram with and without suppression. Image credit: (*57*).

phase. The stationary phase is paired with the eluent, therefore if the eluent of choice is KOH then a hydroxide selective analytical column will be selected. The frequency of the partitioning, the movement of the analyte from the mobile phase to the stationary phase, results in the separation of the sample mixture. If the analyte does not have affinity for the stationary phase it will pass quickly through the column, eluting at the beginning of the chromatogram. A typical chromatogram is shown in Figure 1.10. The diameter of the beads used to compose the stationary phase are usually < 10 μm and can vary based on the application desired.

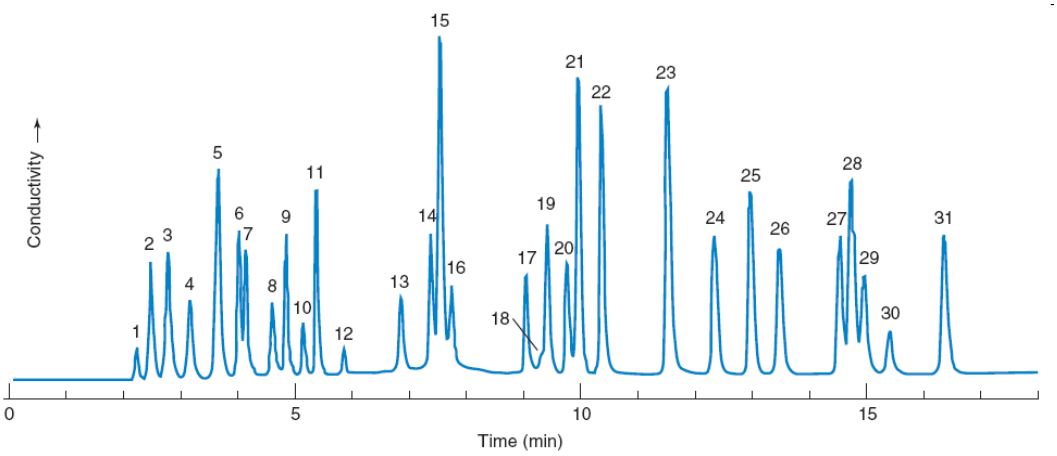

Figure 1.10. A typical anion chromatogram using a Dionex IonPac AS11 column. Peaks are (1) quinate; (2) F^-; (3) acetate; (4) propanoate; (5) formate; (6) methylsulfonate; (7) pyruvate; (8) valerate; (9) chloroacetate; (10) BrO_3^-; (11) Cl^-; (12) NO_2^-; (13) trifluoroacetate; (14) Br^-; (15) NO_3^-; (16) ClO_3^-; (17) selenite; (18) CO_3^{2-}; (19) malonate; (20) maleate; (21) SO_4^{2-}; (22) $C_2O_4^{2-}$; (23) tungstate; (24) phthalate; (25) PO_4^{3-}; (26) chromate; (27) citrate; (28) tricarballylate; (29) isocitrate; (30) *cis*-aconitrate; (31) *trans*-aconitate. Image from Thermo-Scientific.

1.5 Future Chemical Instrumentation for Mars

Phoenix provided the first *in-situ* wet electrochemical analysis of another planet's soil. Scientists use the data from the mission in combination with several other

mission results to characterize Mars. The Phoenix data is still being analyzed and reanalyzed, but recent work has focused on the development of future instrumentation. In order to have wet chemistry experiments on Mars, the advantages and disadvantages of the Phoenix instrumentation must be considered before a future iteration of the WCL can be proposed. Advantages of a WCL type analysis include the real time investigation of soil sample. The use of ISEs also allows for the simple determination of soluble ionic concentrations simultaneously. The WCL type ISEs survived the harsh conditions travelling to and remaining on the Martian surface, and also successfully determined the concentration of several ionic species.

A major improvement that can be made to a potential next generation WCL would be the ability to increase sampling. Only four cells were onboard Phoenix, limiting the analyses performed owing to each cells' one-time use capability. The ability to analyze a greater number of samples would provide a greater characterization of the Martian surface. In a similar vein, the ability for a WCL type instrument to be placed on a rover, instead of a lander, would also help achieve this goal although in order to maximize the number of analyses performed either the WCL must be miniaturized or the overall payload/rover must be much, much larger. Accuracy and precision of the measurements can be increased by incorporating more ISEs, each WCL beaker had only 15, and by implementing redundancy of the ISEs present. These changes allow for greater chemical speciation and the production of more reliable measurements. At the current time of flight, there was not a viable solid-state reference electrode, therefore the Li^+ electrode was used,

under the assumption that no lithium would be present on the surface. Although this turned out to be the case, a solid-contact reference electrode should be used in future analyses that does not rely on a specific ion in the background matrix. An active delivery of the soil sample should also be incorporated to ensure that the sample is successfully added to the leaching solution. Lastly, WCL analyses assumed that a 1 cc sample of soil was added to each cell, with an approximate weight of 1 g. The ability to weigh the sample prior to analysis would greatly increase the accuracy and precision of the calculations.

The inclusion of an IC on a payload to Mars, or another planetary body, would eliminate the stability and selectivity issues that exist with ISEs. An IC in an extraterrestrial environment would allow the separation and detection of the various ionic species at lower detection limits than ISEs and would also be able to differentiate ions in the Hofmeister series, therefore eliminating the perchlorate problem when trying to quantify the amount of nitrate. The amount of sulfate could also be determined directly, instead of using titrimetric methods. The major obstacle of this is the sheer amount of instrumentation required. Although advancements are being made for a miniaturized IC system, the requirement of eluent and the generation of waste poses the greatest obstacles. In order to successfully detect the cations and anions that Phoenix detected three different systems would be required, taking up valuable payload real estate. The use of IC in an extraterrestrial environment might occur sometime in the future, but the current technologies hinder it from being included for several years to come. Currently, the most viable method for the detection of soluble ionic species remains ISEs.

2. Martian Chemistry

The core of any analytical technique consists of three steps: (1) sample acquisition, (2) sample preparation, and (3) sample analysis. In a laboratory setting, the first two can be overlooked and underappreciated. When performing autonomous experimentation in a remote location, or on another planet, the sample is usually acquired by some form of a robotic arm (RA) and sample preparation is often limited. For instance, on Phoenix, the RA delivered the soil sample to the funnel, and it was then dropped into the WCL beaker for analysis (*23*). The TEGA analyses involved the heating of the sample in ovens before analysis (*21*). Complex preparatory experiments require too many resources for an instrument payload, therefore techniques and instruments are usually selected that can perform a sample analysis with limited sample preparation.

Ideally, samples would be returned from the various sampling areas for analysis here on Earth. Mars sample return, although proposed in several decadal surveys, has yet to be accomplished. Scientists and engineers face enough challenges and obstacles when planning a one-way mission to Mars, let alone a mission that caches samples and then returns to Earth. For this reason, Martian analogues are proposed and tested to confirm the various results of the various missions and provide further insight for future missions. Currently, several terrestrial sites provide similar characteristics to those of Martian soil, such as the Antarctic Dry Valleys (ADV) (*59–62*), the Atacama desert in Chile (*63*, *64*) as well as several other sites (*65*, *66*). These environments contain a combination of similar aridity, geological composition, chemical composition or other traits, although no

terrestrial analogue is identical to the Martian surface. For this reason, models are formed based on equilibrium kinetics. Geochemical and equilibrium models are invaluable when a lack of laboratory-based studies have yet to be performed for various samples. This chapter will discuss the results of Phoenix as well as the use of equilibrium modeling software to confirm the results seen on Phoenix, and quantify and characterize the form of sulfates and perchlorates. A brief discussion will also compare the results of the models to the Phoenix results, a Martian meteorite (EETA 79001) and a Mars analogue (Antarctic soil).

2.1. Phoenix Results

Four soil samples, designated Rosy Red, Sorceress-1, Sorceress-2 and Golden Goose were delivered to the sample funnels of cells 0-2, respectively. The only sample that was not successfully delivered for analysis was the Golden Goose sample to WCL cell-3. The location of such samples can be found in (*25*). One of the major results of the Phoenix mission was the determination of the pH of the soil. Using the two pH ISEs as well as an iridium electrode coated with iridium oxide, the pH was determined to be alkaline with a value of 7.7 ± 0.3 (*24*). The Martian soil was buffered by the carbonate system and the presence of CO_2 in the headspace of the WCL beaker. The dominant anion in solution was determined to be perchlorate, ClO_4^-, at a level of 2.7 ± 1 mM in solution (corresponding to ~ 0.4-0.6 wt%) (*24*, *25*). The determination of perchlorate confirmed the Viking results that indicated a strong oxidant was present, indicating that the pyrolytic pretreatment of the sample should not be performed if one wants to detect organics

on Mars. At the very least, without the use of derivatization agents. It should be noted that the Phoenix TEGA results were inconclusive for the presence of organics, most likely from the heating of the soil sample before analysis. However, the presence of a strong oxidant at these levels did not have a drastic impact on the oxidation-reduction potential of the sample, with a moderate value of 253 ± 6 mV (*30*). The soluble cation concentrations were initially reported as: $[Ca^{2+}]$ = 0.56 ± 0.50 mM; $[Mg^{2+}]$ = 2.9 ± 1.5 mM; $[Na^{+}]$ = 1.4 ± 0.6 mM; and $[K^{+}]$ = 0.36 ± 0.30 mM (*24*). A discussion of the error associated with this measurement can be found in (*24*). A graphical representation of the Phoenix results can be found in Figure 2.1, showing a potential versus time plot for numerous ISEs. The response of the Hofmeister electrode (NO_3^-/ClO_4^-) shows the largest response (~200 mV change)

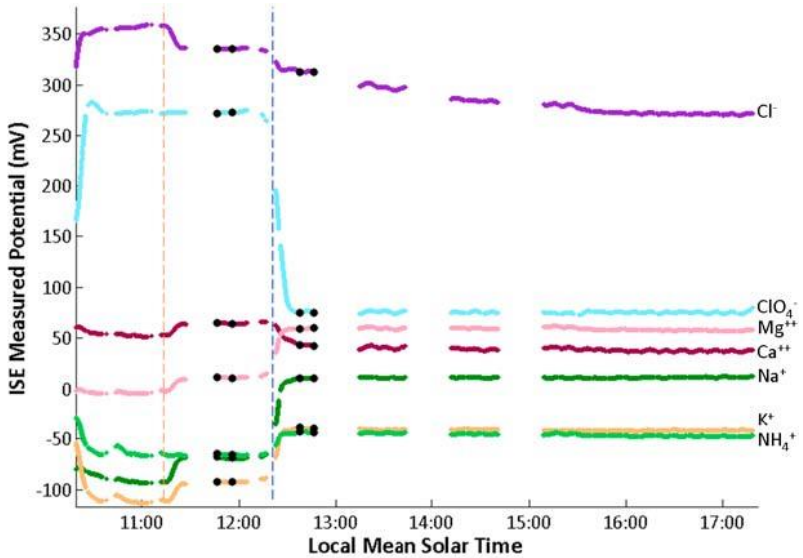

Figure 2.1. Phoenix results represented as a plot of potential (versus the Li^+ electrode) vs. local time. Beginning at time 11:00, the electrodes from top to bottom are: Cl^-, NO_3^-/ClO_4^-, Ca^{2+}, Mg^{2+}, NH_4^+, Na^+, and K^+. The orange dotted line just after 11:00 is the addition of the calibration pellet and the blue dotted line represents the addition of the Rosy Red sample on sol-30. Image credit: (*24*).

indicating the presence of ClO_4^- and not NO_3^-. The calcium ISE is the only other uncharacteristic signal, in that upon sample addition there was a negative response (indicating that the amount of calcium had decreased and/or been eliminated from the system). This will be further investigated in Section 2.3.1.

2.2. Equilibrium Modeling with MINEQL+

The soluble ionic species outlined above and given in (*24*) were used to compose a simulant of salts (and later minerals) for confirmation of the Phoenix results, and determine the amount of sulfate in the Phoenix soil samples. The Rosy Red soil sample was initially chosen because the Ba^{2+} sensor used in the Sorceress-1 sample failed. Results were also later compared with the Sorceress-2 sample.

Chemical equilibrium software, MINEQL+, was used to model the Phoenix results and fabricate a simulant. Each species in Table 2.1 was selected along with H_2O and H^+, which were selected by default. Perchlorate needed to be added via "Edit Mode" and was supplied with its corresponding ionic charge (-1). After all species were selected, the "Scan Thermo" mode was chosen. Under the "Wizard" menu, the concentrations of the various components were varied. The final values selected for modeling are present in Table 2.1 as "Input (mM)". The various other parameters were changed and selected as follows: the pH was calculated by the program based on electroneutrality; the CO_2 was "open to the atmosphere" with a $\log(P_{CO2})$ value of -2.10 (equal to the value of the WCL headspace); and the solids selected included calcite ($CaCO_3$) and magnesite ($MgCO_3$). No parameters were changed for the various menus entitled: "Fixed Entities," "Dissolved Solids," and "Species Not Considered". Based on the Phoenix results, the ionic strength was set

to the value determined for the Rosy Red sample (8.4×10^{-3} M) and the temperature was set to 8.4°C. The results of the model were obtained from the "Summary of All Species for a Single Run" located under the "Special Reports" output type. After several models, a simulant was formulated using commercially available salts including: ammonium chloride (NH_4Cl), sodium chloride (NaCl), potassium perchlorate ($KClO_4$), magnesium perchlorate hexahydrate ($Mg(ClO_4)_2 \bullet 6H_2O$), sodium sulfate ($Na_2SO_4$), magnesium sulfate heptahydrate ($MgSO_4 \bullet 7H_2O$), calcium carbonate ($CaCO_3$), magnesium carbonate ($MgCO_3$), and calcium sulfate dihydrate ($CaSO_4 \bullet 2H_2O$).

Table 2.1. Simulant concentrations for the MINEQL+ program (Input) as well as the physical make-up of the desired simulant (SimRR105). Results from the equilibrium program (MINEQL Output) are compared with the soluble species detected by a WCL testbed (TB2 Output).

Ion	Input (M)*	MINEQL Output (M)	TB2 Output (M)
Ba^{2+}	3.00×10^{-5}	2.92×10^{-5}	6.44×10^{-6}
Ca^{2+}	5.00×10^{-2}	8.99×10^{-4}	1.93×10^{-6}
Cl^-	6.73×10^{-4}	6.73×10^{-4}	6.39×10^{-4}
K^+	4.92×10^{-4}	4.88×10^{-4}	4.61×10^{-4}
Li^+	1.00×10^{-3}	9.94×10^{-4}	NA
Mg^{2+}	9.96×10^{-3}	4.83×10^{-3}	9.27×10^{-4}
Na^+	1.55×10^{-3}	1.53×10^{-3}	4.75×10^{-4}
NH_4^+	3.00×10^{-5}	2.78×10^{-5}	1.17×10^{-4}
NO_3^-	1.09×10^{-3}	1.09×10^{-3}	NA
SO_4^{2-}	3.04×10^{-3}	2.09×10^{-3}	NA
ClO_4^-	2.76×10^{-3}	2.76×10^{-3}	NA

*Includes background contribution from TS21 solution
NA: not analyzed

Experiments were performed on a WCL testbed (TB2) that contained the same make-up and orientation of sensors as the WCL onboard Phoenix. The electrochemical sensors were calibrated with the leaching solution serving as the first calibration point, similar to the procedure performed on Mars. The only differences were: (1) the additions were added in aqueous form, opposed to the addition of a solid calibration pellet, and (2) a full 5-point calibration was

performed before sample addition, compared with a 2-point calibration on Phoenix. The addition of calibrants in aqueous form eliminates the time required for the dissolution of the solid calibrant, allowing the calibration to occur quickly and efficiently. The concentration of the test solutions (TS) are shown in Table 2.2. The leaching solution for the Phoenix WCL cells was TS20. Therefore, with the

Table 2.2. Composition of the test solutions (TS) used for the analysis of Martian simulants.

Ion	TS20 (M)	TS21 (M)	TS21M (M)	TS22 (M)	TS23 (M)	TS24 (M)
Li^+	1.00×10^{-3}	1.00×10^{-3}	1.00×10^{-3}	1.00×10^{-3}	1.00×10^{-3}	1.00×10^{-3}
Na^+	1.00×10^{-5}	3.00×10^{-5}	3.40×10^{-5}	1.10×10^{-4}	1.01×10^{-3}	1.00×10^{-2}
$NH4^+$	1.00×10^{-5}	3.00×10^{-5}	3.40×10^{-5}	1.00×10^{-4}	1.00×10^{-3}	1.00×10^{-2}
K^+	1.00×10^{-5}	3.00×10^{-5}	3.40×10^{-5}	1.00×10^{-4}	1.00×10^{-3}	1.00×10^{-2}
Ca^{2+}	1.00×10^{-5}	3.00×10^{-5}	4.17×10^{-5}	1.00×10^{-4}	1.00×10^{-3}	1.00×10^{-2}
Mg^{2+}	1.00×10^{-5}	3.00×10^{-5}	3.47×10^{-5}	1.00×10^{-4}	1.00×10^{-3}	1.00×10^{-2}
Ba^{2+}	1.00×10^{-5}	3.00×10^{-5}	3.81×10^{-5}	1.00×10^{-4}	1.00×10^{-3}	1.00×10^{-2}
NO_3^-	1.03×10^{-3}	1.09×10^{-3}	1.10×10^{-3}	1.30×10^{-3}	4.00×10^{-3}	3.10×10^{-2}
Cl^-	5.00×10^{-5}	1.50×10^{-4}	1.94×10^{-4}	6.00×10^{-4}	6.00×10^{-3}	6.00×10^{-2}
HCO_3^-	1.00×10^{-5}	3.00×10^{-5}	3.40×10^{-5}	1.00×10^{-5}	1.00×10^{-5}	1.00×10^{-5}

exception of the background concentrations of Li^+ and NO_3^- at ~1 mM, the remaining ionic species were present at 10^{-5} M (10^{-3} mM). A solid calibration pellet with known amounts was then added to bring the concentrations to ~ 3×10^{-5} M, therefore TS21 served as the second point in the calibration. The actual concentrations of TS21 on Mars were calculated as TS21M. On Mars, the ISEs could not be calibrated any further because the background concentrations needed to remain relatively low in order to detect small concentration changes of ionic species. In the laboratory, WCL test-beds and flight units are calibrated from TS20-TS24 before performing any analyses. Simulant experiments were carried out in the Mars chamber, seen in Figure 2.2, with a controlled solution temperature of 10-

15ºC and in an atmosphere of ~8000 mbar CO_2 (balanced by N_2), equal to the headspace P_{CO2} of WCL. The 10-15ºC range corresponded to the temperature of WCL during the thawing/analysis process. At the start of each sol (Martian day) the beaker was thawed and frozen at the end of the analysis/sol to conserve power for the overall payload. A custom lid for the chamber was fabricated to facilitate the addition of spike solutions while under the above conditions, therefore the lid allowed the chamber to act as a glove box.

Figure 2.2. Mars simulation chamber. Courtesy of S.P. Kounaves.

2.1.1. Martian Simulants

The first simulant fabricated, SimRR105, after equilibrium modeling with MINEQL+ compared well with the Rosy Red (RR) soluble concentrations. The makeup of the SimRR105 simulant can be found in Table 2.1, along with the equilibrium modeling and experimental results. Similar to the Phoenix results, there was approximately a 200 mV depression in the "nitrate" electrode signal upon the addition of 2.76 mM ClO_4^- and the characteristic negative response seen by the Ca^{2+} electrode as shown in Figure 2.3 (*24*, *25*). With the exception of Ca^{2+} and Mg^{2+}, the modeling software was in agreement with the soluble concentrations. One reason

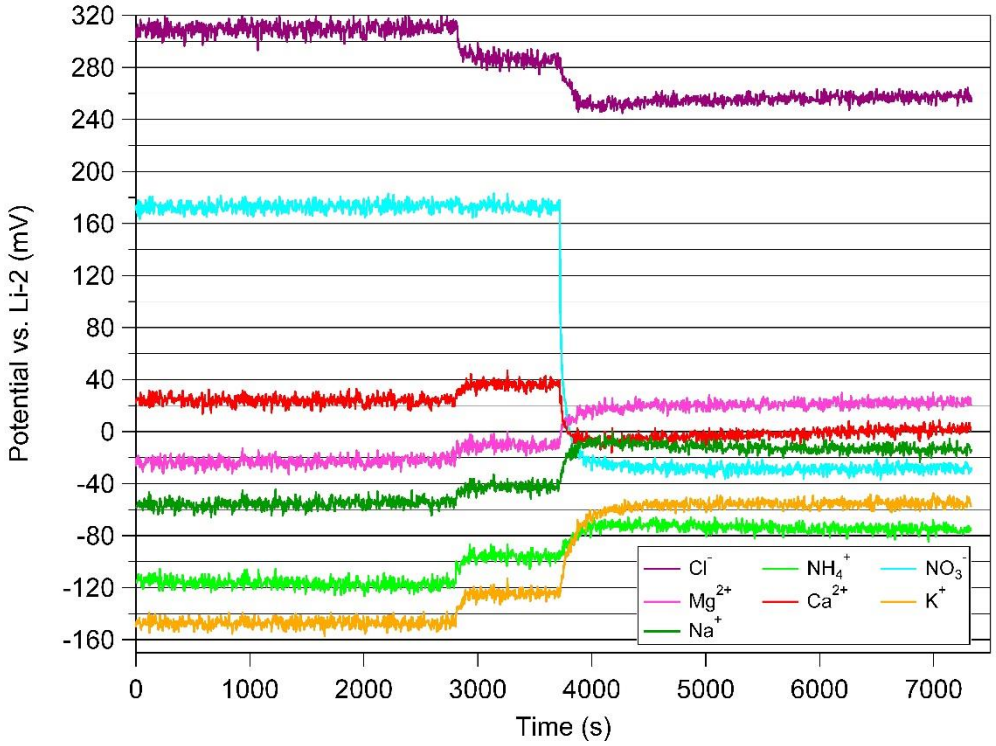

Figure 2.3. Addition of the SimRR105 simulant and the electrochemical response of various electrodes in WCL TB2. The first major potential change ~2800 s is the addition of the first calibrant spike to bring the concentration levels to that of TS21. The next change in potential ~3600 s is the addition of the simulant SimRR105. From top to bottom starting at t = 0 the ISEs were: chloride, nitrate, calcium, magnesium, sodium, ammonium and potassium.

for this discrepancy could be that the simulant was analyzed for only 2 hours, and although it appeared an equilibrium had been reached, various other reactions could continue to occur slowly over time (much slower than experimental conditions). This was also expected since the ionic species originated from chemical salts instead of minerals. The results from the SimRR105 simulant confirmed the Phoenix results and presented evidence of the possible parent salts of the species.

Further simulant analysis looked to elucidate the amount of soluble sulfate in the Phoenix soil. To achieve this, the most prevalent ionic species, ClO_4^-, was removed to ensure no interference with SO_4^{2-}. The formation of simulant SimRR105ii replaced all perchlorates with their respective nitrates as seen in Table 2.3. The simulant SimRR105ii was then run in the Mars chamber in a similar fashion to the previous simulant. A comparison of the results seen in Figure 2.4, with those of Figure 2.3, shows the behavior of the NO_3^- and Ca^{2+} electrodes with no perchlorate present. The nitrate signal, which begins at a background concentration of 1.09 mM increases to 4.10 mM with a potential difference of ~30 mV, opposed to the ~200 mV change when a similar amount of ClO_4^- was added. This clearly showed the selectivity of the electrode ISM toward perchlorate over nitrate. The calcium signal also increased, as was expected due to the amount of calcium in the system, although the majority of the calcium remained as $CaCO_3$. Similar to the previous simulant, the equilibrium model agrees with the experimental results with the exception of Ca^{2+} and Mg^{2+}.

Table 2.3. Simulant concentrations for the MINEQL+ program (Input) as well as the physical make-up of the desired simulant (SimRR105ii). Results from the equilibrium program (MINEQL Output) are compared with the soluble species detected by a WCL testbed (TB2 Output).

Ion	Input (M)*	MINEQL Output (M)	TB2 Output (M)
Ba^{2+}	3.00×10^{-5}	2.88×10^{-5}	4.67×10^{-6}
Ca^{2+}	5.01×10^{-2}	9.02×10^{-4}	8.03×10^{-7}
Cl^{-}	4.92×10^{-4}	4.92×10^{-4}	6.40×10^{-4}
K^{+}	5.44×10^{-4}	5.39×10^{-4}	4.79×10^{-4}
Li^{+}	1.00×10^{-3}	9.94×10^{-4}	NA
Mg^{2+}	9.96×10^{-3}	4.85×10^{-3}	6.53×10^{-4}
Na^{+}	1.42×10^{-3}	1.40×10^{-3}	2.82×10^{-4}
NH_4^{+}	3.00×10^{-5}	2.78×10^{-5}	9.21×10^{-5}
NO_3^{-}	4.10×10^{-3}	4.09×10^{-3}	NA
SO_4^{2-}	2.99×10^{-3}	2.05×10^{-3}	NA
ClO_4^{-}	0.00	0.00	NA

*Includes background contribution from TS21 solution
NA: not analyzed

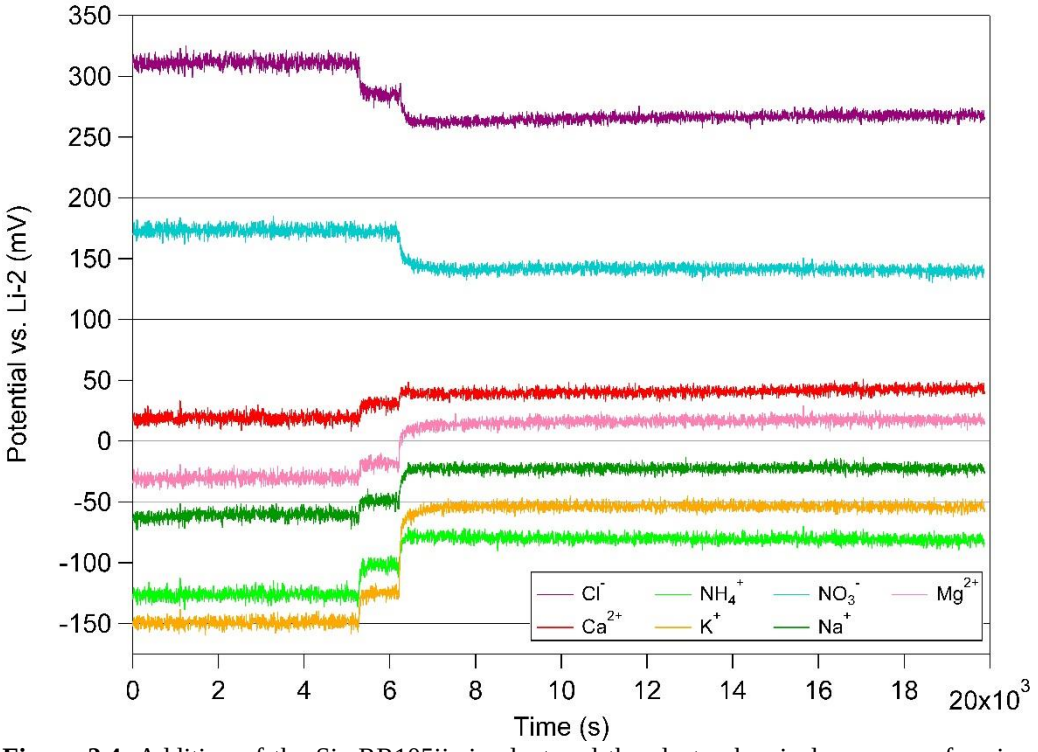

Figure 2.4. Addition of the SimRR105ii simulant and the electrochemical response of various electrodes in WCL TB2. The first major potential change ~5200 s is the addition of the first calibrant spike to bring the concentration levels to that of TS21. The next change in potential ~6000 s is the addition of the simulant SimRR105ii. From top to bottom starting at t = 0 the ISEs were: chloride, nitrate, calcium, magnesium, sodium, ammonium and potassium.

2.2. Determination of Sulfate at the Phoenix Landing Site

2.2.1. Sol-96 and the Golden Goose "Sample"

The total amount of soluble SO_4^{2-} was initially determined to be 4.8 ± 1.5 mM for cell-0 (Rosy Red) and 5.9 ± 1.5 mM for cell-2 (Sorceress-2). This value was estimated by the equation:

$$[SO_4^{2-}]_T = \frac{\Delta[Cl^-]}{2}$$

where $[SO_4^{2-}]_T$ is the total amount of sulfate, and $\Delta[Cl^-]$ is the change in chloride concentration from the addition of the sample until there was an increase in the barium signal, indicating that all the sulfate had been titrated. Figure 2.5 shows the signals of the chloride and barium electrodes from cell-0 and cell-2 used for this calculation. In cell-0 the chloride signal increases, but stabilizes by the end of the sol, while in cell-2 there is a constant increase in the chloride signal over the two

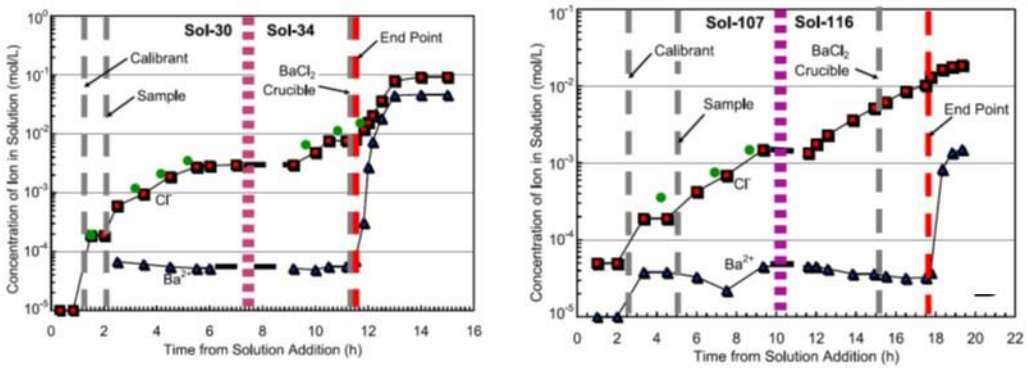

Figure 2.5. Barium (▲) and chloride (■) electrode responses for the analysis of the soluble sulfate in cell-0 of the Rosy Red soil sample (left) and cell-2 of the Sorceress-2 soil sample (right). Chloride was also independently verified by CP (●). The Rosy Red sample was added on Sol-30, the sulfate titration experiment was performed on Sol-34 (left) and the Sorceress-2 sample was added on Sol-107 with the sulfate titration experiment performed on Sol-116 (right). Figure taken from (*28*).

sample time periods. The increase was quantified as ~1.5 x 10^{-3} mol L^{-1} h^{-1}. The increase in chloride was also confirmed with CP.

The increase of the chloride concentration in cells 0 & 2 led to the hypothesis that there was a leak present from the $BaCl_2$ crucibles. This was confirmed upon the analysis of the sol-96 data. The soil sample, Golden Goose, was not successfully delivered, as it got clogged in the funnel and would not drop into the drawer. After the soil addition attempt there was an increase in the amount of barium and chloride seen by their respective electrodes, shown in Figure 2.6. This evidence of a "blank" confirmed that there was in fact a leak of the $BaCl_2$ after soil addition (or attempted soil delivery). The increase in concentration of Ba^{2+} and Cl^- in cell-3 increased at the predicted ratio of 1:2, while increases were not seen for any of the other ionic species. The increase in chloride concentration was also confirmed independently with CP.

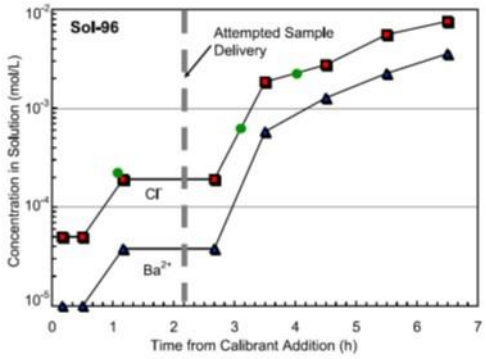

Figure 2.6. Barium (▲) and chloride (■) electrode responses for the analysis of the Golden Goose soil sample on Sol-96. Chloride was also independently verified by CP (●). The attempted sample delivery occurred on Sol-96, although no soil was delivered. The increase of both the barium and chloride signals point to a leak of the $BaCl_2$. Figure taken from (*28*).

2.2.2. Simulant SimSO4RRi

Although the amount of sulfate was initially determined as discussed above, a simulant needed to be fabricated to confirm these results. Formulation of this simulant, SimSO4RRi, increased the amount of initial sulfate to a value ~12 mM. This value was chosen based on previous results relating the S/Cl molar ratio of ~4:1 (*7*, *11*, *12*, *67*). Assuming a value of $[Cl^-]$ = 2.9 mM then it would be assumed that $[SO_4^{2-}]$ would be ~12 mM. This estimate also assumes that all the sulfate is soluble. This simulant was modeled with an initial value of 12 mM SO_4^{2-}, but with the amount of chloride seen by the previous WCL results, ~0.7 mM, shown in Table 2.4. The appropriate amount of perchlorate, ~2.7 mM, was also added to mimic the results detected by the Phoenix WCL electrodes. The experimental values are determined by the WCL testbed are also shown in Table 2.4 and Figure 2.7. The potential responses are very similar to the first simulant, SimRR105 (Figure 2.3), although the amount of SO_4^{2-} has quadrupled.

Table 2.4. Simulant concentrations for the MINEQL+ program (Input) as well as the physical make-up of the desired simulant (SimSO4RRi). Results from the equilibrium program (MINEQL Output) are compared with the soluble species detected by a WCL testbed (TB2 Output) and ion chromatography (IC Output). The leaching calibrant solution was subtracted from the IC Output for comparison purposes. Table adapted from (*62*).

Ion	Input (M)	MINEQL Output (M)	TB2 Output (M)	IC Output (minus TS21, M)
Ba^{2+}	3.00×10^{-5}	2.95×10^{-5}	1.70×10^{-5}	NA
Ca^{2+}	5.01×10^{-2}	2.77×10^{-3}	4.90×10^{-4}	4.54×10^{-3}
Cl^-	6.98×10^{-4}	6.98×10^{-4}	6.67×10^{-4}	9.00×10^{-4}
K^+	3.47×10^{-4}	3.37×10^{-4}	4.15×10^{-4}	3.50×10^{-4}
Li^+	1.00×10^{-3}	9.80×10^{-4}	NA	ND
Mg^{2+}	1.02×10^{-2}	6.64×10^{-3}	1.79×10^{-3}	2.95×10^{-3}
Na^+	1.53×10^{-3}	1.49×10^{-3}	1.10×10^{-4}	1.56×10^{-3}
NH_4^+	3.00×10^{-5}	2.76×10^{-5}	2.25×10^{-4}	2.80×10^{-4}
NO_3^-	1.10×10^{-3}	1.09×10^{-3}	NA	ND
SO_4^{2-}	1.21×10^{-2}	6.88×10^{-3}	NA	1.41×10^{-2}
ClO_4^-	2.87×10^{-3}	2.87×10^{-3}	NA	2.12×10^{-3}

NA: not analyzed
ND: not detected

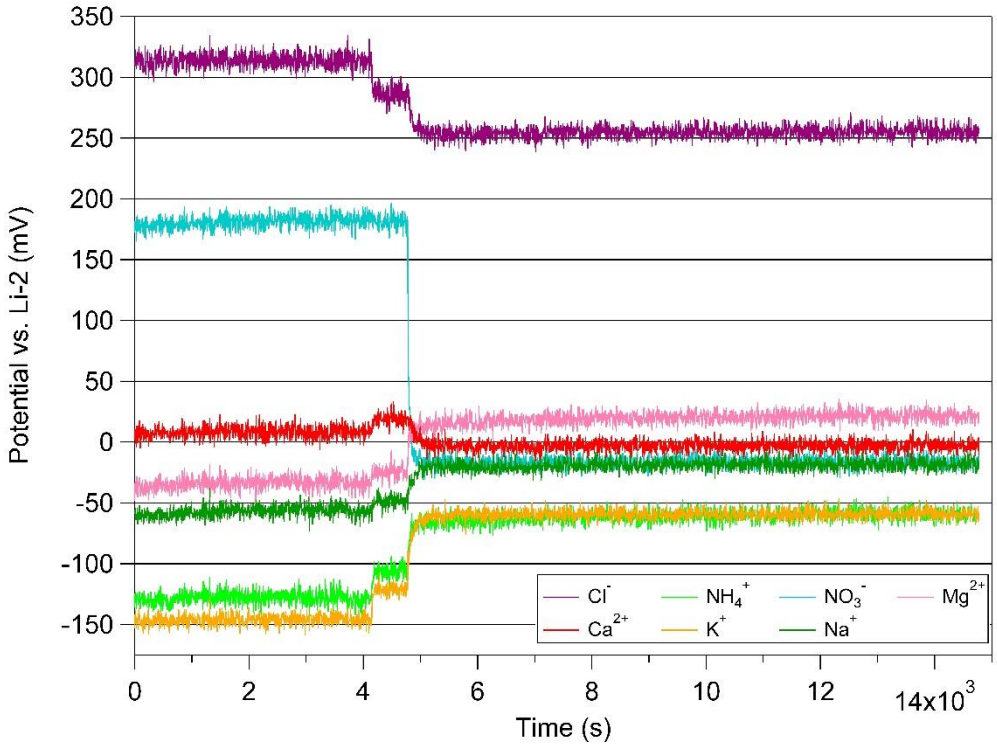

Figure 2.7. Addition of the SimSO4RRi simulant and the electrochemical response of various electrodes in WCL TB2. The first major potential change ~4000 s is the addition of the first calibrant spike to bring the concentration levels to that of TS21. The next change in potential ~4800 s is the addition of the simulant the SimSO4RRi. From top to bottom starting at t = 0 the ISEs were: chloride, nitrate, calcium, magnesium, sodium, ammonium and potassium.

2.2.3. Determination of Sulfate Parent Salts

The previous calculation of the soluble sulfate of 4.8 ± 1.5 mM for cell-0 (Rosy Red) and 5.9 ± 1.5 mM for cell-2 (Sorceress-2) corresponds to 1.2 ± 0.5 and 1.4 ± 0.5 wt% SO_4^{2-} in the Phoenix soil. The molar ratio of S (as SO_4^{2-}) to Cl (Cl^- and ClO_4^-) is ~ 2:1, opposed to the aforementioned predicted 4:1. This discrepancy, as discussed in (*28*) is said to be due to the fact that not all the SO_4^{2-} is soluble, therefore resulting in a low determination from the WCL analyses, or that the soil analyzed in the previous studies was different from the soil analyzed by Phoenix. In order to determine the parent salt form(s) of the sulfate ion, the soluble cations,

Na^+, K^+, Ca^{2+}, Mg^{2+} and $Fe^{2/3+}$ must be considered. An updated soluble species is presented in Table 2.5, showing the results of the SO_4^{2-} analysis (*28*).

Table 2.5. Updated soluble concentration of species likely present in the Phoenix soil. Taken from (*28*). Model assumes that 1 g of soil was added to 25 mL pure H_2O. The equilibrium concentrations is the amount of the required species/mineral to give the measured and calculated ionic concentrations.[a]

Species	Equilibrium Concentration in Solution (mM)	Concentration in Soil (wt%)
$CaCO_3$ (calcite)	Saturated	3 – 5[b]
$MgCO_3$ (magnesite)	Saturated	≥ 1.8[c]
$MgSO_4$ (epsomite)	Dissociated	3.3[d]
ClO_4^-	2.5	0.6
Na^+	1.4	0.08
Cl^-	0.4	0.04
K^+	0.4	0.04
Mg^{2+}	6.4	-
SO_4^{2-}	3.9	-
HCO_3^-	5.4	-
$MgSO_4$ (aq)	1.2	-
Ca^{2+}	0.75	-
$CaSO_4$ (aq)	0.17	-

[a] Equilibrium calculated using GWB *React* at 7ºC and a 4 mbar CO_2 headspace. This model takes into account the presence of the $BaCl_2$ from the leaking crucible. The rate of Ba^{2+} addition appears to have been sufficient in all analyses to maintain $[SO_4^{2-}] < 0.5$ mM and fully dissociate all SO_4^{2-}
[b] As determined by TEGA and WCL.
[c] Minimum required by model to give saturate Mg^{2+} in 25 mL of solution.
[d] Equivalent to 5.3 mM total SO_4^{2-} in solution. At such concentration, other hydrates give similar values.

The presence of sulfate with K^+ or Na^+ would, at most, result in as 0.2 mM K_2SO_4 and 0.7 mM Na_2SO_4. This would only be a fraction of the soluble sulfates, while the presence of $Fe^{2/3+}$ would have resulted in the poisoning of several ISEs, and since this did not occur it can be assumed that $Fe^{2/3+}$ was not present at any appreciable levels. The cations left as the most likely candidates were Ca^{2+} and Mg^{2+}, and after further modeling with *Geochemist's Workbench* (GWB)® it was shown that if $[SO_4^{2-}] \geq 6$ mM then the $[Ca^{2+}]$ and $[Mg^{2+}]$ would have to be ≥ 3 mM

and ≥ 7 mM respectively, which is not the case. A more plausible explanation is that the majority of the sulfate was present as $MgSO_4$, which would result in an increase in the Mg^{2+} response and a decrease in the Ca^{2+} response upon the addition of $BaCl_2$ and the dissolution of SO_4^{2-}. Due to the presence of magnesium bearing minerals, it is extremely likely that the most prevalent form of SO_4^{2-} is $MgSO_4$.

Operating under the assumption that the Phoenix soil was wet at some time in the past based on results from WCL and TEGA (*26*) further studies based on evaporation models could deduce the dominate minerals present in the WCL soils. The values in Table 2.5 were used in GWB over temperature ranges of 0-25°C and P_{CO2} ranges of 0.004-1 atm to yield the dominant evaporates. These included calcite ($CaCO_3$), gypsum ($CaSO_4 \bullet 2H_2O$), magnesite ($MgCO_3$), epsomite ($MgSO_4 \bullet 7H_2O$), $KClO_4$ and $NaClO_4$. This data provides insight into the possible sulfate mineralogy, and is consistent with the finding of previous landers and rovers. The implications of the SO_4^{2-} mineralogy with the dominant salts found at the WCL site provide a basis for the presence of the possibility of past life at the Phoenix landing site. A model (Figure 2.8) comparing the precipitated minerals of 1 L of terrestrial seawater to 1 L of water containing the salts found in (an extrapolated) 40 g of Phoenix soil show that upon dilution of a small amount of Phoenix soil by, for example, a melting snowpack (*68–70*), could result in a water activity consistent with terrestrial halophilic microbes ($a_{H2O} \geq 0.75$) (*71*). Again, this assumes that the soil was wet recently.

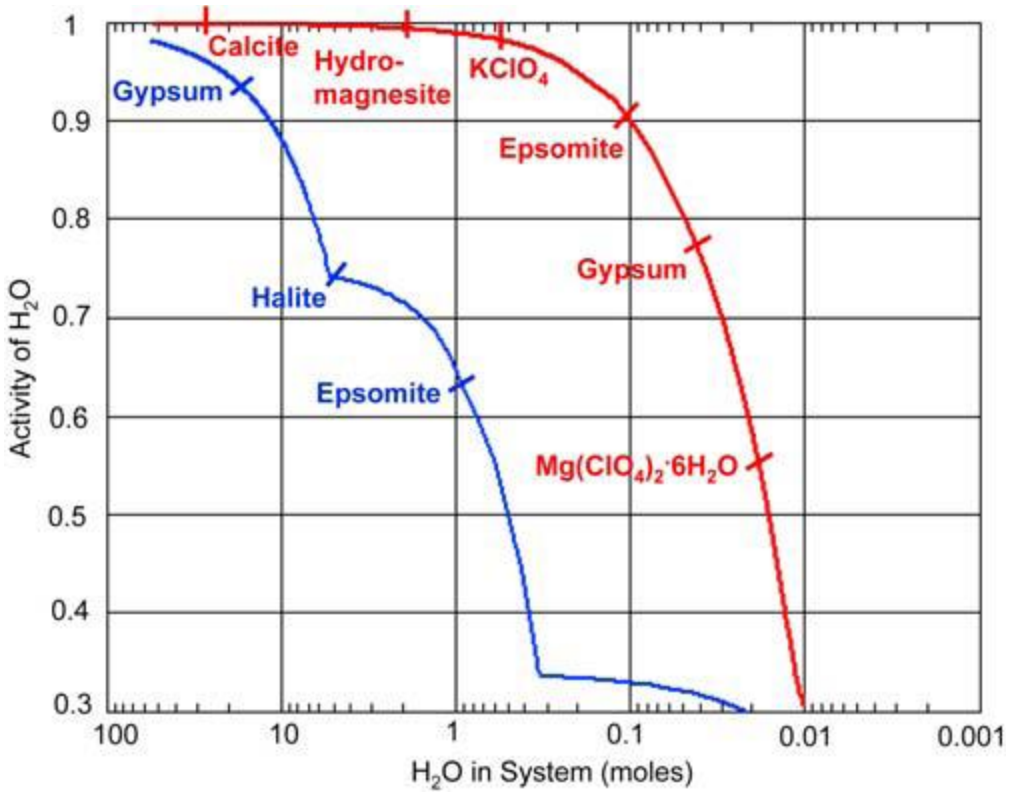

Figure 2.8. *Geochemist's Workbench ® React* model showing the precipitated minerals in 1 L of terrestrial seawater (blue) and 1 L solution containing the ionic species found in 40 g of the Phoenix soil (red). Model for the Phoenix solution was taken at 7°C and P_{CO2} = 4 mbar. Figure taken from (*28*).

2.3. Determination of Perchlorate Parent Salts

Perchlorate was found to be prevalent in the Northern Poles of Mars at the Phoenix landing site in 2008 (*25*). Recent results initially reported by the Curiosity scientists indicate the presence of a chorine-oxygen species and it is hypothesized to be perchlorate (*72*). This find has major implications for the global distribution of perchlorate and the possible detection of organics. An investigation into the effect of perchlorate on the other sensors, mainly calcium and magnesium, was proposed to deduce the chemical composition of the perchlorate parent salts.

The determination of the parent salts of the perchlorate ion yields information regarding the mineralogy, chemistry and history of the Martian soil. The Phoenix WCL cells did not contain an electrode for the direct determination of perchlorate, as previously discussed. Confirmation of the presence of ClO_4^- was determined by testing the Hofmeister ISEs with many interfering species, while constraining the amount present to be similar to the soil delivered by the robotic arm on Phoenix. An investigation into the effect on the calcium sensor showed that there was a negative response upon sample addition, due to the ClO_4^- in solution. This was a characteristic of the presence of perchlorate and led to the determination that ClO_4^- was present in the Phoenix soil.

2.3.1. Investigation of the Calcium Electrode Response

The results from the Phoenix mission yielded information into the soluble species in solution, and did not directly yield parent salts. A closer examination of the electrode responses, mainly the Ca^{2+} ISE, was used as an attempt to determine if ClO_4^- was present in the form of $Ca(ClO_4)_2$ or $Mg(ClO_4)_2$ (*73*). Figure 2.9 shows the response of the Ca^{2+} electrode for the Rosy Red soil sample on Mars. The signal starting at t = 7700 s was the response due to the second calibration point, where the concentration of Ca^{2+} was ~3.0×10^{-5} M and ClO_4^- was not present. A steady decrease in the negative direction occurred until an equilibrium with the carbonates in the system stabilized the signal upon sample addition. The same signal behavior is seen in Figure 2.10, with the successful delivery of the Sorceress-1 soil sample. Initial tests on a WCL spare unit done after the mission show the Ca^{2+} signal

without ClO_4^- present, shown in Figure 2.11. Important features to highlight in Figures 2.9 and 2.10 were that there was no increase in signal upon soil delivery; this decrease did not occur immediately after soil addition but instead happened over a few minutes (~300 s); and the signal stabilized at a potential corresponding to the carbonate equilibrium.

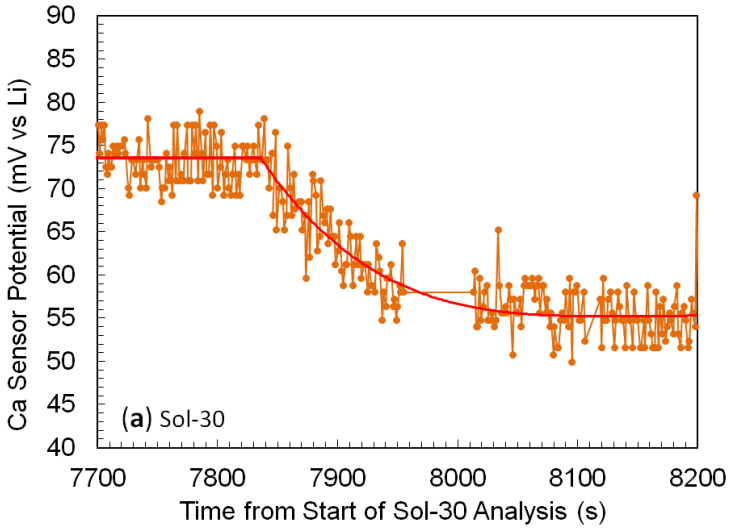

Figure 2.9. Calcium signal from sol-30 upon the addition of the Rosy Red soil sample. The red line is an average of the data to reduce the noise.

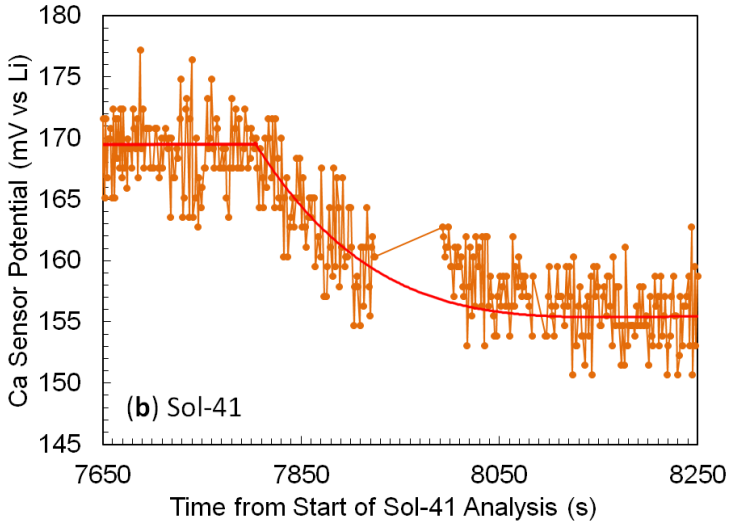

Figure 2.10. Calcium signal from sol-41 upon the addition of the Sorceress-1 soil sample. The red line is an average of the data to reduce the noise.

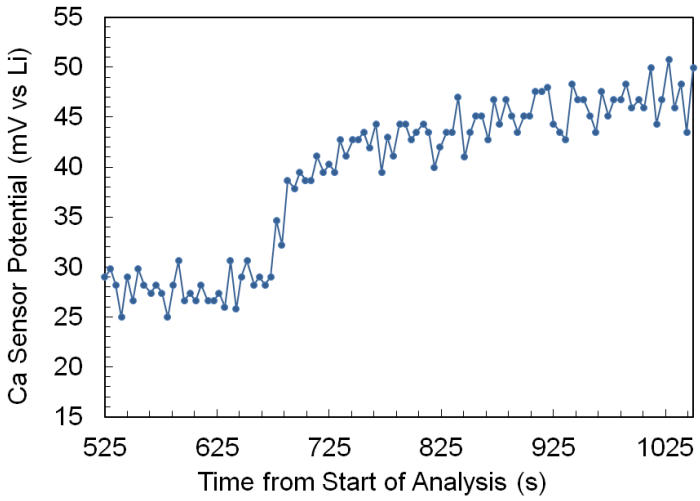

Figure 2.11. Calcium signal obtained on a WCL spare unit with no ClO_4^- present.

2.3.2. Ratio of Calcium:Magnesium Perchlorates

When performing tests to determine the amount of calcium perchlorate versus magnesium perchlorate, the Ca^{2+} sensor appeared to behave differently depending on the amount of each salt present in solution. Figure 2.12 shows a summary of these results, where the shape of the Ca^{2+} ISE signal was monitored while the ratio of Ca:Mg-$(ClO_4)_2$ was changed from 100% $Ca(ClO_4)_2$ to 100% $Mg(ClO_4)_2$. All perchlorates were added to correspond to the amount present in solution detected by Phoenix, as ~0.7 wt% ClO_4^-. When a sample containing 4 wt% calcite (Icelandic spar, $CaCO_3$) and 100% $Ca(ClO_4)_2$ was added to the calibrant solution there was an initial increase in potential, indicating some response by the Ca^{2+} electrode to Ca^{2+} (or interfering species) in solution, followed by a steady decrease in potential. As the ratio is changed to 70:30 Ca:Mg, this initial increase in potential decreased in magnitude but still exhibited a steady decrease until the equilibration with the carbonates occurs. At 60:40 Ca:Mg the initial potential increase is no longer present, but the steady decrease was. When equal amounts of $Ca(ClO_4)_2$ and

$Mg(ClO_4)_2$ were used in the sample there was a more rapid negative response and a slight dip in potential ~85 s (normalized). At 100% $Mg(ClO_4)_2$, there was an immediate decrease and pronounced dip in potential before an increase to the carbonate equilibrium. The shape of the Ca^{2+} ISE seen in the Phoenix WCL cells (Figures 2.9 and 2.10) is most consistent with the curve seen for a ratio of 60% $Ca(ClO_4)_2$: 40% $Mg(ClO_4)_2$.

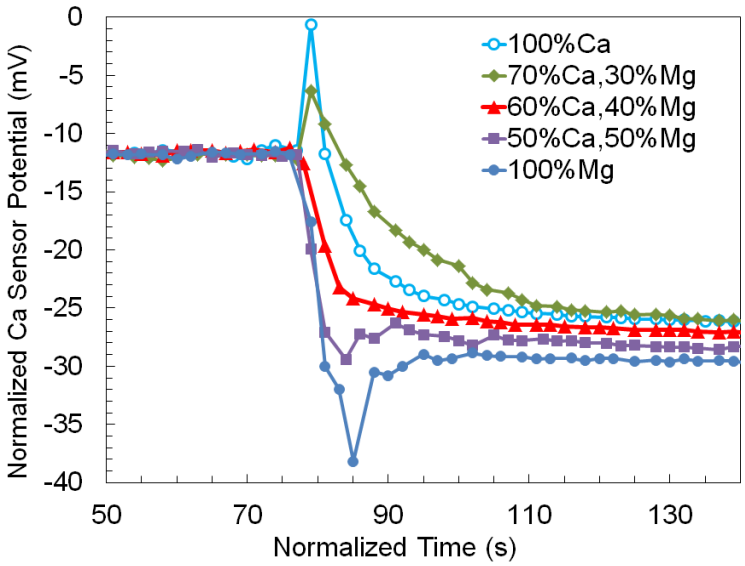

Figure 2.12. Calcium response as the ratio of $Ca(ClO_4)_2$:$Mg(ClO_4)_2$ was varied. All plots were normalized to show the addition of the sample at the same time.

2.3.3. The Effect of Sodium Perchlorate

The presence of calcium and magnesium containing minerals was the major factor in the selection of those species as the perchlorate counterion. The WCL soils also contained other cationic species, mainly Na^+ and K^+. These species could also serve as a counterion for perchlorate. Potassium, present in the WCL soil at a level of 0.4 mM would only account for ~15% of the perchlorate, while Na^+ would only account for ~60% of the perchlorate, assuming that all K^+ and Na^+ were present as

$KClO_4$ and $NaClO_4$, respectively. Another possibility would be the presence of $Fe^{2/3+}$, although the presence of iron would have been detrimental to several of the halide sensors, which was not the case, therefore $Fe^{2/3+}$ was not present in any appreciable amounts. Assuming that the K^+ is insignificant compared to the amount of soluble ClO_4^-, the primary candidate left is Na^+. Similar studies to those found in Figure 2.12 were conducted to investigate this hypothesis.

The Ca^{2+} electrode response was studied upon the addition of various perchlorates. Samples were fabricated with a total amount of 1.4 mM $NaClO_4$ (accounting for ~60% of the ClO_4, assuming all Na^+ present as $NaClO_4$) as well as the combination of various other salts including: $Mg(ClO_4)_2 \bullet 6H_2O$, $CaCl_2 \bullet 2H_2O$ and $Ca(NO_3)_2 \bullet 6H_2O$. Similar to the previous studies, all samples contained 4 wt% calcite. Various sample mixtures are presented in Figure 2.13. The presence of only $NaClO_4$ does not exhibit a similar behavior of the Ca^{2+} electrode experienced by WCL and it also does not account for the total amount of perchlorate. The addition of the remaining ClO_4^- in the form of $Mg(ClO_4)_2$, produced the characteristic depression seen when no $Ca(ClO_4)_2$ was present (Figure 2.12), which was also not consistent with the WCL results. The introduction of soluble calcium species, in the form of $Ca(NO_3)_2$ or $CaCl_2$, at concentrations of ~0.5 mM Ca^{2+} in the presence of ~2.5 mM ClO_4^- (counterion: Mg^{2+}) does not produce any increase in Ca^{2+} signal. Each sample caused an immediate drop in potential upon addition and remained constant for the remainder of the test period. The magnitude of the decrease, ~30 mV, was also greater than that seen on Mars for the Rosy Red and Sorceress-1 samples (Figures 2.9 and 2.10) as well as the Ca-/Mg-$(ClO_4)_2$ studies (Figure 2.12).

These studies confirmed that perchlorate is most likely present as $Ca(ClO_4)_2$ and $Mg(ClO_4)_2$ in a ratio of 60:40.

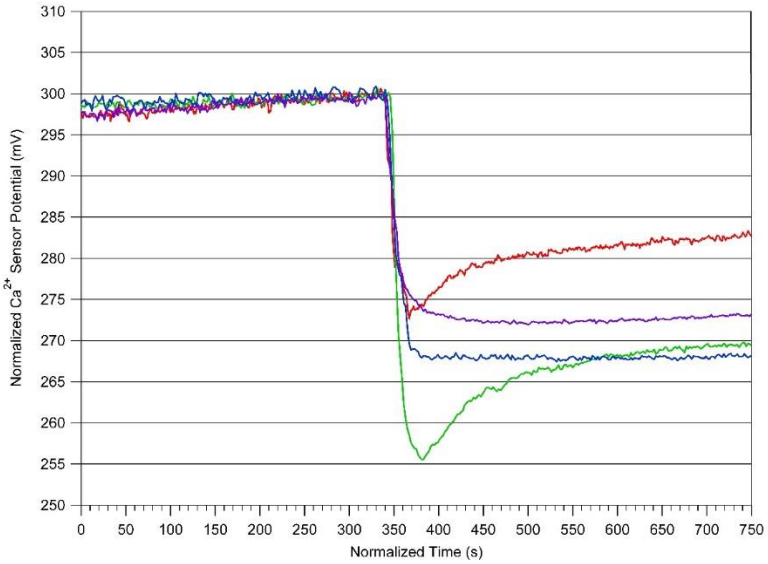

Figure 2.13. Calcium response of various samples containing $NaClO_4$ and other salts. The response at t=0 is the signal attributed to the TS21 concentration of Ca^{2+} (0.03 mM) and the sample was added at t=350 s. The signal and time were normalized so that the sample was added at the same time. From top to bottom at t=750 s, the samples were: 1.41 mM $NaClO_4$ (red); 1.22 mM $Mg(ClO_4)_2 \bullet 6H_2O$ and 0.52 mM $CaCl_2 \bullet 2H_2O$ (purple); 1.44 mM $NaClO_4$ and 0.45 mM $Mg(ClO_4)_2 \bullet 6H_2O$ (green); 1.18 mM $Mg(ClO_4)_2 \bullet 6H_2O$ and 0.52 mM $Ca(NO_3)_2 \bullet 2H_2O$ (blue). All samples contained 4 wt% Icelandic spar (calcite, $CaCO_3$).

2.3.4. Implications of Calcium Perchlorate

Calcium, opposed to magnesium, as the dominant counterion for perchlorate has implications for the recent chemical history of the Phoenix landing site. Originally, the perchlorate was assumed to be mainly present as $Mg(ClO_4)_2$, which would imply a recently wet Phoenix landing site (*26*, *27*, *74*). The results of the work presented above suggests that the perchlorates at the Phoenix landing site were a mixture of $Ca(ClO_4)_2$ and $Mg(ClO_4)_2$ at a ratio of 60:40. The ratio of Ca:Mg is also consistent with the Ca:Mg ratio of the respective carbonates (*26*, *75*). The

implication that perchlorate was present as $Ca(ClO_4)_2$ would suggest that the Phoenix landing site has not been wetted recently, and would have been arid (possibly since the formation of the Heimdall Crater, where Phoenix landed (*76*)). Calcium perchlorate, a highly soluble chemical species, should not be present if the landing site had been in contact with any water, especially in the presence of carbonates and sulfates. Independent evaporation and sublimation models confirmed this hypothesis (*77*, *78*).

2.4. Comparison of A Martian Analogue to Phoenix, A Martian Meteorite and Model Predications

The above models used for the fabrication of the sulfate simulant were also compared to other results beyond Phoenix, mainly Antarctic soils and a Martian meteorite, EETA 79001. These studies investigated the viability of Antarctic soils as a Martian analogue. The EETA 79001 meteorite and soils from ADVs were analyzed using IC, the simulant data was used to formulate a physical sample which was analyzed by both IC and a Phoenix WCL test-bed unit. The simulant investigated, SimSO4RRi, was described previously and results were shown in Table 2.4. The concentrations of the simulant were leached in a similar manner to the Phoenix WCL soil, and the leachate was analyzed by IC (IC Output). The background contribution from the leaching/calibration solvent (TS21) was subtracted to yield the concentration of the simulant. Leachates from several ADVs, the Coastal Thaw Zone (CTZ) and the Stable Upland Zone (SUZ), and the Martian

meteorite (EETA 79001) were analyzed in similar manners. Experimental conditions are outlined elsewhere (*62*).

The environments of the CTZ and SUZs vary in elevation and mean annual temperatures. The CTZ is lower in elevation (0-700 m) but higher in mean temperature (~-20°C) than the SUZ (1700-1800 m, ~-33°C) (*79*). The hyperarid cold desert conditions of the SUZ yield a terrestrial area that serves as a possible Martian surface environment. The Martian meteorite was found ~200 km near the NW ADV during the 1979-1980 field season in *Elephant Moraine (EET)*. Several groups have characterized the meteorite in terms of age and geology (*80*, *81*). The first studies of the soluble ionic species were performed in 2010 (*82*). All samples were compared to the Phoenix results, presented in previous sections.

A comparison of the five samples shows general agreement between the ionic species with the meteorite existing at usually lower concentrations, as shown in Figure 2.14. The meteorite samples were collected sawdust from a cross-sectional cut. It is possible that the Martian surface was different for the Phoenix experiments compared with the meteorite location origin. This is one plausible explanation of the lower concentrations. Most species are also within one order of magnitude when comparing the ADV soils to the Phoenix results and the simulant. The largest deviation is exhibited when comparing ClO_4^-. While the simulant and Phoenix soil are in agreement in the concentration of ClO_4^-, the perchlorate seen in the ADV are drastically lower. Several possibilities for this decrease in ClO_4^- are: (1) the presence of any water would cause the migration of ClO_4^- in the ADVs, while the lack of water on Mars would cause it to remain in place; (2) perchlorate

was not deposited at similar rates on Earth as on Mars, resulting in higher concentrations on Mars than on Earth; or (3) perchlorate is not as prevalent in high concentrations on Earth as it is on Mars.

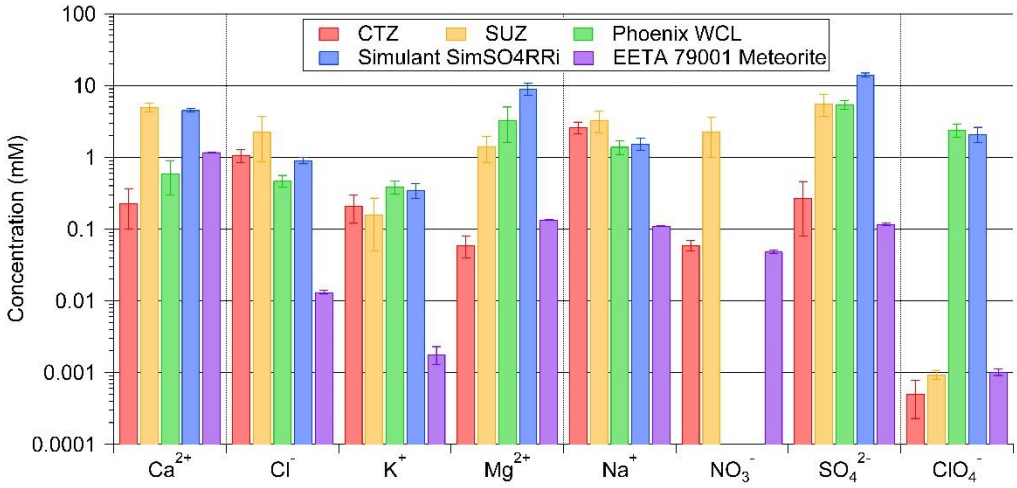

Figure 2.14. Comparison of various samples including: the Antarctic Dry Valleys (Coastal Thaw Zone, CTZ; and the Stable Upland Zone, SUZ), the average of the Phoenix results (Rosy Red, Sorceress-1 and -2), the simulant SimSO4RRi, and the EETA 79001 Martian meteorite. The two points for the NO_3^- data for Phoenix and the simulant are excluded based on the presence of perchlorate. Adapted from (*62*).

The various samples were also comparable in pH and conductivity, as shown in Figure 2.15. All samples had pH values in a neutral range (6-8 pH units) and with the exception of the meteorite were in general agreement when comparing conductivity. The CTZ sample was one order of magnitude lower than the SUZ, while the conductivities of the SUZ, Phoenix soil and simulant samples were all ~1-1.5 mS/cm. Overall, the soils gathered from the ADVs serve as near-ideal Martian analogues. A further analysis of the results suggest that the Phoenix landing site was much more arid than the SUZ, and most likely was arid for a longer period of time (*62*). This conclusion is also in agreement with the $Ca(ClO_4)_2$ argument that

if the parent counterion of ClO_4^- is in fact Ca^{2+}, that the Phoenix landing site would not have seen liquid water longer than initially expected.

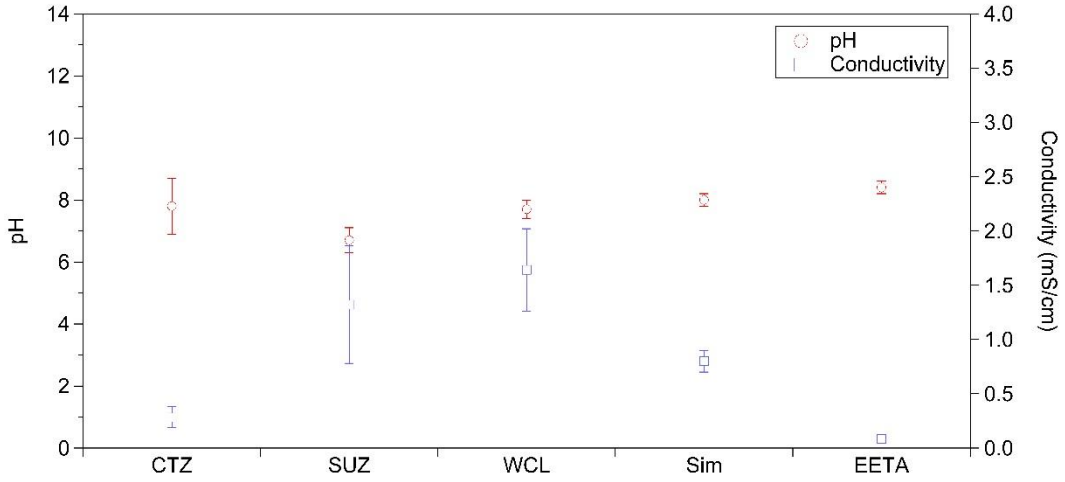

Figure 2.15. A comparison of the pH (○) and conductivity (□) of the various samples. CTZ and SUZ are the Antarctic soils, WCL is the Phoenix analyses, Sim is simulant SimSO4RRi and EETA is the results from the Martian meteorite.

3. The Robotic Chemical Analysis Laboratory (RCAL)

3.1. Functionality of RCAL

The Phoenix WCL cells provided invaluable information into the soluble chemistry of the Martian surface. As previously stated, its major shortcomings were the fact it could only analyze a maximum of 4 samples (one-time use) and that each WCL contained only 15 ISEs. In an attempt to address these concerns, an instrument was developed concurrently with WCL, the Robotic Chemical Analysis Laboratory (RCAL, Starsys Research, Boudler, CO). One of the major differences between RCAL and WCL was the location of the sensors. A carousel of 20 hermetically sealed sample tubes spun to four different positions for analysis, each performing a specific function. The first position punctures the seal of the sample tube to facilitate the delivery of sample. This station could also be revisited to stir the sample by spinning the tip of the puncture mechanism. The other three positions each contained sensor arrays that would be lowered into the sample tube to perform the chemical analysis. Figure 3.1 shows a view of the RCAL unit, with a look inside, highlighting the carousel and dipping mechanisms.

3.2. RCAL Electrodes

Previous work (*83*) investigated the fabrication of a sensor array that would encompass more sensors than the WCL beakers. This was achieved by miniaturizing the WCL type electrodes and creating an array of 15-20 ISEs that could vertically be dipped into a sample tube (O.D. ~15 mm). The replacement of

Figure 3.1. The Robotic Chemical Analysis Laboratory (RCAL) with its cover on (left). The dipping mechanism shown with the puncture mechanism installed (top right) and a view of the carousel (bottom right).

faulty ISEs was difficult, which was the major drawback of this design. The array would have to be disassembled and reassembled, which could also cause further damage to other sensors. For this reason an array where sensors could easily be removed and replaced was proposed. Although the array accommodated fewer sensors, it utilized the previously characterized WCL-type ISEs. The heritage of the WCL sensors provided electrodes that could survive pre-flight and cruise conditions, and were well characterized. Multiple arrays could be used to account for the decrease in quantity of ISEs per array.

Ideally, the sensor array would be located at the tip of the dipping mechanism which is difficult when the O.D. of the dipping mechanism is ~10 mm. RCAL has its ISEs located along the side of a dipping mechanism, shown in Figure

Figure 3.2. RCAL sensor dipping mechanism with five WCL type electrodes installed.

3.2. The top-most sensor could potentially not be submerged in the sample solution depending on how deep the dipping mechanism goes into the sample tube. For this reason, coated-wire ISEs (CW-ISE) were fabricated and characterized in an attempt to maximize the number of sensors available in the same plane. CW-ISEs, in various configurations and compositions, have been used in various applications (*31*, *32*, *84–89*), although usually in a disposable manner. The lifetime of CW-ISEs are usually much lower than larger electrodes due to a decrease in the active area of the membrane and the smaller amounts of electroactive components. The leaching of electroactive components from the membrane to the sample solution occurs more quickly than with electrodes 5-10 times their size. Despite these disadvantages, CW-ISEs were proposed to initially test their incorporation with RCAL. A schematic of the CW-ISEs used can be found in Figure 3.3.

The CW-ISEs utilized were fabricated in a similar fashion to the previously discussed WCL electrodes, except on a much smaller scale. A silver wire was encased in PVC heat-shrink tubing and the tip of the wire was chloridized to form

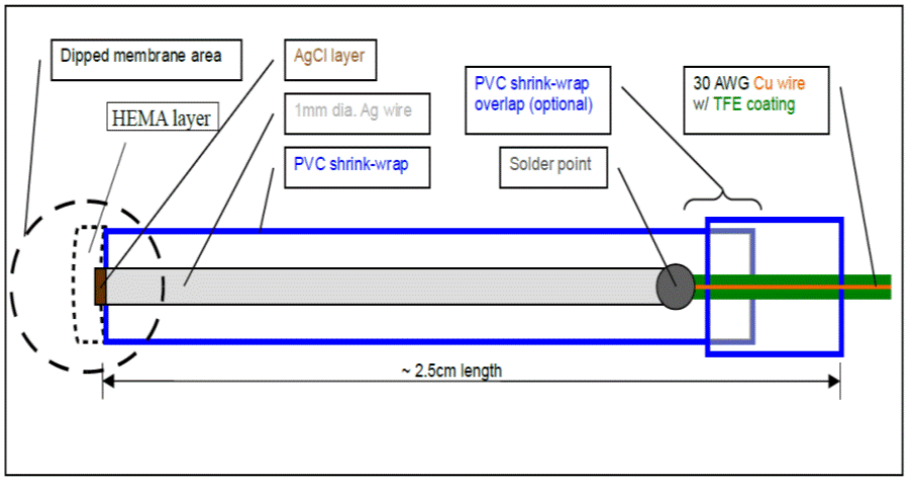

Figure 3.3. Schematic of coated-wire ISEs.

an internal reference element (Ag/AgCl). The polymeric hydrogel, pHEMA, was then pipetted (1 µL) on the tip of the chloridized wire and cured with a 365 nm UV light. The electrode was then dipped into the corresponding plasticized PVC membrane solution. Nine electrodes could be placed around a solid support and then successfully lowered into the RCAL sample tube.

3.3. RCAL Goes for a Ride

A main goal of the RCAL research was to see how it would interface with a rover for an autonomous mission while collecting electrochemical data for a delivered sample. Previous tests had been performed with non-ISE based sensors after sample addition but no field tests had been performed upon the incorporation of ISEs. A successful field test would incorporate RCAL onto a rover and the operational sequence would be fully tested. The operational sequence was to: (1) have a robotic arm (RA) acquire and deliver a sample to RCAL; (2) successfully puncture the sample tube and deliver the soil sample from the RA; (3) successfully move the carousel into the proper position for deployment of the sensor array; (4)

successfully deploy the sensor array and collect data; and (5) repeat steps 1-4. Before a field test of RCAL could occur, the electronics had to be miniaturized and optimized. In its original form RCAL was controlled by a switch board that was approximately 1 m x 1 m. In collaboration with Draper Laboratory (Cambridge, MA) the electronics and software were rebuilt and designed to facilitate the incorporation of RCAL onto the back of a rover.

A series of FieldPoint controllers were used to miniaturize the hardware for RCAL. The FieldPoint controllers were interfaced with a laptop using LabView software to control the various aspects of RCAL. The software used to control RCAL was changed to facilitate easier use and the viewing of ISE data directly in the same graphical user interface (GUI). A view of the software GUI can be found in Figure 3.4. Several buttons were programmed to easily run a series of actions.

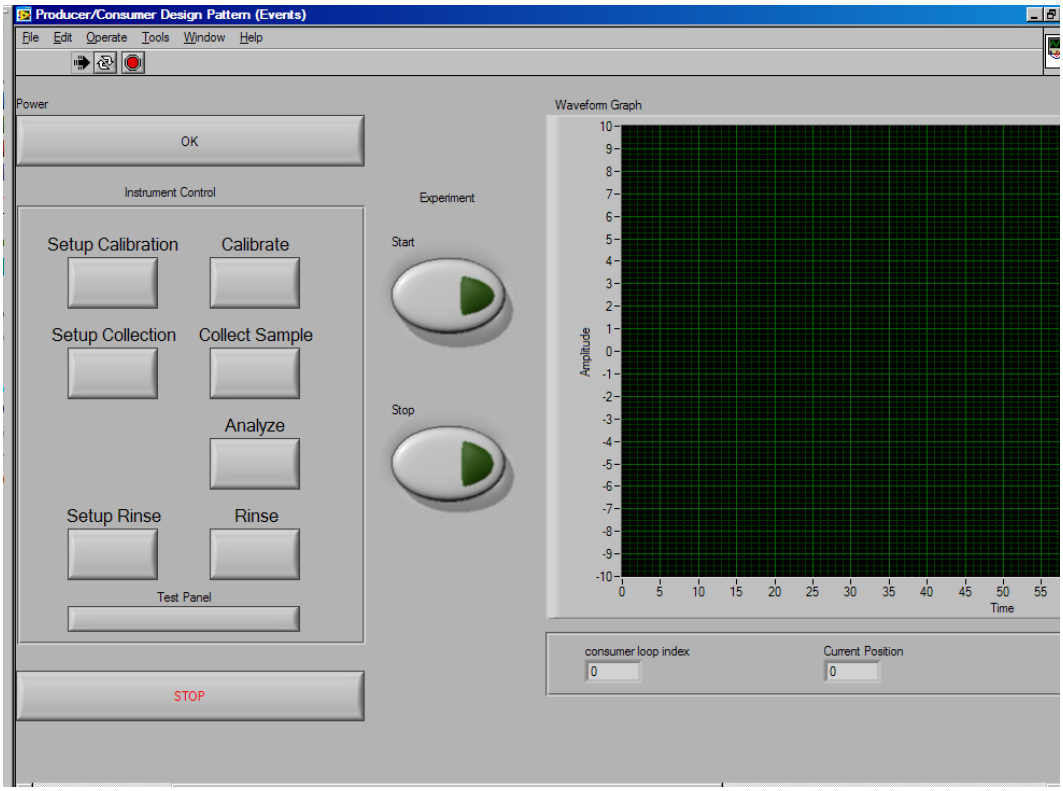

Figure 3.4. Graphical user interface (GUI) for the control of RCAL. Developed for the Death Valley field tests by Draper Laboratory.

To manually control the various operational characteristics, the "Test Panel" button can be selected. Each dipping mechanism and the carousel could be selected and controlled from this sub-menu. An optical sensor inside the carousel determined the location of the sample tube, which allowed for the proper movement of the appropriate sample tube under each dipping mechanism.

3.3.1. Death Valley

The first field test of the newly engineered RCAL took place in Death Valley, CA in November of 2009. The experiments were conducted to address how RCAL would perform in a desert environment with new hardware/software and with limited resources. The power was supplied by two 12 V batteries and the CW-ISE data was obtained externally by use of a Lawson Labs EMF16 data acquisition system. At the time of the test, the software had not been completed to collect data in the same interface, therefore the software from Draper Laboratory was only used to operate the various mechanical functions of RCAL. The entire set-up was placed in a single suitcase and ultimately operated out of the back of a car, while samples were delivered by hand instead of a RA. The set-up can be seen in Figure 3.5.

Overall, the test was a success, showing that the current incarnation of RCAL could be brought into the field and successfully operated. The operation was also conducted on limited power resources which would be desirable for future incorporation onto a rover or other payload. The test also solidified the necessity of a software interface that could collect sample data, and the need for more reliable

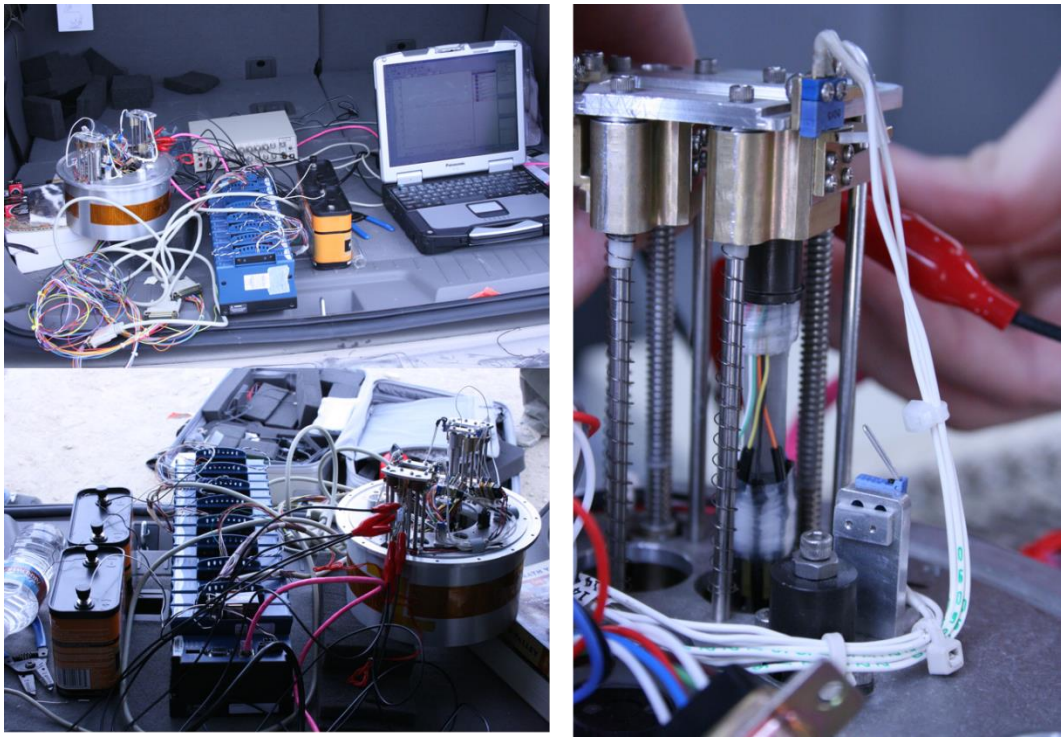

Figure 3.5. A view of RCAL in Death Valley, CA. The entire set-up was run out of the trunk of a car (top left) where RCAL is on the far left, the FieldPoint controllers, Lawson Labs EMF16 interface and 12 V batteries are centrally located with the laptop computer running the RCAL GUI on the right. An alternative view of the set-up (bottom left) and a close up of the CW-ISEs installed (right).

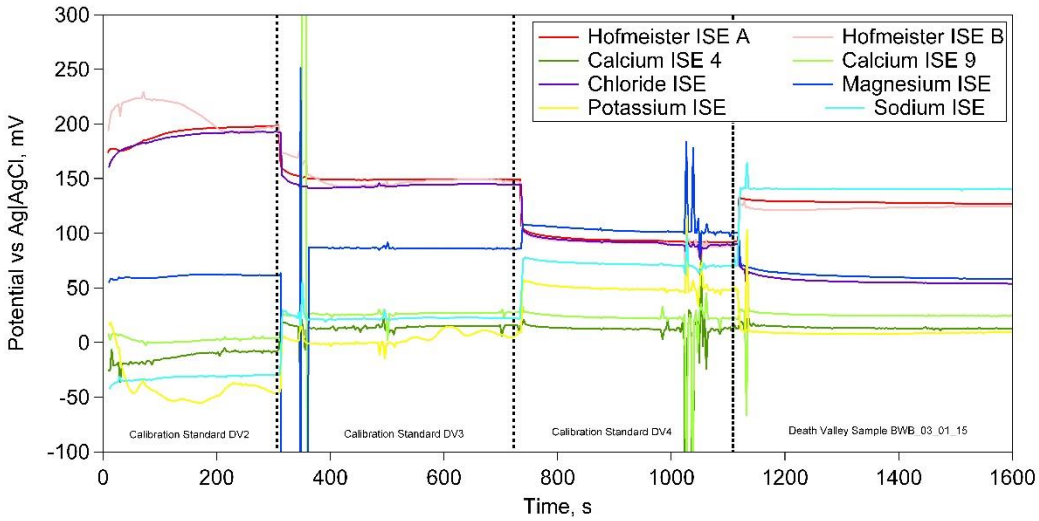

Figure 3.6. Potential versus time plot for the CW-ISEs used in Death Valley, CA in 2009 of sample DV_BWB_003_04_15. The calibration standard DV2 was comprised of ~1.0×10^{-5} M Na^+, K^+, NH_4^+, Ca^{2+}, Mg^{2+}; ~3.0×10^{-5} M NO_3^-; and ~4.0×10^{-5} M Cl^-. DV3 and DV4 increased by an order of magnitude successively. Beginning from the top, at t = 1600 s, the electrodes are as follows: sodium; Hofmesiter A; Hofmeister B; magnesium; chloride; calcium 9; calcium 4; and potassium.

electrodes. A potential versus time plot is shown in Figure 3.6, where the noisy signal from the ISEs can be seen. Although the CW-ISEs collected data *in-situ* in the desert, if the project were to move forward, sensors would need to have a greater stability to ensure the operation of the ISE for the various samples. If RCAL was placed on a rover and sent to a remote location sampling could occur within days or weeks of each other, requiring sensors to function over a long period of time, which the CW-ISE electrodes do not in their current form. Therefore, a sacrifice of quantity of sensors was proposed and the WCL type HEMA electrodes were used for future testing.

3.3.2. SRR2K Rover

The subsequent test of RCAL occurred in March 2012, after integration with the SRR2K rover at the Jet Propulsion Laboratory (JPL) in Pasadena, CA. The primary objective of these experiments was to test the operational sequence from sample acquisition to analysis while placed on a rover. The SRR2K rover was built in 2000 as a technology prototype for a sample return mission (SRR: sample-return rover) and can be seen in Figure 3.7 with RCAL incorporated. It was built to have four wheels that can move independently with an arm that has four degrees of freedom (*90*). The sensors for this test were WCL type with a few modifications. Two sets of electrodes were fabricated, HEMA based electrodes and porous carbon electrodes. The latter configuration replaced the pHEMA of the WCL-type electrodes with a solid support, porous carbon. Due to the configuration of the

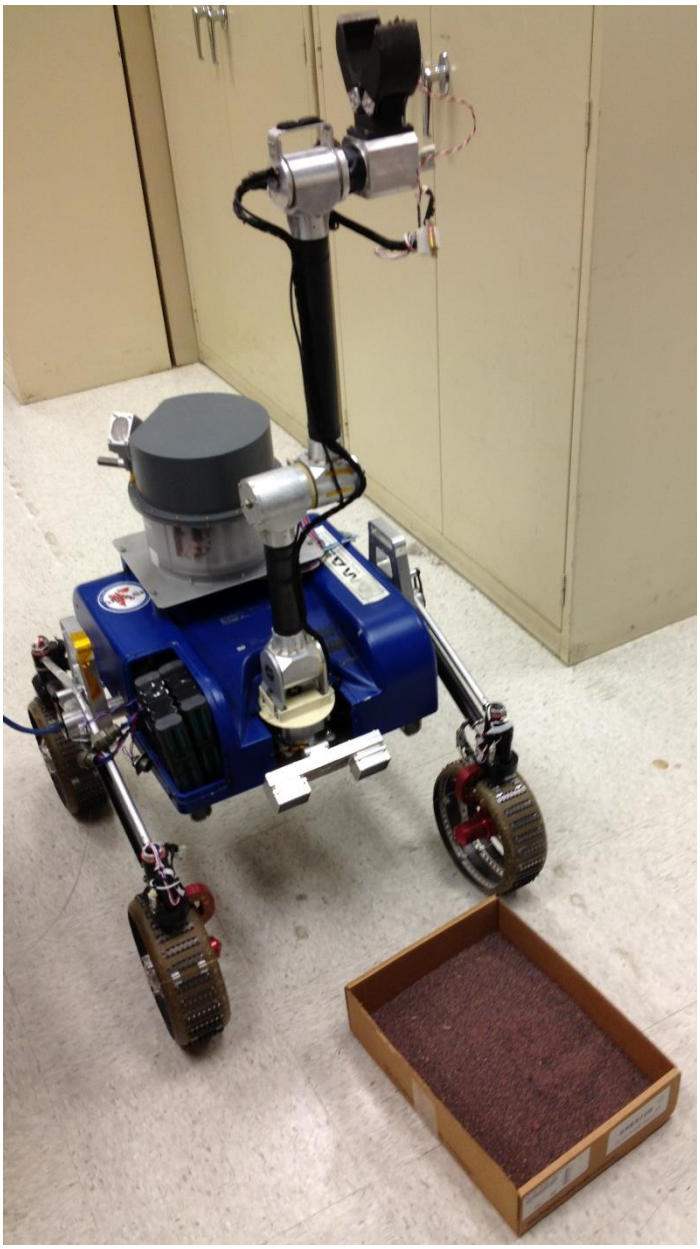

Figure 3.7. Sample-return rover (SRR2K) with RCAL integrated.

dipping mechanism, only 5 electrodes were incorporated into the array: two K^+ ISEs, two NO_3^- ISEs and one Li^+ ISE, which served as the reference electrode. The electrodes that were fabricated with pHEMA were the Li^+ ISE, one K^+ ISE and one NO_3^- ISE. In addition to these three electrodes, one K^+ ISE and one NO_3^-

ISE were fabricated with porous carbon. The replacement of pHEMA with porous carbon will be elaborated further in Chapter 5. All electrodes were characterized before arrival at JPL, and only the best were incorporated into RCAL. A summary of the characterization tests can be found in Figures 3.8 and 3.9. The sensitivity of the NO_3^- ISE shown was -51 mV/decade, near-Nernstian while the the Li^+ ISE exhibited little potential differences over the calibration range. The Li^+ ISE was calibrated in the TS20 solutions (TS21-24) and remained stable even with concentrations of several ionic species at 10^{-2} M levels. This was the desired response since it was going to be used as the reference electrodes for the system.

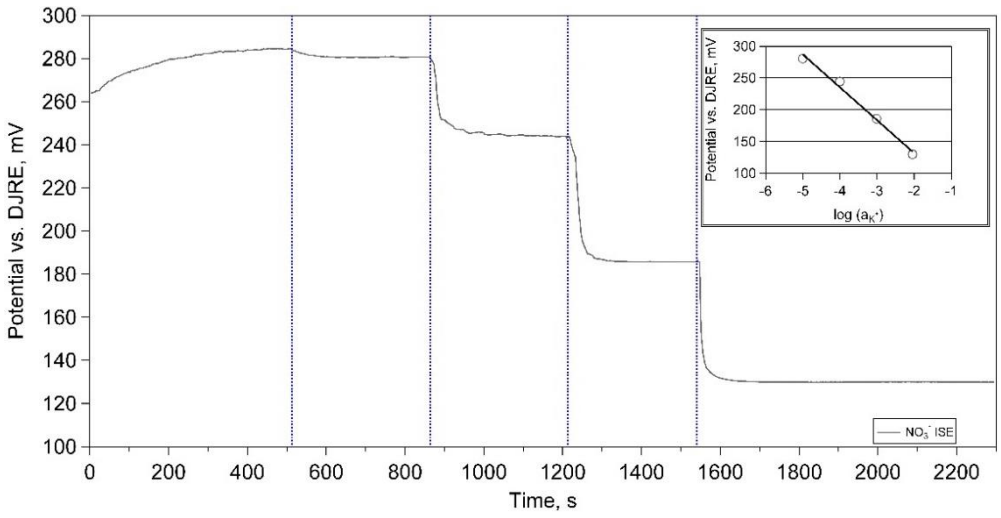

Figure 3.8. Potential vs. time plot of the NO_3^- ISE before integration into RCAL on the SRR2K rover. Blue lines represent the addition of a solution to calibrate the sensors. The concentrations were as follows: bulk water, 10^{-5} M NO_3^-, 10^{-4} M NO_3^-, 10^{-3} M NO_3^-, and 10^{-2} M NO_3^-. Inset shows the corresponding calibration curve.

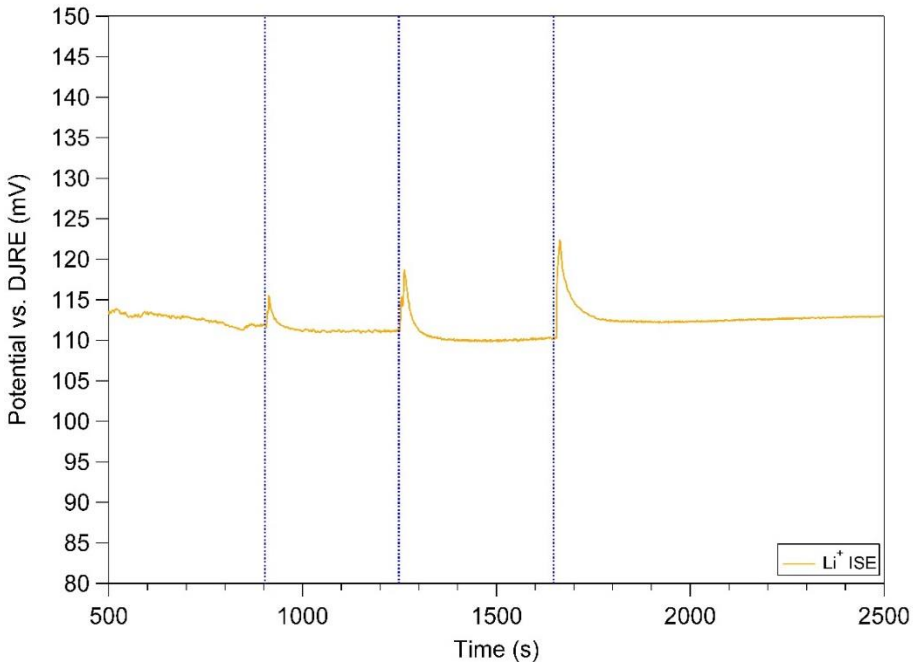

Figure 3.9. Potential vs. time plot of the Li^+ ISE before integration into RCAL on the SRR2K rover. Blue lines represent the addition of a solution to calibrate the sensors. The Li^+ ISE was calibrated in TS21, TS22, TS23 and TS24 (see Table 2.2).

All electronic hardware was supplied by the rover, and the software was built to control all operational characteristics, including the rover, RCAL dipping mechanisms and carousel, as well as data acquisition. Commands were programmed to control the movement of all aspects of the robotic arm including the scoop and the three joints (at the scoop, mid-arm and the base of the arm). Commands also existed for the movement of the scoop to invert as well as to open and close. In terms of the control of RCAL, the carousel was programmed to function without an optical sensor designation for each location. Instead the location of each individual tube was controlled by the movement along the inner wheel of gears. The carousel could be "homed" where the carousel would rotate until a magnet passed between two oppositely poled magnets. This ensured that the carousel rotated the correct number or units for a reliable determination of location. After the carousel was homed, it could then be programmed to rotate in either

direction (depending on which sample tube was being moved) under the appropriate dipping mechanism. The five available positions were the puncture/stirring mechanism (position 0), instrument 1 (1), instrument 2 (2), right drawer for sample delivery (3) and left drawer for sample delivery (4). The third instrument position was not functioning at the time of the tests, therefore only allowing two instruments for analysis. Each dipping mechanism could then be programmed to be lowered and raised (0 indicated the dipping mechanism being lowered, and 1 for being raised).

After the electrodes were placed in the dipping mechanism and wired into the electronics for the collection of data, the sensors were calibrated. After various tests, it was apparent that the dimensions of the RCAL unit at JPL were slightly different than the one present at Tufts. For this reason, the dipping mechanism needed to be shortened from 5 electrodes to 4 electrodes. After further tests it was also apparent that the topmost sensor was not being lowered into the solution. This left three electrodes available, one being the reference electrode. Therefore, one porous carbon NO_3^- ISE and one porous carbon K^+ ISE were placed on either side of the Li^+ reference. A sequence was programmed to allow the automation of the calibration and sampling process. This sequence can be found in Table 3.1. Sample tube 4 was used as the rinse and sample for this scenario, where in an actual run, commands 8 and 13 would be changed for a different sample tube location. After data was collected for a desired period of time, the sequence would either be run again (changing the sample tube location) to obtain information for another calibration tube (or sample tube) or manually programmed to raise the dipping

mechanism and cease testing. Table 3.2 shows the concentrations of the various ion in the calibration solutions (CS).

Before field-testing RCAL on the rover, a set of simulants was fabricated to test the viability of the sample analysis. Simulants consisted of 1 g of silicon dioxide and a constant amount of potassium nitrate. After calibration, the sensors were lowered into the sample solution to quantify the amount of KNO_3 that was in the sample (4.33 mg KNO_3 corresponding to 5.35 mM NO_3^- in the sample tube), and the results are presented in Figure 3.10. Although the NO_3^- sensitivity was less than

Table 3.1. Programmed commands for the autonomous collection of data. The sequence could be easily changed by changing the tube number or the dipping mechanism.

	Command	Purpose
1	cmd_setMoveDipper2_Dist40	Sets sensor dipping mechanism distance to 40
2	cmd_moveDipper2 1	Moves sensor dipping mechanism up (ensuring carousel can turn)
3	cmd_homeCarousel	Homes the carousel
4	cmd_turnCarouselTubeAbs 4, 2	Places tube 4 under the sensor dipping mechanism
5	cmd_moveDipper2 0	Lowers sensors into tube 4, as a rinse
6	cmd_moveDipper2 1	Raises sensors
7	cmd_homeCarousel	Homes the carousel
8	cmd_turnCarouselTubeAbs 4, 0	Places tube 4 under the puncture mechanism
9	cmd_PunctureTest 0	Lowers the puncture mechanism to puncture the foil of the sample tube
10	cmd_runStirr 1, 5	The puncture tip will stir for 5 seconds
11	cmd_PunctureTest 1	Raises the puncture mechaism
12	cmd_homeCarousel	Homes the carousel
13	cmd_turnCarouselTubeAbs 4, 2	Places tube 4 under the sensor dipping mechanism
14	cmd_moveDipper 2, 0	Lowers sensors into tube 4, to collect data.

Table 3.2. Calibration solutions (CS) I-IV for the RCAL testing.

Ion	CS I (M)	CS II (M)	CS III (M)	CS IV (M)
Li^+	1.00×10^{-3}	1.00×10^{-3}	1.00×10^{-3}	1.00×10^{-3}
Cl^-	1.00×10^{-3}	1.00×10^{-3}	1.00×10^{-3}	1.00×10^{-3}
K^+	1.00×10^{-5}	1.00×10^{-4}	1.00×10^{-3}	1.00×10^{-2}
NO_3^-	1.00×10^{-5}	1.00×10^{-4}	1.00×10^{-3}	1.00×10^{-2}

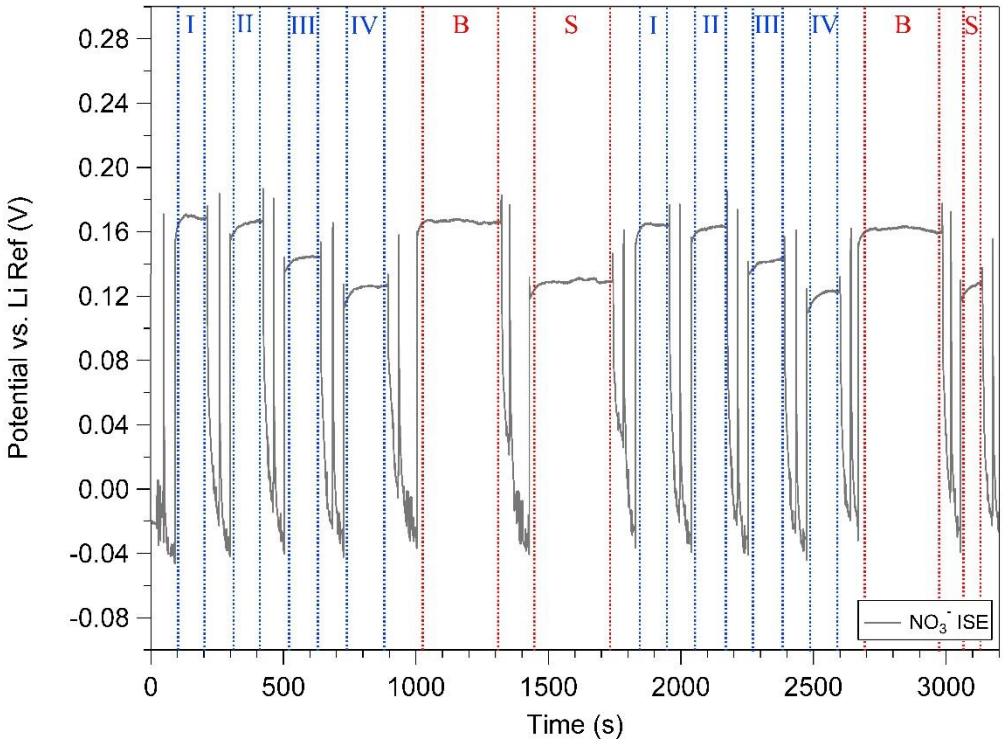

Figure 3.10. Laboratory based experiment (Pre-Mars Yard Test 2) investigating the calibration (I-IV) of the NO_3^- ISE and the detection of NO_3^- in two samples: a blank sand (SiO_2) sample (B) and a mixture of SiO_2 and KNO_3 (S). Each calibration solution and sample was located in a separate sample tube. The noise associated between samples is due to the sensor not being in solution and the electrical noise of the carousel and dipping mechanism moving.

ideal (~30 mV/decade) it still detected the amount of NO_3^- in solution with recovery values of > 75%. A summary of the three pre-Mars Yard tests can be found in Table 3.3. For the testing of the RCAL operational sequence, this accuracy was suitable and therefore the full operational sequence was tested in the Mars Yard at JPL.

Table 3.3. Summary of the pre-Mars Yard and Mars Yard sample results. The amount of KNO_3 added was converted from mg to mM based volume of the sample leaching solution, 7 mL.

	KNO_3 Added (mM)	KNO_3 Detected (mM)	% Recovered
Pre-Mars Yard Test 1	8.65	7.82	90.4
Pre-Mars Yard Test 2	5.35	4.69	87.7
Pre-Mars Yard Test 3	6.49	5.04	77.7
Mars Yard Test	1.49	0.14	9.40

3.3.3. Mars Yard Testing

The Mars Yard at JPL is an area that various payloads and rovers are tested. RCAL was tested running off battery power (and later from an outlet). The full operational sequence was tested including: (1) sample acquisition; (2) sample delivery; (3) control of RCAL carousel and dipping mechanisms; and (4) acquisition of data. A video of the process has been included with this work. For the testing of RCAL, a sand simulant was fabricated in a similar manner to the previous tests. A sample containing 19.9 g SiO_2 and 103.08 mg KNO_3 was homogenized with a mortar and pestle. The sample delivery of RCAL is ~0.25 cc, and assuming that the density of the soil is 1 g/mL (a similar assumption was made for the Phoenix experiments) then a completely homogenized sample would contain 1.29 mg KNO_3, corresponding to 1.59 mM NO_3^-. Figure 3.11 shows the calibration and the analysis of a blank (only SiO_2) as well as the sample containing KNO_3. A longer calibration method was employed to ensure the accuracy of the measurement. The results after a subsequent calibration and the addition of the simulant are also presented in Table 3.3.

The recovery of NO_3^- from the sample was less than expected. The amount detected was 0.14 mM NO_3^-, instead of the assumed 1.59 mM. This was expected because the assumption was that the KNO_3 would be equally dispersed in the mixture and that 1.59 mM would be the amount in each 0.25 cc of the sample. Some of the sample was also lost upon the delivery and inversion of the scoop. As previously stated, the nitrate ISE was less than ideal, as it was not ideally stored for the various weeks of testing. The sensor was stored partially lowered into a sample

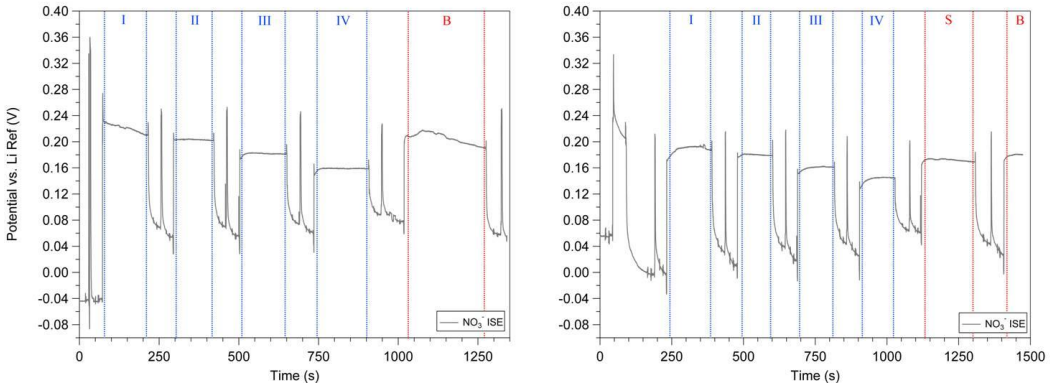

Figure 3.11. Mars Yard field test of RCAL on the SRR2K rover. The NO_3^- ISE was calibrated (I-IV) before the ISE was lowered into a blank sample (left). The ISE was calibrated again before the delivery of a sample that was acquired and delivered by the robotic arm of RCAL (right, S). The blank was again analyzed (right, B).

tube that contained 1.0 mM KNO_3, although not submerged. The lid of RCAL was then placed on and was left this way. Ideally, a smaller closed humid environment would have been used, but this was the best option given that the sensors could not be removed once wired in place. The detection of any NO_3^- proved that the programming of the operational sequence could be successfully carried out in a field test environment.

3.4. Lessons Learned from RCAL

Overall, the integration of RCAL with the SRR2K rover was a success. The full operational sequence was tested, including sample acquisition, delivery and analysis. Initially, all power was supplied by batteries, while later power was switched to a wall power supply. The capabilities of RCAL on a rover provide increased sampling over a lander, and allow for greater characterization of a remote terrestrial or extraterrestrial environment. The software used to control RCAL was user-friendly and allowed for a great amount of flexibility when controlling both RCAL and the rover.

Although the operational sequence of RCAL was successfully tested, there were many lessons learned for future missions or instruments. The number of samples that could be analyzed was increased by a factor of ~5, however, the number of sensors was much lower. Future instrument sample beakers (or tubes) should contain their own ISE arrays. As shown above, if sensors are less than ideal or non-functioning, the results of subsequent analyses are affected. A sample beaker can be discarded, if there is an array of such beakers, if sensors prove less than ideal or non-functioning. The sample can then be delivered to the next beaker for analysis. In a remote or extraterrestrial environment, sensors will not be removed or replaced, but when characterizing the instrument it should easier to exchange ISEs. The necessity of a proper reference electrode was also apparent. The above studies were performed using a Li^+ ISE as a reference, as was done on Phoenix. The ability to have a solid-contact reference electrode would have decreased the noise associated with the ISEs as well as required a background solution with a

much lower concentration. Moving forward from RCAL, new instrumentation should mainly: (1) include beakers with sensors included (avoid the dipping method); (2) consist of an array of sample beakers; and (3) contain ISEs with increased stability for extended periods of time to ensure functionality during a rover mission.

4. The In-Situ Wet Chemical Analysis Laboratory and Sensor Array (CHEMSENS): Instrument Development

An advantage of the Phoenix WCL analyses was its *in-situ* detection of the soluble species in the Martian soil sample. This information provided insight into the dissolution rates of the available species. The current MSL rover Curiosity contains the largest number of scientific instruments compared with previous payloads, although no instrumentation capable of *in-situ* aqueous chemistry. The inclusion of instrumentation that can perform wet chemical analyses is a necessity for future missions to Mars and other planetary bodies. Future missions should address the objectives outlined in Section 1.1.1, pertaining to life detection, the characterization of climate and geology, as well as determining if the Martian surface is harmful to humans (with a goal of potential human exploration). Discussed here, is the development of the next generation WCL, the *In-Situ* Wet Chemical Analysis Laboratory and Sensor Array (CHEMSENS).

The objectives of the CHEMSENS project were: (1) to develop an improved sensor array (compared with WCL) that is redundant and capable of quick and accurate analyses; (2) fabricate a smaller RCAL-like instrument to provide a greater number of sample analyses while incorporating sample analysis units with individual sensor arrays; and (3) demonstrate that an autonomous and robotic chemical analysis is as reliable as laboratory initiated experiments. These objectives will be achieved by designing and fabricating instrumentation and sensors that provide an accurate and precise measurement of the soluble chemical components in an environmental sample. At its core, the CHEMSENS project can

be divided into two parts: instrumentation (hardware/software) and sensor development. The latter will be discussed in the subsequent chapter. The focus of this chapter, will pertain to the design and production of instrumentation including the sample beaker, the sample delivery and weighing mechanisms as well as the mechanism for calibrant delivery.

4.1. Instrument Design

The proposed design of CHEMSENS incorporated the carousel design utilized in RCAL to analyze the greatest number of samples while taking up the least amount of space. Instead of relying on a dipping mechanism with ISEs, each individual sample analysis module contained its own ISE array as well designated areas for leaching and calibration solution storage. An overview of these designs can be seen in Figure 4.1. This design increased the number of ISEs by an order of magnitude compared with WCL and addressed the concerns of the ISE array associated with

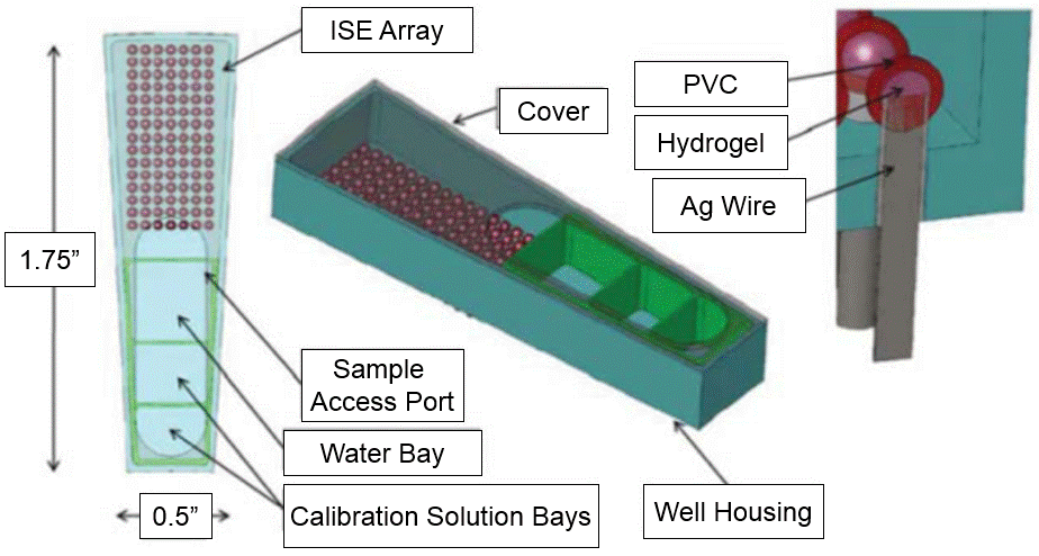

Figure 4.1. Sample analysis unit for the originally proposed CHEMSENS instrument.

using a dipping probe. The design at its originally proposed size would allow for the analysis of 60 samples, while a similar area (ignoring height; WCL ~12 cm, CHEMSENS ~3 cm) would only encompass 16 WCL beakers/actuator assemblies. Upon successful funding of the CHEMSENS project, many aspects of the design changed. Presented here is the evolution of the CHEMSENS hardware through its various iterations with a discussion and evaluation of each design for an optimal chemical analysis.

4.1.1. Sample Analysis Unit

Each sample analysis unit (SAU), or beaker, was developed to house the ISEs for the characterization of an environmental sample. The orientation of the beaker can aide or hinder the analysis of the sample, and therefore careful consideration was placed on the design and production of this aspect of CHEMSENS. The initially proposed SAU, shown in Figure 4.1, was designed to have an array of CW-ISEs for the redundant analysis of 20 chemical species, yielding an array of > 100 ISEs. An access point was planned for the delivery of the samples, while three compartments contained various solutions. The first would contain the leaching solution, while the latter two would contain calibration solutions to provide a possible 3-point calibration of the ISEs in the array. The carousel design modified from RCAL would turn so that the sample could be delivered and the solution compartments could be punctured, shown above in Figure 4.2.

Although this design increased the number of ISEs by an order of

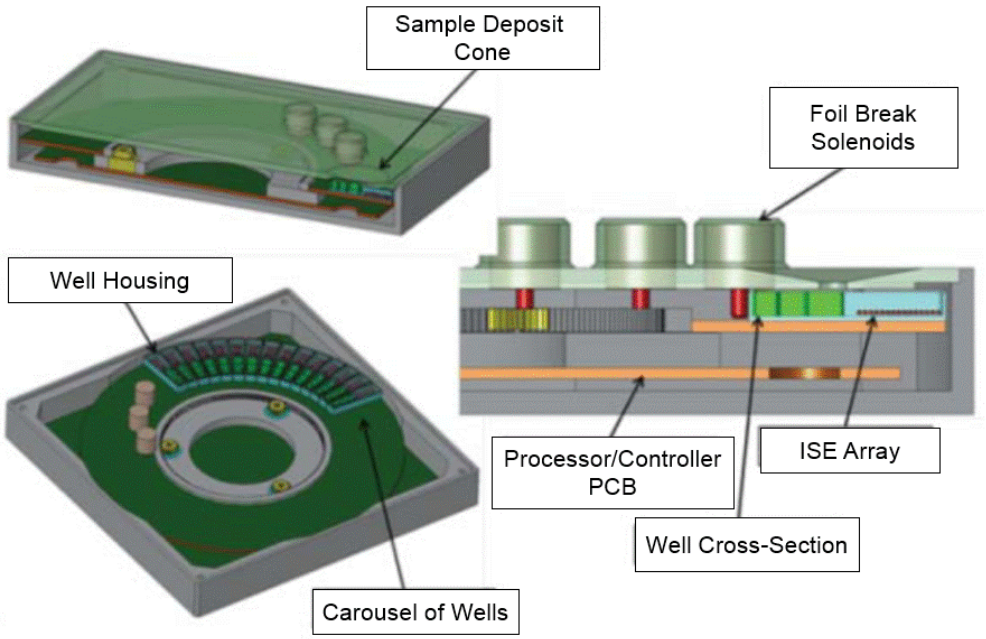

Figure 4.2. Original CHEMSENS instrument.

magnitude, the current stability and lifetime of the proposed CW-ISEs would not be sufficient for the demanding qualifications of space-hardening. Due to the location of the ISEs along the bottom of the SAU, the sample could potentially land on the ISEs blocking them from the sample solution. This type of orientation also hinders the ability of stirring to be present, resulting in a potentially non-uniform solution. The accuracy and precision of the measurement would suffer from this non-uniformity, resulting in the presence of redundancy being for naught. This design of SAU provided a valuable starting point leading to various iterations of SAUs. The initial design studies stated that: (1) the number of SAU should be maximized; (2) the number of ISEs per array should also be maximized; (3) the size of each SAU should be minimized; (4) the sample solution should be homogeneous; and (5) the system should consider the possibility of spilling due to the movement of the parent rover.

In order to optimize the number of SAUs, concentric rings of SAU were designed with multiple sample introduction sites. This design also relocated the ISEs to the sides of the SAUs, instead of the bottom of the unit, shown in Figure 4.3. The problem with this design was that due to the geometry, each circle of SAUs would be a different size. Therefore, the number of sensors per unit could change, and the analysis might be slightly different for each sample analyzed, resulting in a SAU that is not easily mass producible. Overall, the inclusion of multiple sample delivery sites yielded a complex system where multiple front-end sample processor might need to be employed. The increased complexity does not implicitly yield a

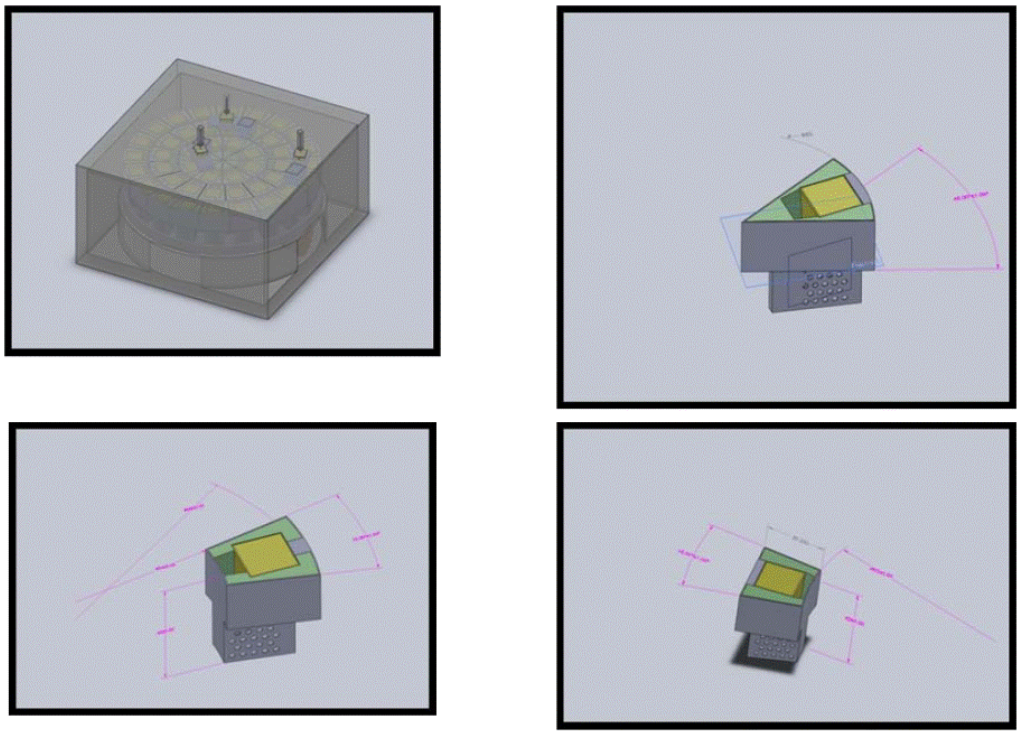

Figure 4.3. Carousel design proposed for CHEMSENS with a view of the SAUs contained in the concentric circles. Each circle of the carousel would contain a different size SAU,

better system. On the other hand, if one of the sample introduction sites or sample processors failed this would introduce a fail-check that would allow the system to continue functioning. The replacement of the carousel with a track system provided a design that would have uniform SAUs and could function with either a single or multiple sample introduction sites.

The track system would employ a movable shuttle that would deliver sample as well as provide other functionality over an array of immobile CHEMSENS SAUs. The proposed design was threefold: (1) a self-propelled shuttle on a track; (2) four shuttles on parallel tracks; and (3) a single shuttle on perpendicular tracks. Of the three designs, shown in Figure 4.4, the first, the self-propelled shuttle on a single track, would be the most complex. A less intricate track design was desired, therefore this design was the first to be eliminated. The

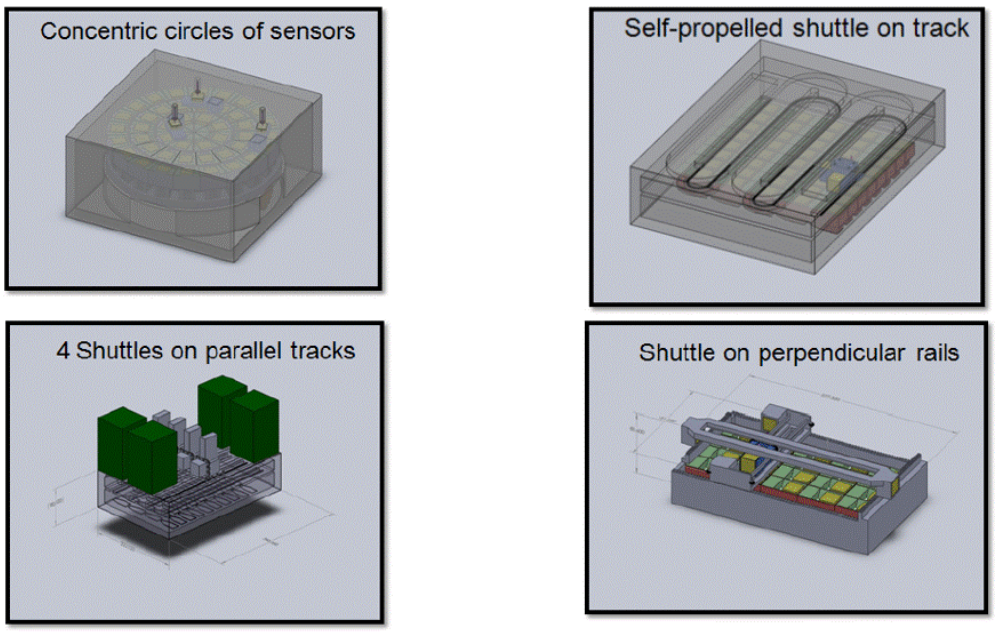

Figure 4.4. CHEMSENS designs proposed and hypothesized.

subsequent two designs differed in the number of sample introduction sites. The four shuttle system on parallel tracks would provide the greatest redundancy and fail-checks, while if only one sample introduction site was included with the science payload the shuttle on perpendicular tracks would be preferred. Each of the systems would contain similar SAUs, and although both designs were considered extensively, the likelihood of having a single sample introduction site led to the selection of the shuttle on perpendicular rail design.

The SAU itself was further designed to incorporate the ISEs onto the sides of the beaker for a more WCL-like analysis. The location of the stirrer and the leaching reservoir was also varied in multiple fashions, shown in Figure 4.5. Upon the movement from a carousel to a track design, the overall shape of the SAU became more rectangular. The shape of the SAU drastically influenced the number of sensors that can be incorporated and the tilt angle if the rover traverses an incline. A maximum of 20° was chosen based on the current rover technologies. Figure 4.6 shows a SAU that can accommodate 1 cc of soil and 5 mL of leaching solution. The SAU on the left contains ISEs that are ~6.5 mm in diameter, similar to those used in WCL, while the SAU on the right contains ISEs that are ~3 mm in diameter. The tilt angle of 20° had a limited effect on the SAU with WCL sized electrodes, while at most 12 ISEs would be partially covered by the soil sample or partially out of solution for the smaller ISEs. Assuming that the bottommost and topmost rows of sensors were removed in the 3 mm ISE SAU, the amount of ISEs increased from 16 to 32 compared with the WCL sized ISE system. It should be noted that the

amount of leaching solution available in both SAUs presented in the previous figure was 5x less than that of WCL.

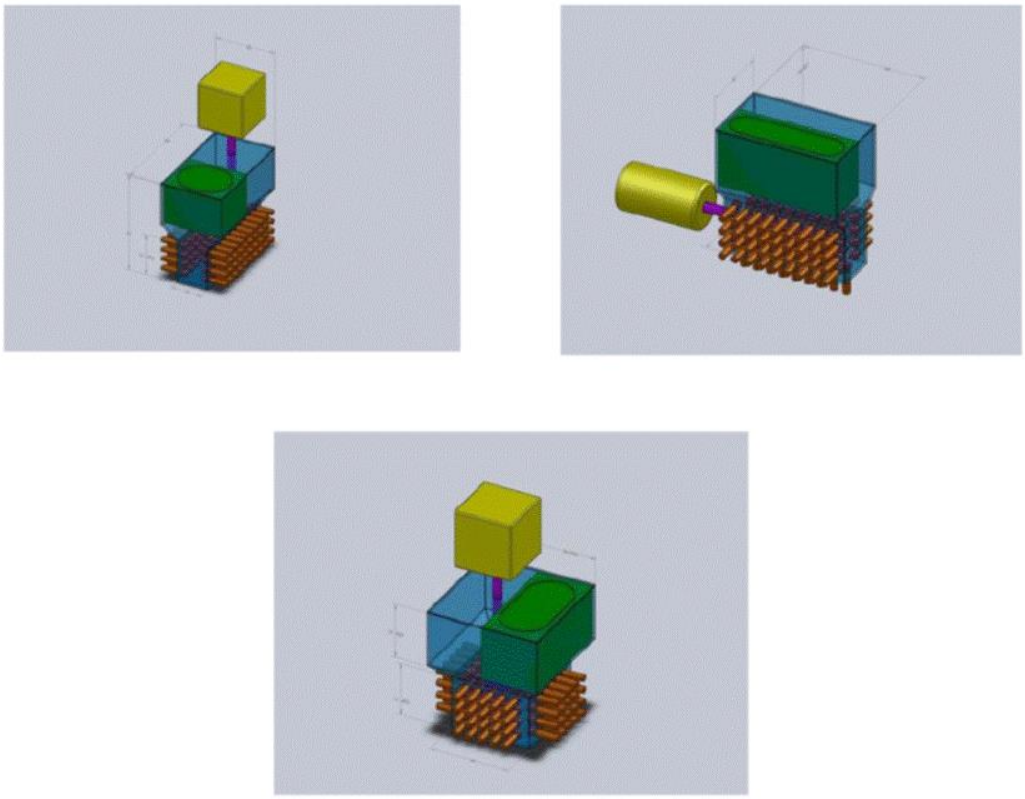

Figure 4.5. Location of the leaching solution tank and the stirrer with a populated array of ISEs in the SAU.

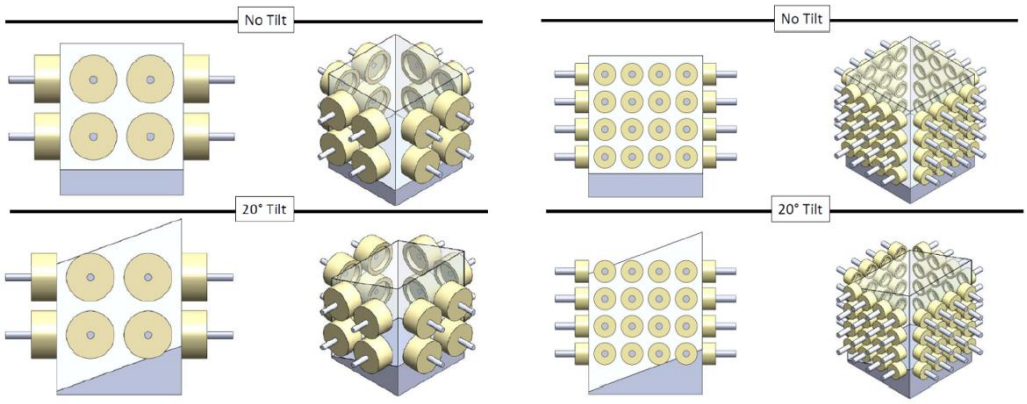

Figure 4.6. Mock-up of a proposed CHEMSENS SAU with WCL-sized ISEs (~6.5 mm O.D. left) and ~3 mm O.D. ISEs (right). Each SAU has 1 cc of soil delivered and the application of a 20° tilt angle is shown for the four views on the bottom row.

The rectangular SAU design proved more flexible in terms of possible future changes and more easily mass produced to provide a system with redundant arrays of SAUs. Although several minor modifications were made, of which those iterations will be omitted, the current SAU design is shown in Figure 4.7. The figure shows a cross-section of the SAU, where there is an array of 15 ISEs per wall (populating three walls, the fourth wall was reserved for other electrochemical sensors to be determined at a later date). In order to provide a more realistic

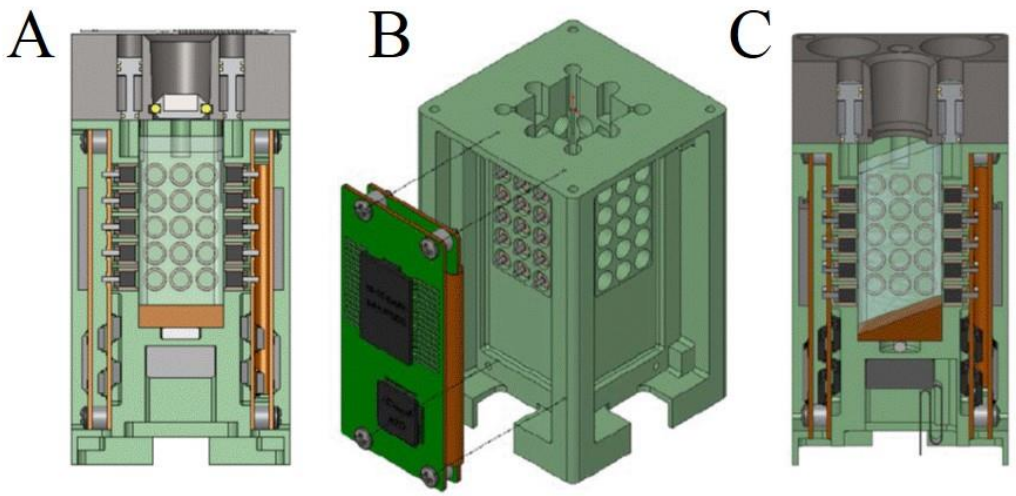

Figure 4.7. Design of the CHEMSENS SAU shown as a cross-section (A,C). A view of how the electronics board will be fashioned to the SAU with the sensors installed (B). Considerations for tilt angles are also shown (C).

experimental design (compared with the traditional laboratory) the inclusion of a stir plate and bar were proposed as indicated in Figure 4.7A. Discussed in the subsequent section is the development of the liquid calibration mechanisms, also shown Figure 4.7A. The electronics required to relay the potential measurement for the ISEs are shown here on a board that is screwed into place on the side of the SAU, shown in Figure 4.7B and discussed further in Section 4.1.4. To address the

concerns of possible tilt angles, the amount of leaching solution was increased from 5 mL to ~8 mL, and the design in Figure 4.7C shows that limited sensors are affected by an angle of 20°. The overall design of the beaker, which started as a more RCAL-like instrument, in fact became a miniaturized WCL unit with increased functionality.

4.1.2. Sample Delivery and Weighing

The track design discussed previously provided more redundancy and also would allow for a centralized shuttle instead of each individual SAU containing its own actuator assembly functionality, which reduces the overall mass of the instrument. Although multiple sample introduction sites would increase the redundancy and provide fail-checks, the design proposed using a single shuttle on perpendicular tracks. A custom XY gantry was designed, shown in Figure 4.8, which contained a shuttle that would actively deliver and weigh the sample, shown in Figure 4.9.

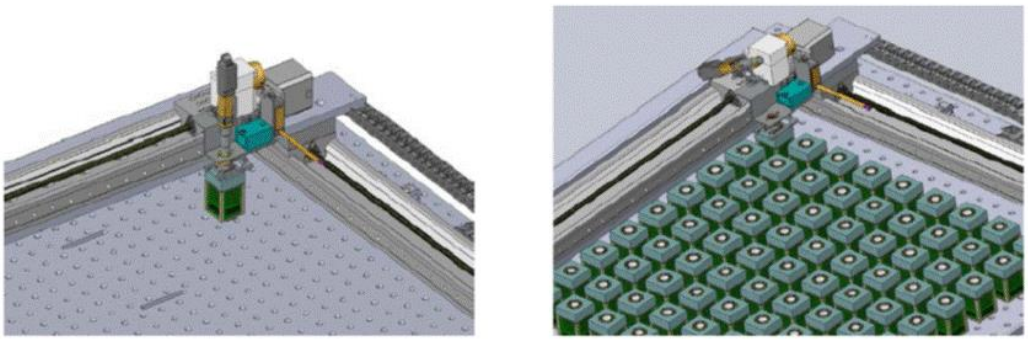

Figure 4.8. A view of the XY gantry with shuttle over a single SAU (left) and a populated array of SAUs.

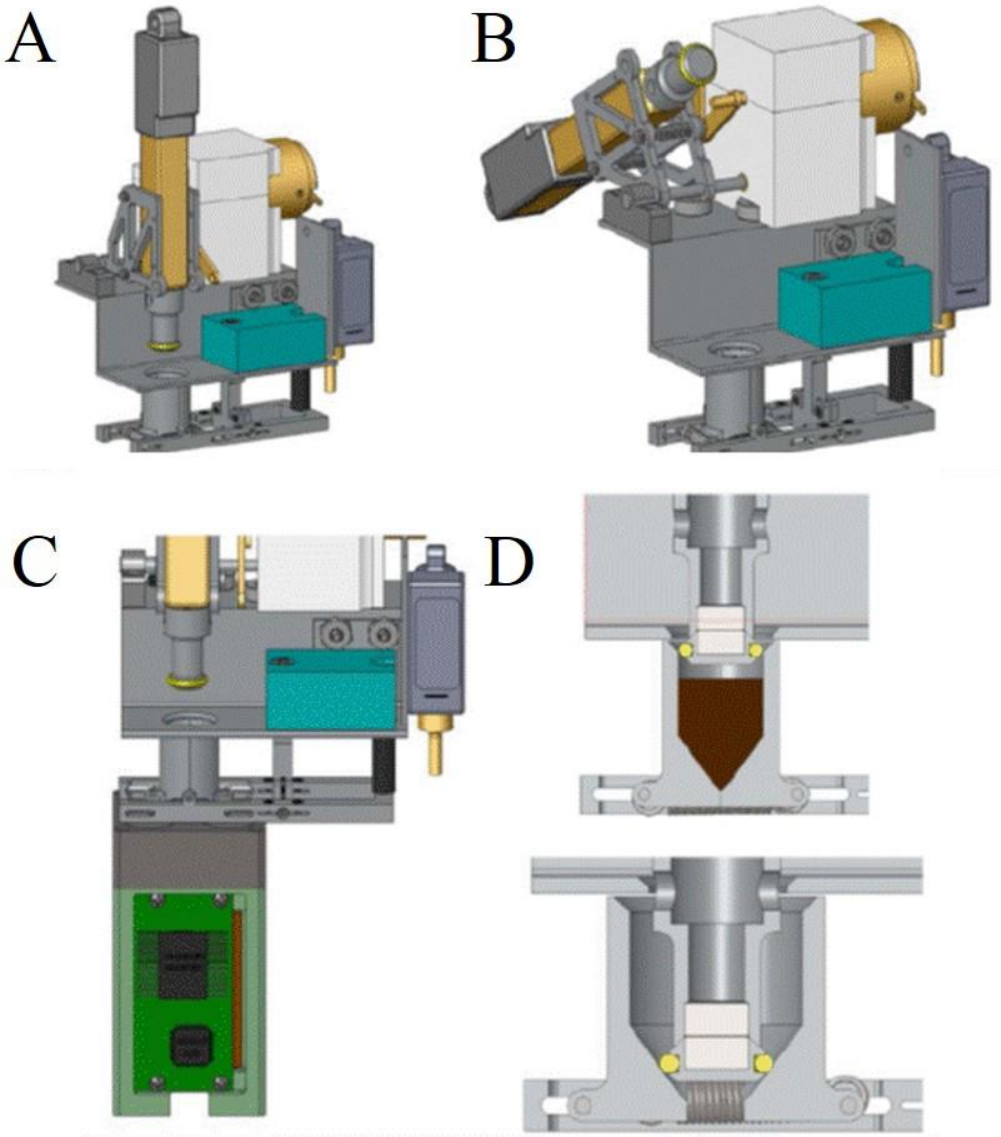

Figure 4.9. The shuttle located on the XY gantry. The shuttle would actuate to deliver the soil to the SAU (A), and turn out of plane for the introduction of the subsequent sample (B). The shuttle located over the SAU, with a focus on the sample weighing mechanism (teal, C) and a view of the sample delivery after being weighed (D).

The weighing mechanism, shown in the previous figure, would be a custom system that contain cantilever beams and strain gauges to determine the weight of the soil sample. In Figure 4.9A, upon sample addition the weighing configuration is shown before displacement of the soil sample from the sample tray into the SAU, shown

in Figure 4.9D. The Phoenix results assumed that the density of the soil sample was 1 g = 1 cc, although no sample had been weighed on Mars. The weighing of a sample before analysis would yield a more accurate measurement instead of relying on assumptions and visual confirmation of sample delivery.

4.1.3. Calibration

Calibration on Phoenix was performed by adding solid calibration pellets which contained known amounts of solid ionic species to bring the background leaching solution (TS20) to a higher concentration (TS21). When performing an *in-situ*, real time analysis of a soil sample, the background concentration should be as low as possible to ensure higher detection limits. For example, the background leaching solution after the first calibrant addition (TS21) contained ~ 1 mM Li^+ and NO_3^- while most other ionic species were ~ 0.03 mM. The addition of a sample would therefore not detect small changes of Li^+ and NO_3^- due to their high concentrations while the remainder of the ionic species were low enough that the detection limits were on the same order of magnitude. In a laboratory setting, calibrations are usually performed via standard addition. In order to mimic this laboratory practice the delivery of liquid calibration solutions was proposed instead of the previously used solid pellets.

The incorporation of liquid calibrants would allow for a quicker calibration versus the time it would take the solid to diffuse when using solid pellets. The idea behind the inclusion of liquid calibrants was to include a high concentration solution (containing various ionic species) that would be frozen and thawed upon

delivery of the payload. Eight concepts were designed and explored to achieve this function. The majority of the concepts were designed to deliver a solution from a housing with a similar diameter to the proposed size of the ISEs in the SAU (~4 mm). A summary of all concepts is shown in Figure 4.10. The first concept optimized the idea behind the liquid calibration methods. A housing would be fabricated and sealed with a foil membrane. The back of the housing would contain a resistive heating element to heat a paraffin slug located behind a silicone diaphragm. The pressure applied to the internal cavity containing the liquid calibrant would cause the foil to rupture releasing it into the SAU. The main purpose of the silicone diaphragm was to separate the paraffin from both the liquid calibrant and ultimately the sample solution. An advantage of this concept was its simplicity and utilization of paraffin, which was successfully used on Phoenix. The main drawback of this concept was the dependency of the puncture mechanism on the pressure supplied by the heating the paraffin slug. If the foil was ruptured, the ISEs would detect the changes in the solution, while if no changes occur it would by hypothesized that the calibration mechanism failed. This concept would not have an easy way to pinpoint the failure.

The second concept still would be housed in an ISE sized housing but would rely on a solenoid piston instead of paraffin. A similar foil membrane would seal the calibrant inside the housing, but an internal piston (polymer with an iron core) would be used to puncture the foil. Outside the housing, insulated copper would be coiled around the housing so that a current could be flowed through the coils

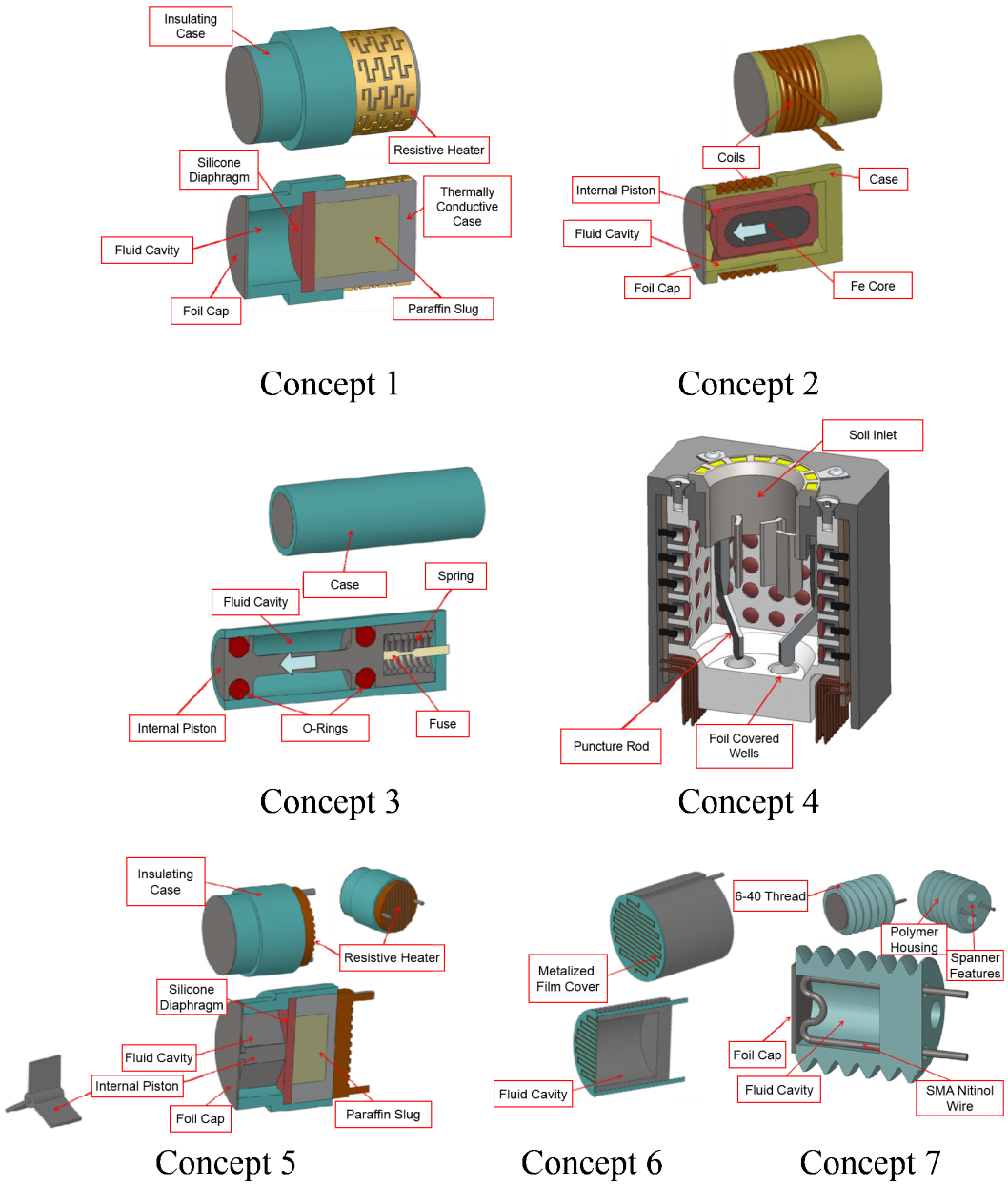

Figure 4.10. Calibration concepts proposed for CHEMSENS.

resulting in the forward motion of piston via a magnetic repulsion. The solution, which would located around the piston would then mix with the leaching solution. This concept required few components and the force supplied by the piston would be determined experimentally. The force supplied by the piston would be

characterized by its size and speed. If the solenoid produced enough force the probability of foil puncture would be high. Although this concept would be easily mass producible, the use of the insulated copper around each calibration housing could increase the overall size of the beaker and provide a complex overall fabrication of the SAU.

The third concept explored the use of a puncture mechanism without the inclusion of paraffin or a solenoid, instead utilizing a fused spring. This concept does not utilize a foil seal to separate the calibrant solution from the bulk solution, instead it used the front end of the internal piston. The internal piston would be held in place by two o-rings separated by a known distance. Contained in this distance would be the calibrant solution. The application of a current to the small fused metal wire will cause it to heat and eventually melt, releasing the spring and pushing the calibrant into the bulk solution. The active delivery of the calibrant is advantageous, while the major drawbacks are the fabrication and utilization. The fabrication of the fused spring would be tedious and difficult, while the filling of the fluid cavity with the calibrant is also no easy matter. The major risk with this concept is that the fuse could break prematurely during launch, cruise or landing conditions. If this were to occur, upon the commencement of the experimentation the leaching solution would be added, resulting in a background solution of higher activity and the loss of the ability to calibrate the ISEs reliably.

The fourth concept moved away from the design concept of using a housing in the SAU wall, instead utilizing an external punch mechanism. This concept would have foil sealed wells at the bottom of the SAU, with puncture rods extended

from the sample inlet. A proposed method to activate these puncture rods was a solenoid, composed of shape memory alloy (SMA). The actuators for these puncture mechanisms would be located on the shuttle, discussed previously, which allowed the inclusion of less actuators for the overall system, while decreasing the redundancy of the calibration method. The failure of this actuator would result in the lack of calibration for the remainder of the SAUs included. Another drawback of this concept, was its lack of functionality after sample addition. The addition of other solutions to perform further chemical analyses, such as an acid addition for the determination of pH or the addition of a barium solution for the titrimetric determination of sulfate, could not occur due to the placement of the sample on top of the wells. This would result in another method for the delivery of such solutions, increasing the complexity. For this reason, this concept was abandoned and the final three concepts reverted to the ISE housing design.

The fifth concept combined two advantageous aspects from concepts 1 and 2. Instead of relying on pressure or the use of a solenoid, a paraffin slug would push an internal piston. The resistive heater was also moved to the back of the housing (versus around the perimeter of the housing) to ensure a quick and effective heating of the paraffin. This concept shared in some the advantages and disadvantages of its two parent concepts, with a few newly introduced. Due to the inclusion of the internal piston as well as the diaphragm and paraffin, there is limited space for the calibrant (2-3 μL). The inclusion of a diaphragm could also result in the limited forward motion of the piston.

Concepts 6 relied on a metalized foil that upon activation (current) would cause the desired path to be melted, creating a way for the calibrant to flow into the bulk solution. The geometry of the design could be problematic and the heat transfer between the bulk solution and the resistive element are not desirable. Concept 7 was proposed to use a SMA actuator composed of nitinol. The foil cap would be ruptured upon the change of the shape of the SMA from its initial (preflight) position to a permanent activated position. The loop located just before the foil seal would invert from its "U" position to form a complete loop through the seal. An advantage of this method is that the distinct temperature required for the transition of the SMA yields a system that avoids the activation prematurely.

The final concept, shown in Figure 4.11, was the design ultimately chosen for inclusion in CHEMSENS. This concept abandoned the use of an ISE housing and instead proposed to use a syringe-like design that could be installed around the sample introduction well. The syringe-like design was inspired by the previous

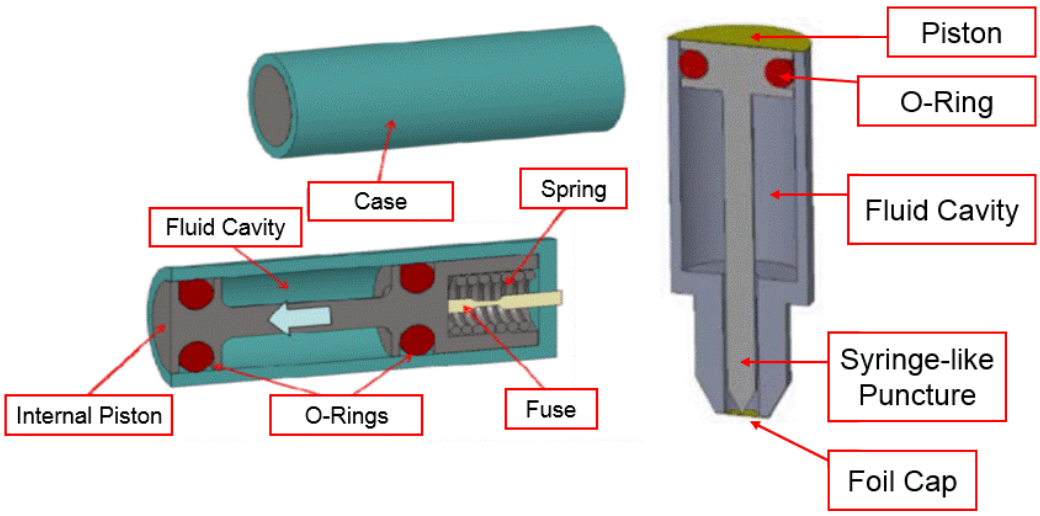

Figure 4.11. Calibration concept 3 (left) with the final calibration design (right).

concept 3 and the typically used syringes in a laboratory setting. An actuator located on the shuttle would push the internal piston, actively pushing the calibrant into the bulk solution from the top of the SAU. The stir bar will result in a quick equilibration to the concentration of the subsequent calibration(s). A view of the calibration design located in the SAU was shown previously in Figure 4.7.

4.1.4. Electronics and Software

The entire CHEMSENS system will be controlled by two subsystems: one for the shuttle and one for each SAU. These feed into a central processor, as shown in Figure 4.12. Both sets of subsystems can be repeated as needed to accommodate

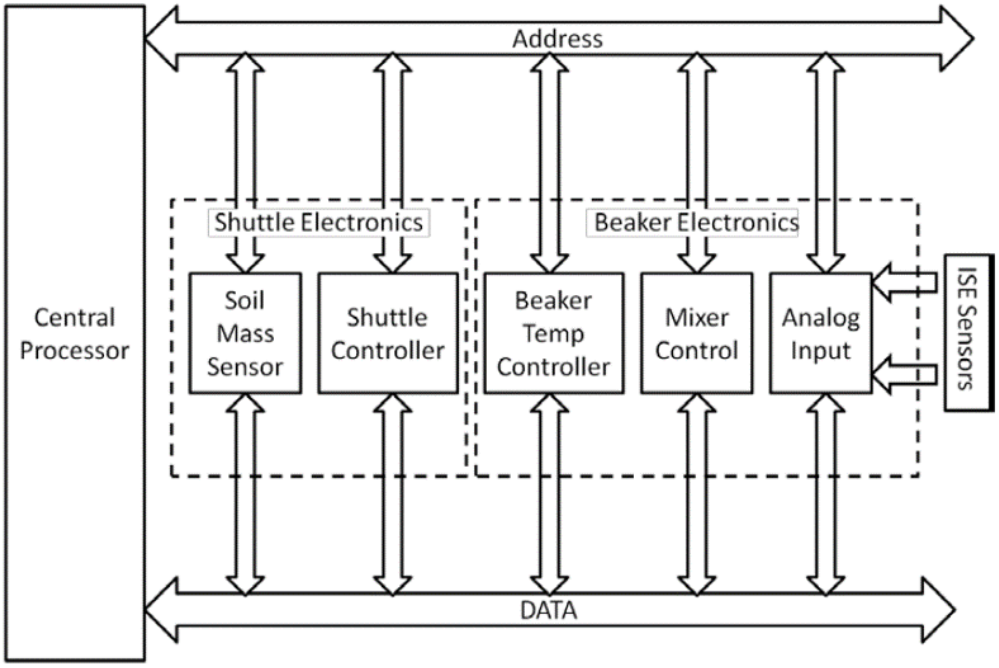

Figure 4.12. CHEMSENS control system.

multiple SAUs and possible subsequent shuttles, if needed. As indicated, the shuttle electronics will incorporate the weighing of the soil as well as the shuttle controller, which determines the location of the shuttle at any given point. Each SAU will contain electronics to control the beaker temperature sensors, the stirrer and the analog inputs from the ISEs. The current design will rely on an external computer for data storage while future iterations will include local memory for this purpose.

One of the most difficult aspects of the development of hardware for the ISEs was the miniaturization of the electronics. The ISEs themselves are high impedence systems (MΩ – GΩ), the input impedence of the electronics must be approximately 1000x greater than the ISEs, which require input impedences in the GΩ – TΩ range. This level of impedence is difficult to achieve in the laboratory setting, let alone upon the miniaturization of the electronics for the CHEMSENS SAUs. For this reason, several breadboards were designed and ultimately tested. The first of which, seen in Figure 4.13, shows a block diagram for ISE measurement using an analog input and central processor. A typical system used for the measurement of ISEs with a single reference can also be seen in Figure 4.13 for comparison. A difficulty of this design is that each ISE requires its own reference electrode. This would half the number of ISEs per wall. Therefore, the use of a single reference electrode for each SAU wall was explored. A modification to the design yielded Figure 4.14 (top), where each ISE is referenced to the ground, while the ISE potential can then be referenced after the signal is multiplexed. An updated system could be envisioned as seen in Figure 4.14 (bottom), where parts are listed for purchase.

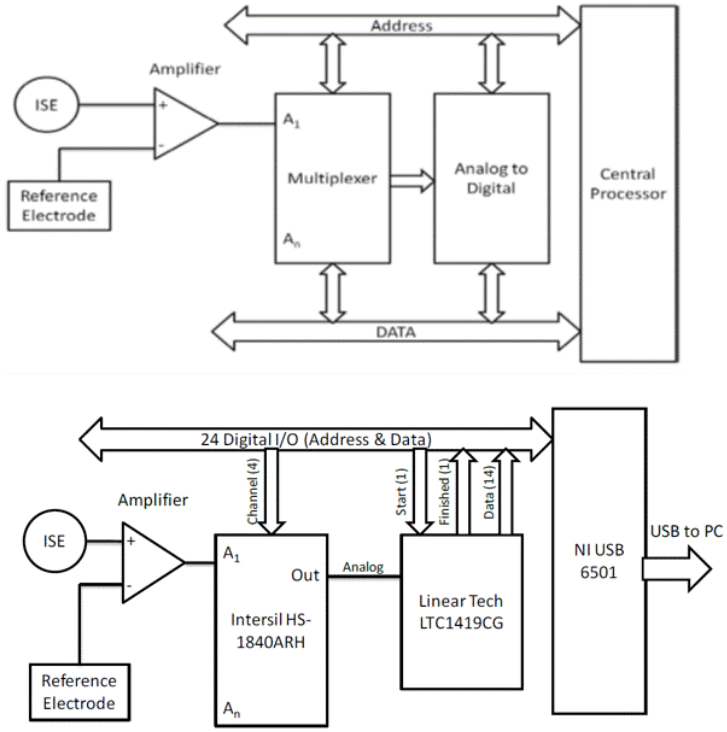

Figure 4.13. Block diagram to measure the ISE signal (top) and the breadboard with parts listed (bottom).

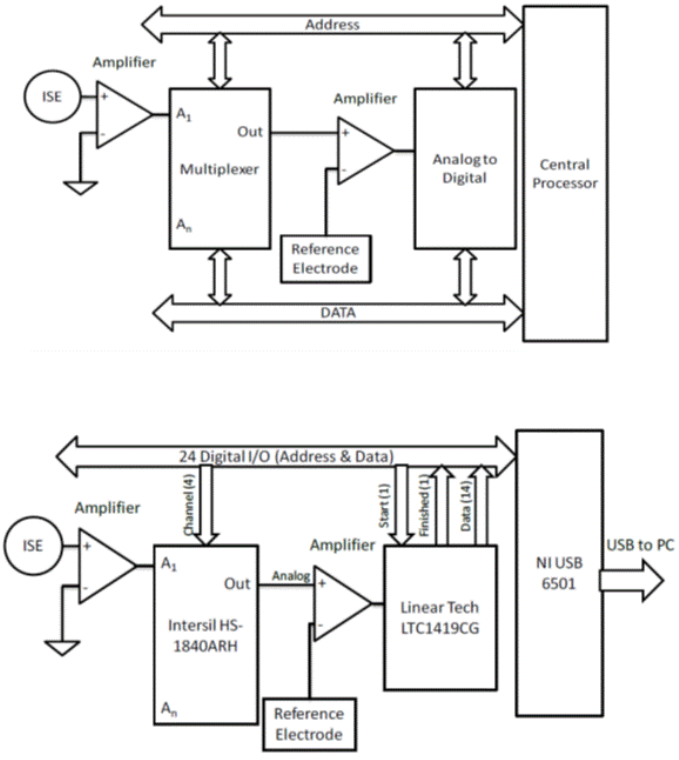

Figure 4.14. Block diagram for an array of ISEs with a single reference electrode (top) and a similar block diagram with parts listed (bottom).

4.2. CHEMSENS Hardware Manufactured

After designing each component, as discussed in the previous sections, the manufacture or purchase of the components occurred. The XY gantry was commercially available, complete with motors and controllers and is shown in Figure 4.15. For other shuttle components, a small linear actuator (Firgelli PQ12) was obtained to actuate the calibration pistons; a large linear actuator (Figelli L12) was obtained to deliver the sample into the beaker; and a low-speed, brushless motor (Faulhaber 2622-012-B-SC) was obtained to move the large actuator out of position so that soil could be delivered to the sample cup before delivery to the SAU. These can be seen in Figure 4.16, showing the shuttle system above a SAU as well as the weighing mechanism.

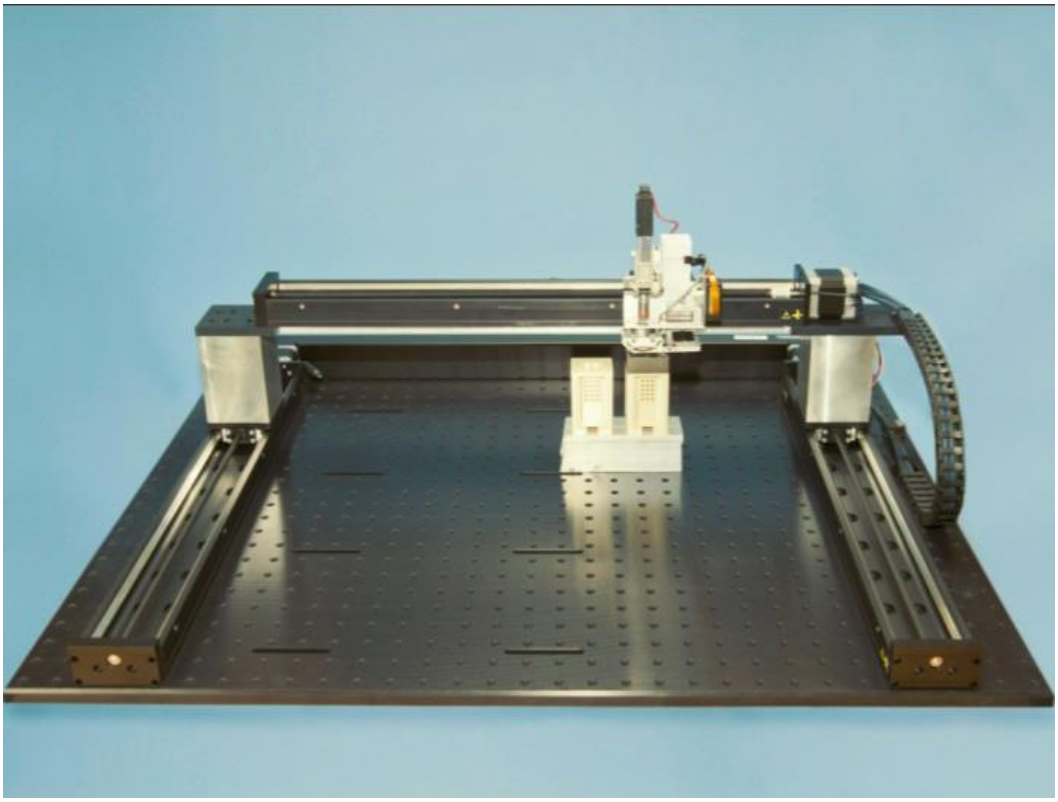

Figure 4.15. The XY gantry with shuttle located over a SAU.

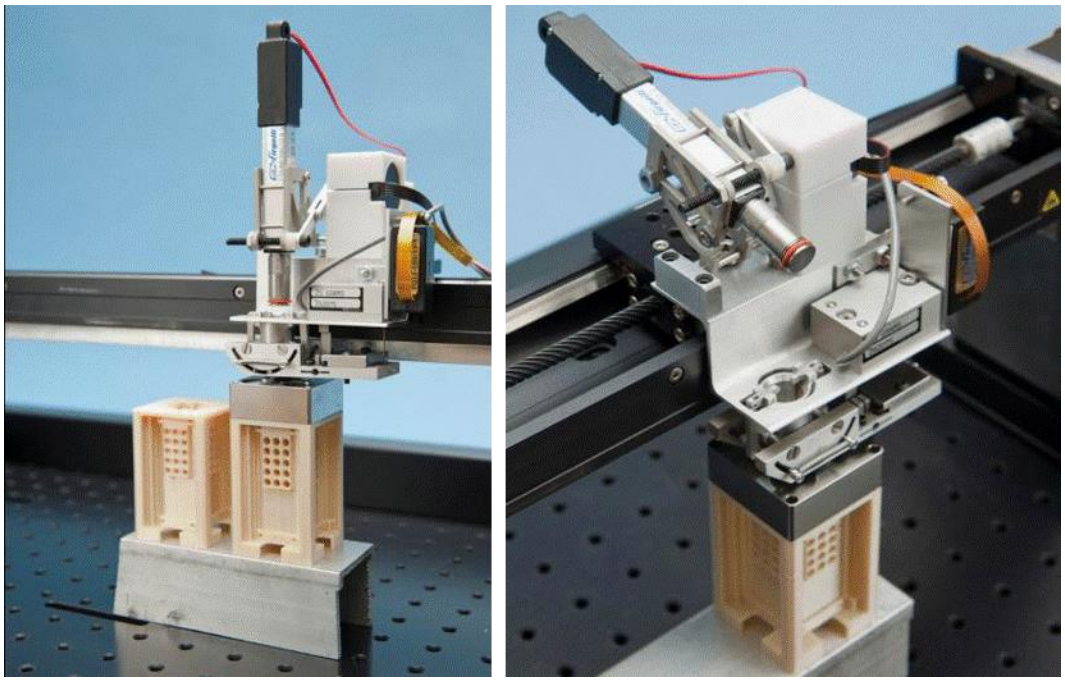

Figure 4.16. Zoomed in figure of the shuttle system where the actuator to deliver the sample to the SAU (left) and out of plane for the introduction of a new soil sample (right).

The final design of the SAU (shown previously in Figure 4.7) was manufactured and shown in Figure 4.17. The majority of the SAU was ultem, while the solution leaching tank was stainless steel. The final design consisted of each SAU wall containing five rows of three ISEs and could accommodate ~8 mL of leaching solution and 1 cc of soil. The gap at the bottom of the SAU is where the stir plate will be located. The stir plate was obtained from is shown in Figure 4.18. After the ISEs are placed in each beaker, the electronics will be screwed in place in the back of them. A view of the boards can is shown in Figure 4.19, where the circular holes are where the ISEs would be interfaced. The supporting circuit diagram and system schematic can be found in Figure 4.20.

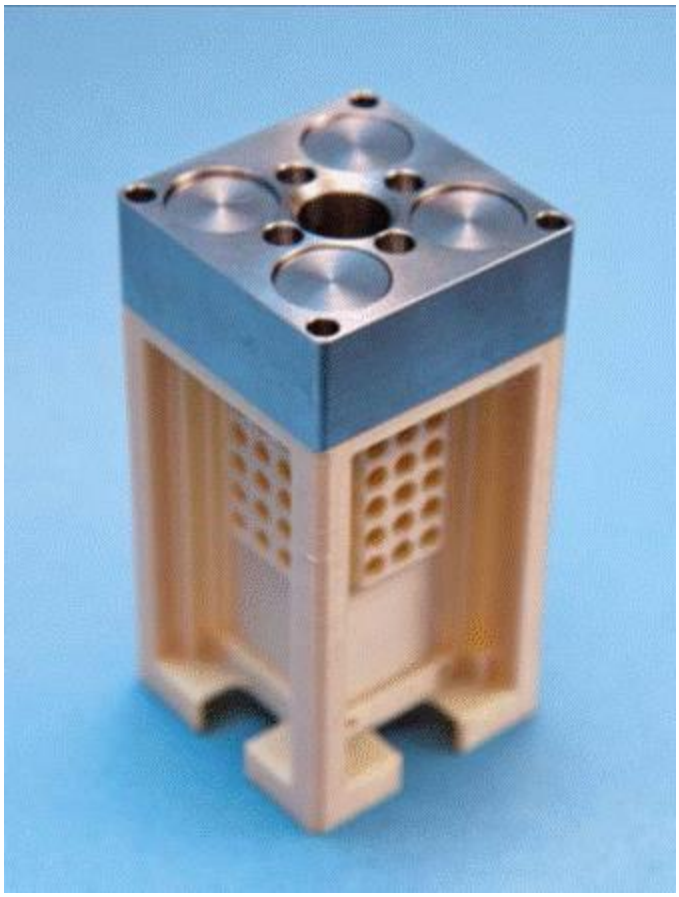

Figure 4.17. The CHEMSENS SAU which was machined using ultem for the bottom and stainless steel for the leaching solution tank.

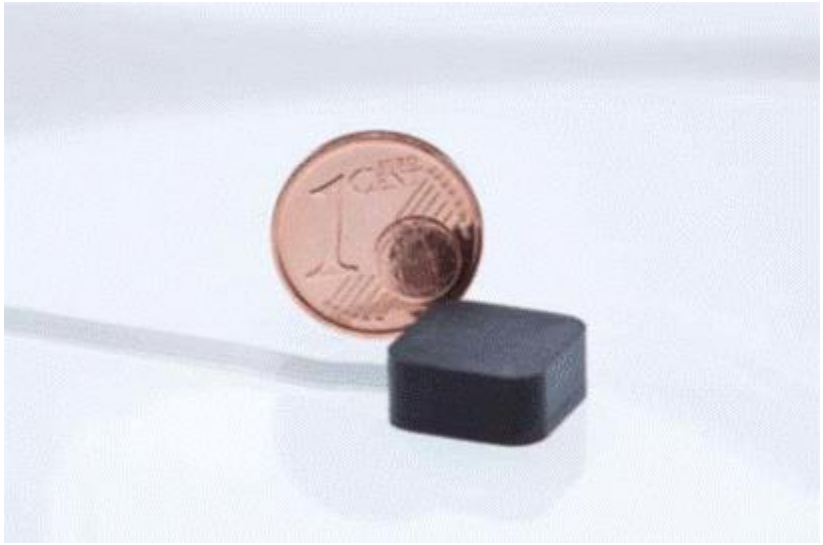

Figure 4.18. The stir plate which will be located at the bottom of the SAU, with a size comparison of a 1 cent Euro piece.

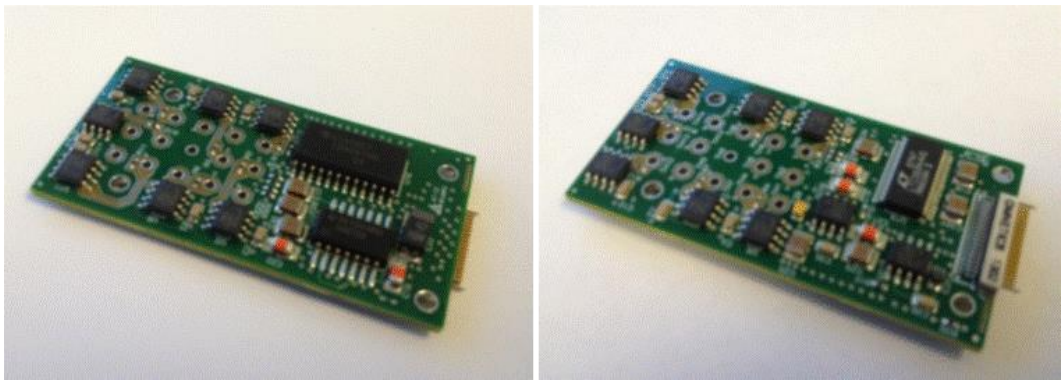

Figure 4.19. Electronics boards for each SAU wall.

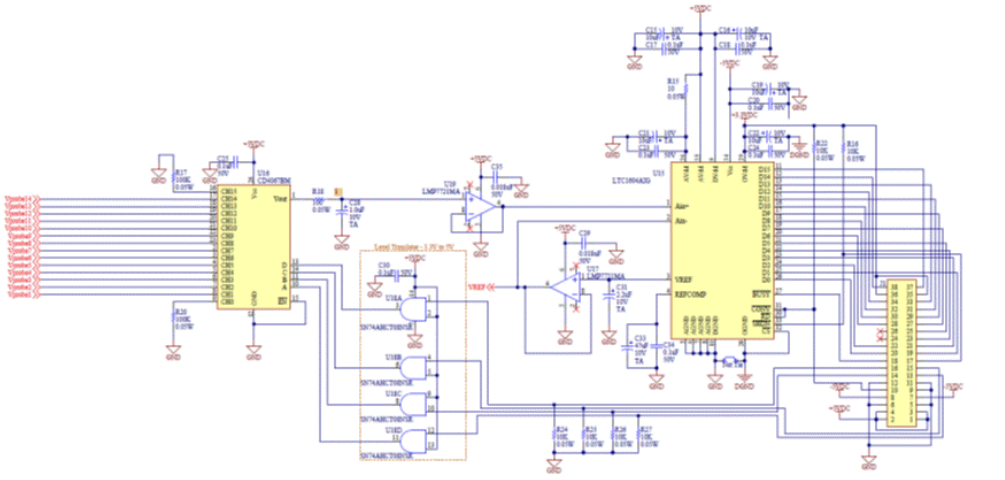

Figure 4.20. Circuit diagram of the CHEMSENS electronics board

4.3. CHEMSENS Test Platform

To facilitate laboratory bench-top testing, a simpler system was fabricated. This system, referred to as the CHEMSENS testbed, modified a SAU to only have ISEs on one wall. This would allow the testing of ISEs without having to populate the remainder of the ISE wells with blank housings. This system would also only use a single electronics board located directly in front of the ISEs with connectors fabricated to bridge from the ISE to an intermediate pin-board before the electronics board. A view of the design of the testbed is shown in Figure 4.21. The external

sensors shown in the figure correspond to a conductivity sensor and possibly a temperature sensor. The entire testbed was encased in an aluminum enclosure to ensure limited noise interference for the ISE measurements. A view of the fabricated system is shown in Figure 4.22.

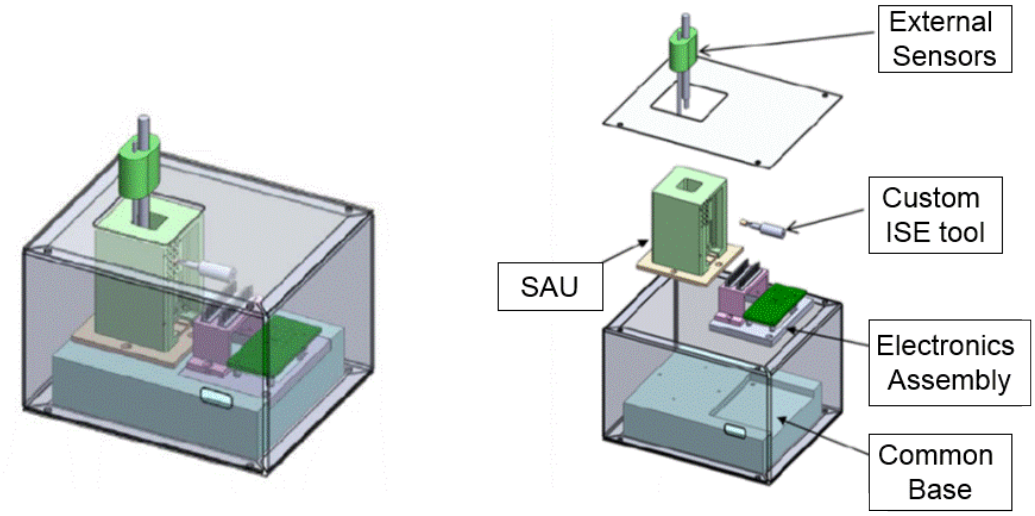

Figure 4.21. Design of the CHEMSENS test platform assembled (left) with parts (right).

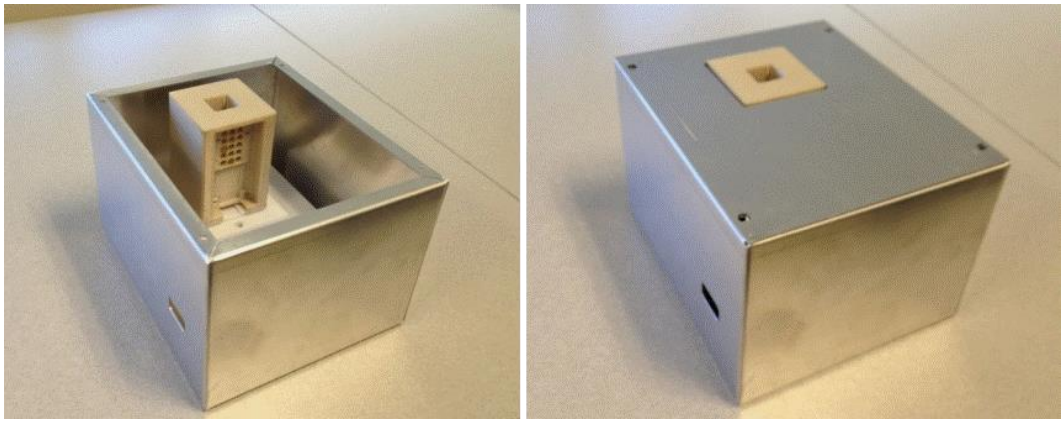

Figure 4.22. The fabricated CHEMSENS test platform with shield box.

4.4. Conclusions

Overall, the entire CHEMSENS unit was designed and fabricated over the course of the grant period. The system was envisioned as the next generation WCL, and through various design iterations resembled a similar design, although miniaturized

with a greater number of overall sensors. CHEMSENS evolved from the successes of Phoenix WCL as well as the previously discussed RCAL. The inclusion of CHEMSENS would be advantageous for a future mission payload due to its various measurement capabilities as well as its multiple SAUs. The overall system was fabricated to be completely scalable, so that if a future payload could accommodate 4 to 100 SAUs it can be built to encompass that many SAUs. The analysis of a soil sample by CHEMSENS resembles an analysis performed in a laboratory setting, as indicated by the inclusion of a stir plate and bar and the addition of calibrants in solution form. These technologies will provide a quicker and more accurate measurement as it will ensure dissolution and migration of the ionic species to the analytical devices, the ISEs. Omitted from this section was the development of the ISEs, as this will be discussed at length in the subsequent section.

5. The In-Situ Wet Chemical Analysis Laboratory and Sensor Array (CHEMSENS): Sensor Development

The goals outlined for the proposed CHEMSENS instrument included: (1) a system capable of analyzing several samples; (2) a SAU that contained the maximum number of sensors possible, therefore increasing the redundancy for increased precision; and (3) a SAU will a small footprint. The design and production of the CHEMSENS SAU was previously discussed, and ultimately finalized to have a size that can accommodate ~8 mL of leaching solution, approximately 3 times smaller than the sample volume used on Phoenix. As the SAU was shrunk, the necessity of miniaturized ISEs became overwhelmingly apparent. The ISEs used for the Phoenix mission were approximately 6.5 mm in diameter, limiting the number of ISEs for the current design. The use of such large diameter ISEs would not satisfy the second goal stated above. This chapter will discuss the modification and miniaturization of ISEs for use in CHEMSENS with a focus on sensitivity, stability and lifetime.

5.1. Miniaturization of WCL-type Electrodes

The maximization of the number of ISEs per SAU whilst miniaturizing the overall size of each unit resulted in a careful analysis of the construction of the Phoenix WCL electrodes. The use of such electrodes provides heritage to a future payload, owing to its successful characterization of the Martian soils by Phoenix. As seen previously in Figure 4.6, if WCL-sized ISEs were used at their current size the number of overall sensors would be less than on Phoenix. Therefore, the overall

size of the sensors needed to be miniaturized in order to maximize the total number of ISEs in the smaller area. Briefly discussed in Section 1.3.1.2, the major obstacle when miniaturizing ISEs is the replacement of the inner filling solution, or in WCL's case, the pHEMA. In their current form, the WCL/RCAL ISEs were ~6.5 mm in diameter, with a pHEMA well ~3 mm in diameter and ~1.25 mm deep, a membrane well ~5.5 mm in diameter and ~0.5 mm deep and a thru hole for the 1 mm Ag wire.

A potassium ISE was fabricated by curing the pHEMA with a high intensity UV light (365 nm) for 10 min, then applying a plasticized PVC membrane containing the ionophore valinomycin (2-3 wt%), the ionic additive sodium tetrakis[3,5-bis(trifluoromethyl)phenyl]borate (NaTFPB, 1 wt%), poly(vinyl-chloride) (32-35 wt%) and the plasticizer bis(2-ethylhexyl) sebacate (DOS, remainder), all dissolved in tetrahydrofuran (THF) on top of the cured pHEMA. The electrochemical cell for a potassium ISE constructed in this manner is:

Ag|AgCl | 3 M KCl | 0.1 M NaCl || Sample | ISM | pHEMA, KCl | AgCl|Ag

which shows that the double-junction reference electrode used contained an inner filling solution of KCl and an outer filling solution (salt bridge with the sample solution) of 0.1 M NaCl. The K^+ pHEMA ISE was tested in a background solution of 0.1 M NaCl to investigate its selectivity over Na^+ and its stability over time. Figure 5.1 shows results from this electrode. The pHEMA ISE was extremely sensitive, selective and exhibited a moderate lifetime of ~1 week. The potential over the 6-day period averaged to -79 ± 3 mV at an activity of 7.5×10^{-4} M (0.1 M

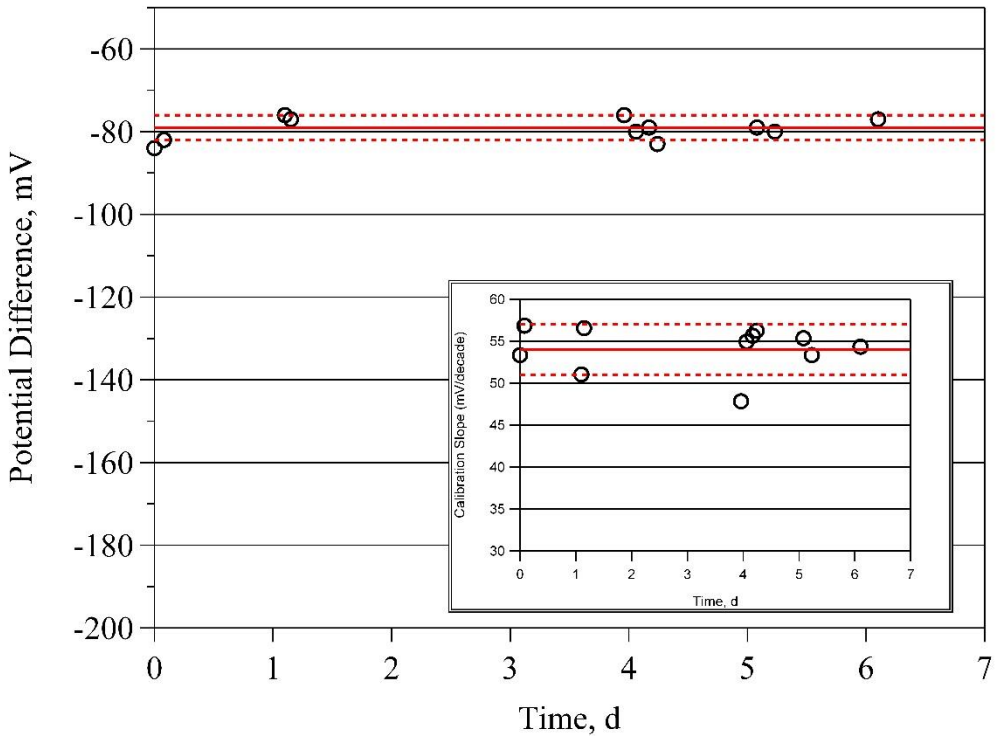

Figure 5.1. Potential response versus an Orion double-junction reference electrode for the pHEMA ISE at an a_{K+} of 7.5×10^{-4} M (0.1 M NaCl background solution and 10^{-3} M KCl). The solid line represents the mean potential, and each dashed line represents ± 1σ. Inset: calibration slope, where the ISE was calibrated for a_{K+} range of 7.5×10^{-6} and 7.5×10^{-3} M (0.1 M NaCl with between 10^{-5} and 10^{-2} M KCl).

NaCl + 10^{-3} M KCl) while exhibiting a calibration slope value of 54 ± 3 mV/decade. These values will serve as a baseline for the remainder of the chapter, as the miniaturization process is further discussed.

The first step in the modification and miniaturization of ISEs for use with CHEMSENS was to miniaturize the pHEMA component well. The new housing was ~3 mm in diameter, with a pHEMA well ~2 mm in diameter and ~1.25 mm deep, a membrane well ~2.5 mm in diameter and ~0.5 mm deep and a thru hole for the 1 mm Ag wire. This was approximately half the size (diameter) of the WCL electrode. Two sensors were identically fabricated with an ISM composition of 65.7 wt % DOS, 32.7 wt% PVC, 1.1 wt% valinomycin and 0.5 wt% NaTFPB and tested

over two days. Although linear, the sensitivity and potential stability were less than ideal. The first sensor exhibited a calibration slope of 14.4 and 15.3 mV/decade on days 0 and 1 while the second sensor exhibited slope values of 16.0 and -14.7 mV/decade. The values are approximately 4 times less ideal than a traditional Nernstian ISE. The reason for this inadequate response was attributed to the decrease of the pHEMA and membrane size. The electroactive components were suspected to leach from the ISM to the bulk solution. The decrease in the size of the electrolyte reservoir was also suspected to decrease the stability. One possible solution to this predicament was to replace the pHEMA with a support than could replenish the electroactive component upon its leaching into the bulk solution, while increasing the overall diameter of the electrolyte reservoir.

5.2. Replacement of the pHEMA with Porous Carbon

The stability and sensitivity of a sensor was carefully considered upon the replacement of the pHEMA in the electrode construction. A solid-support that exhibited a similar stability and response to the Phoenix WCL ISEs, while robust enough for the pre-flight characterization, cruise and landing conditions was a necessity. Another factor considered was the ease of fabrication. Porous carbon was ultimately selected to investigate its characteristics based on previous research that showcased stability, sensitivity and lifetime upon incorporation (*42*). The electrode presented by Vamvakaki and Chaniotakis did not discuss miniaturization beyond 5.5 mm, an ISE slightly smaller in diameter than the Phoenix WCL electrodes. This section will present various ISEs fabricated with porous carbon, focusing on the

stability, sensitivity and lifetime of the ISEs. Figure 5.2 shows a comparison of the electrodes that will be discussed. For comparison purposes, the pHEMA WCL type housing, an intermediate housing and the final CHEMSENS design housing are shown in Figure 5.3.

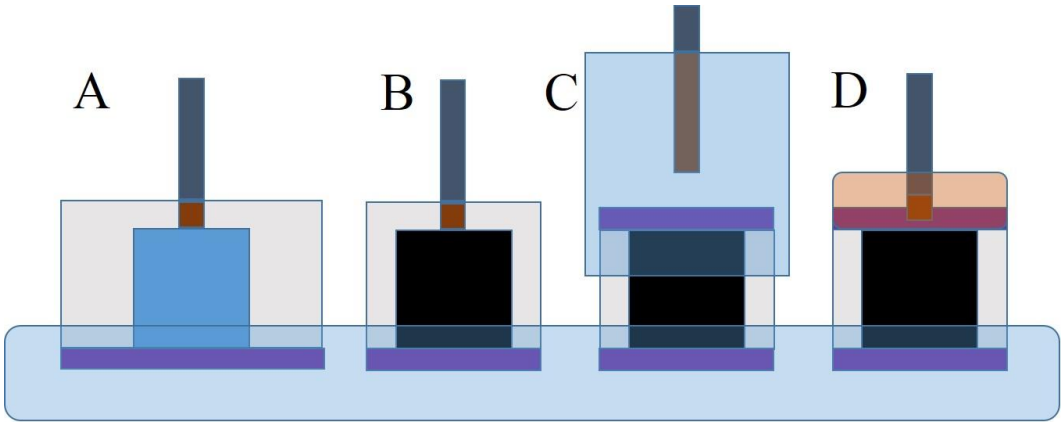

Figure 5.2. Electrode configurations (not to scale) shown in contact with a sample solution. (A) pHEMA based electrode, (B) asymmetric membrane SC-ISE, (C) symmetric membrane ISE, and (D) symmetric membrane SC-ISE.

Figure 5.3. Size comparison of the housings proposed all placed on a nickel. On the far left is the WCL/RCAL type housing, in the middle is an intermediate design for CHEMSENS, with the housing on the far right being the final CHEMSENS threaded housing with an O.D. ~4 mm.

5.2.1. Asymmetric Membrane Sensor

The first ISE fabricated, henceforth referred to as an asymmetric membrane solid-contact ISE (AM-SC-ISE), placed a 3 mm dia. porous carbon slug in a PVC housing with an overall diameter of 4.5 mm shown in Figure 5.2B. The internal reference element, the chloridized Ag wire, was in direct contact with the porous carbon which had been impregnated with the associated ionophore, used for the ISM, dissolved in the corresponding plasticizer. Unless otherwise noted, all sensors subsequently discussed were K^+ ISEs with a membrane composition of 32-35 wt% PVC, 1 wt% NaTFPB, 2-3 wt% valinomycin and the remainder DOS. The porous carbon saturation solution was comprised of 4 wt% valinomycin and the remainder DOS. To ensure homogeneity for the saturation solution, after application the electrode housing was placed in vacuum to dry. The membrane was then applied as previously described. Further experimental details can be found here (*43*). The electrochemical cell for the AM-SC-ISE was:

$$\text{Ag|AgCl | 3 M KCl | 0.1 M NaCl || Sample | ISM | porous carbon,}$$

$$\text{valinomycin + DOS | AgCl|Ag}$$

The AM-SC-ISE was tested for approximately 15 days in a background a solution of 0.1 M NaCl before it ceased functioning. Between tests the electrode was stored in 0.1 M NaCl, ensuring that the electrode was in constant contact with solution for the duration of the testing period. The first day of testing (day 0) yielded a potential response of 194 ± 13 mV at an activity of 7.5×10^{-4} M K^+, as shown in Figure 5.4. The first few days of testing any SC-ISE is usually where the greatest instability occurs (with the exception of before the failure of the sensor). This

instability is attributed to the uptake of water by the plasticized PVC membrane, and the possible formation of a water layer between the solid support and the ISM (*91*).

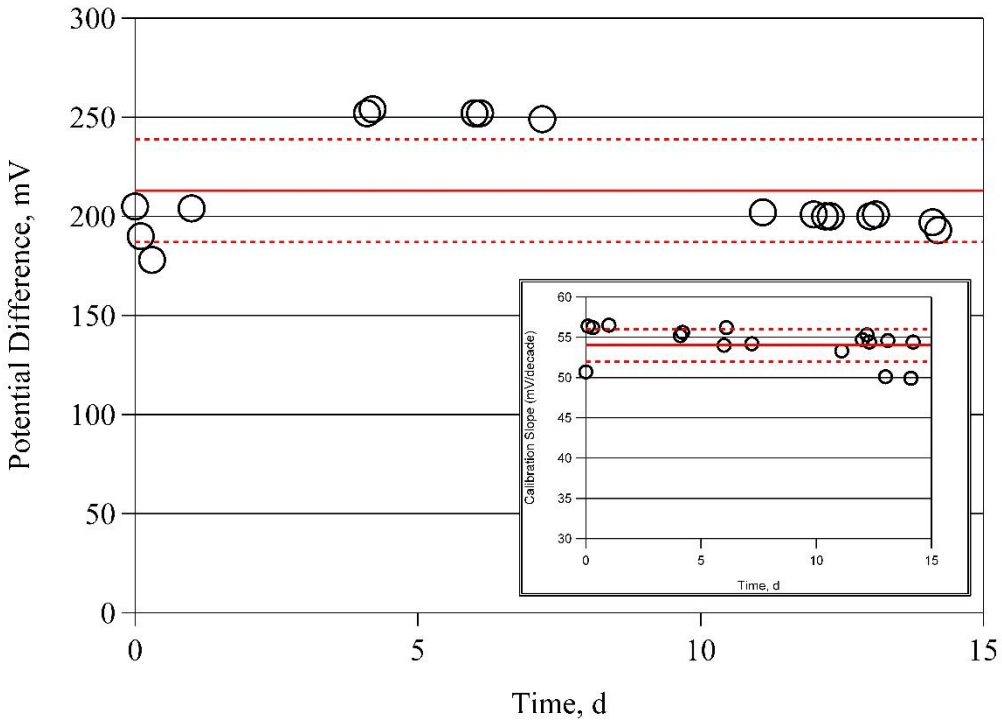

Figure 5.4. Potential response versus an Orion double-junction reference electrode for the AM-SC-ISE at an a_{K+} of 7.5×10^{-4} M (0.1 M NaCl background solution and 10^{-3} M KCl). The solid line represents the mean potential, and each dashed line represents ± 1σ. Inset: calibration slope, where the ISE was calibrated for a_{K+} range of 7.5×10^{-6} and 7.5×10^{-3} M (0.1 M NaCl with between 10^{-5} and 10^{-2} M KCl).

Calibrations performed between days 4 and 7 resulted in an increased, stable potential of 252 ± 1 mV. The increase of ~50 mV was not expected and was hypothesized to occur due to a combination of the evaporation of reference electrode filling solution and storage solution. The sensor returned to its original potential of 199 ± 3 mV between days 10-15 before the sensor ceased functioning. The potential stability over the entire time period of 15 days was 213 ± 26 mV while the sensitivity was near-Nernstian with a value of 54 ± 2 mV/decade. The

hypothesized reason for the failure of this sensor was that the internal reference element, the chloridized Ag wire, was no longer in contact with the porous carbon due to handling over the 15-day time period. The change in absolute potential compared to the pHEMA is a result of the electrode components and the change in the redox couple present. In order to create a sensor that would be more robust than the AM-SC-ISE, the Ag|AgCl wire would need to stay in contact with the porous carbon, therefore a symmetric membrane ISE was fabricated.

5.2.2. Liquid Junction Symmetric Membrane Sensor

To ensure that the internal reference element remained in contact with the porous carbon, an ISE with a back, non-sensing membrane was proposed, henceforth referred to as a symmetric membrane ISE (SM-ISE) shown in Figure 5.2C. The characterization of such a configuration was performed by incorporating a traditional liquid junction before fabricating a solid-contact version. For the construction of the SM-ISE, a similar housing to the AM-SC-ISE was fabricated but instead of machining a 1 mm hole for the Ag wire, the porous carbon well was made throughout the entire housing. The membrane was applied to the front of the housing, as previously described, while also repeating this step for the back of the housing. The entire back side of the housing was then placed in clear PVC tubing that was subsequently filled with 10^{-3} M KCl. A chloridized Ag wire was then placed in this solution, and the tubing was sealed. The electrochemical cell for this configuration was:

Ag|AgCl | 3 M KCl | 0.1 M NaCl || Sample | ISM | porous carbon,

valinomycin + DOS | ISM | 10^{-3} M KCl | AgCl|Ag

Multiple ISEs were fabricated and tested over an extended period of time, with a single SM-ISE shown in Figure 5.5. Each SM-ISE was tested for 50 days in a background/storage solution of 0.1 M NaCl. Again, the only time the electrodes were not in solution (sample/storage) was when they were being transported to/from testing. Throughout the 50 day test period each SM-ISE exhibited a potential standard deviation of ±10-16 mV and a sensitivity of 56 ± 1 mV/decade.

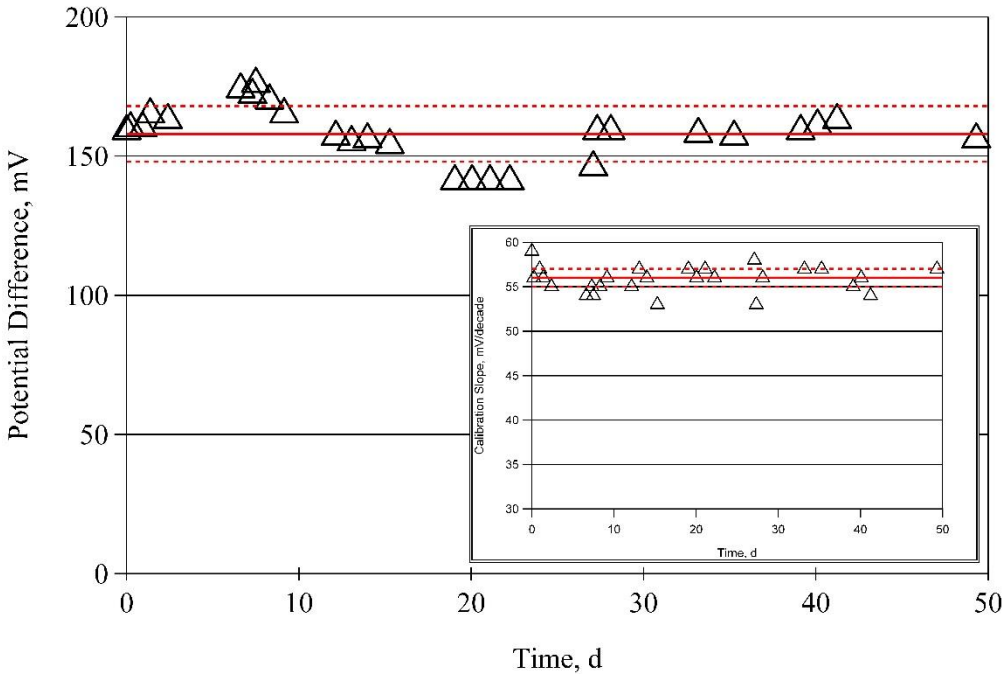

Figure 5.5. Potential response versus an Orion double-junction reference electrode for the SM-ISE at an a_{K+} of 7.5×10^{-4} M (0.1 M NaCl background solution and 10^{-3} M KCl). The solid line represents the mean potential, and each dashed line represents ± 1σ. Inset: calibration slope where the ISE was calibrated for a_{K+} range of 7.5×10^{-6} and 7.5×10^{-3} M (0.1 M NaCl with between 10^{-5} and 10^{-2} M KCl).

The SM-ISE configuration yielded an electrode with increased sensitivity, stability and lifetime over the previously tested AM-SC-ISEs and compared similarly to the pHEMA ISE. The configuration was successful and it was

hypothesized that the stability benefited from the back, non-sensing membrane due to the symmetric response between the bulk sample with the front ISM and the back ISM with the internal electrolyte reservoir. In order to fabricate a miniaturized electrode for inclusion in the CHEMSENS instrument, the liquid component of the SM-ISE needed to be eliminated. Therefore, a sensor was proposed to eliminate this liquid reservoir and placed the internal reference element directly in the back, non-sensing ISM.

5.2.3. Solid-Contact Symmetric Membrane Sensor

A symmetric membrane solid-contact ISE (SM-SC-ISE) was fabricated building on the successful testing of the SM-ISE, shown in Figure 5.2D. The SM-SC-ISE was fabricated similarly to the aforementioned AM-SC-ISE and SM-ISE, except the chloridized Ag wire was placed directly in the back, non-sensing ISM. The exposed Ag wire was then encased in heat-shrink tubing and silicone rubber to ensure the aqueous solution did not interfere with the response of the electrode as constructed. The electrochemical cell for the constructed ISE was:

$$\text{Ag|AgCl | 3 M KCl | 0.1 M NaCl || Sample | ISM | porous carbon,}$$

$$\text{valinomycin + DOS | ISM | AgCl|Ag}$$

The SM-SC-ISE was extremely stable, 241 ± 3 mV after the initial stabilization attributed to the water uptake by the plasticized PVC ISM, shown in Figure 5.6. This time-frame for a SC-ISE was similar to those found in the literature (*38*). The initial tests, days 0-2, exhibited a sensor with a potential stability of 323 ± 19 mV, and as the stabilization due to the water uptake continued, days 5-15

exhibited a potential stability of 260 ± 20 mV. The remainder of the tests, between days 12-29, exhibited the aforementioned potential stability of 241 ± 3 mV. The potential stability over the entire range was 267 ± 37 mV, with a sensitivity of 53 ± 2 mV/decade. It should be noted that the first value obtained for the calibration slope was excluded from the determination via a Q-test, performed as outlined in (*43*) and according to Rorabacher (*92*). The tests performed with the SM-SC-ISE yielded results consistent with those reported in the literature for the K^+ ion, while surpassing some of the stability characteristics (*41*).

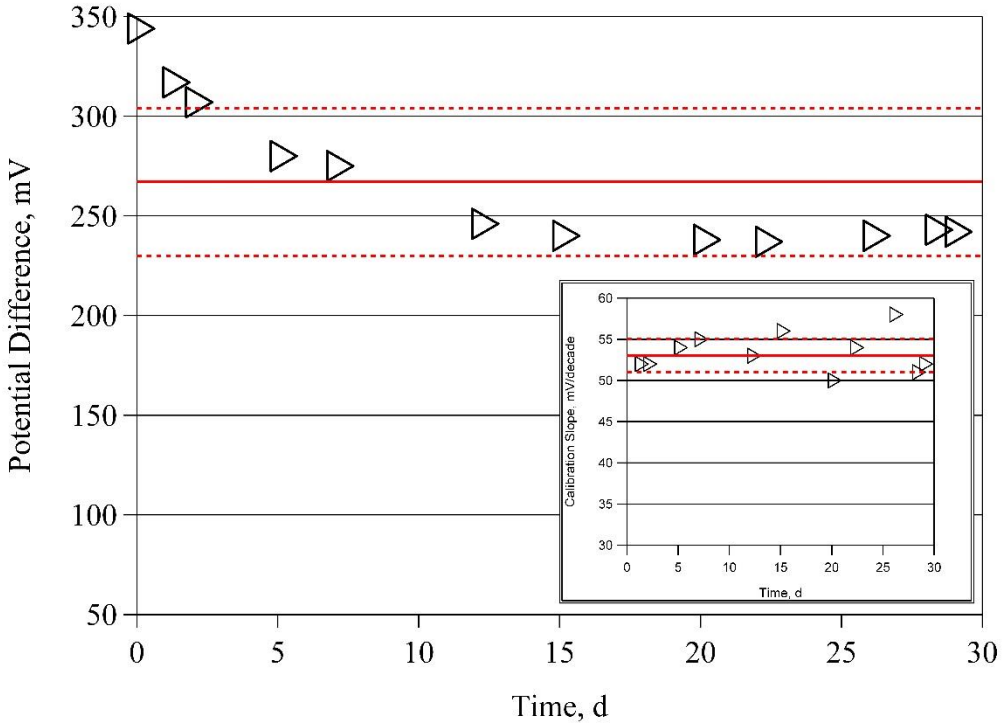

Figure 5.6. Potential response versus an Orion double-junction reference electrode for the SM-SC-ISE at an a_{K+} of 7.5×10^{-4} M (0.1 M NaCl background solution and 10^{-3} M KCl). The solid line represents the mean potential, and each dashed line represents ± 1σ. Inset: calibration slope where the ISE was calibrated for a_{K+} range of 7.5×10^{-6} and 7.5×10^{-3} M (0.1 M NaCl with between 10^{-5} and 10^{-2} M KCl).

5.2.4. Symmetric Membrane Configuration for Other Ionic Species

Symmetric membrane SC-ISEs were also fabricated for other ionic species. Mainly, Ca^{2+} and Mg^{2+}, and were similar to the previously discussed K^+ SM-SC-ISE with minor exceptions. The Ca^{2+} ISM and porous carbon saturating solution were fabricated with Calcium Ionophore I and the plasticizer 2-nitrophenyl octyl ether (*o*-NPOE). This particular ISM was composed of 3.6 wt% ionophore, 0.8 wt% ionic additive (NaTFPB), 30.6 wt % PVC and 65 wt% *o*-NPOE. The Mg^{2+} ISM and porous carbon saturation solution were fabricated with Magnesium Ionophore VI, the ionic additive potassium tetrakis[3,5-bis(trifluoromethyl)phenyl]borate (KTFPB) and the plasticizer *o*-NPOE in a ratio as follows: 1.2 wt% ionophore, 1.5 wt% ionic additive, 30.1 wt% PVC and 6.4 wt% *o*-NPOE. Porous carbon soaking solution contained the same weight percentages as the ISM dissolved in plasticizer (remainder wt%). These electrodes were fabricated with the purpose of high-pressure testing in ocean water, therefore they were not examined for lifetime. The calibrations for these sensors can be found in Figure 5.7. Both the Ca^{2+} and Mg^{2+} SM-SC-ISEs functioned in the commercially recommended background solution of 0.08 M KCl and a seawater simulant of 0.50 M NaCl. The calibration slopes were 29.41 and 26.24 mV/decade for the Ca^{2+} electrode, respectively for each background solution, and 31.46 and 28.12 mV/decade for the Mg^{2+} electrode, respectively. The sensors compared well with the Nernstian value of 29.58 mV/decade and calibrated well in high concentration background solutions. Electrochemical cells are similar to those presented for the K^+ SM-SC-ISE with the exception of the composition of the ISM and porous carbon soaking solutions.

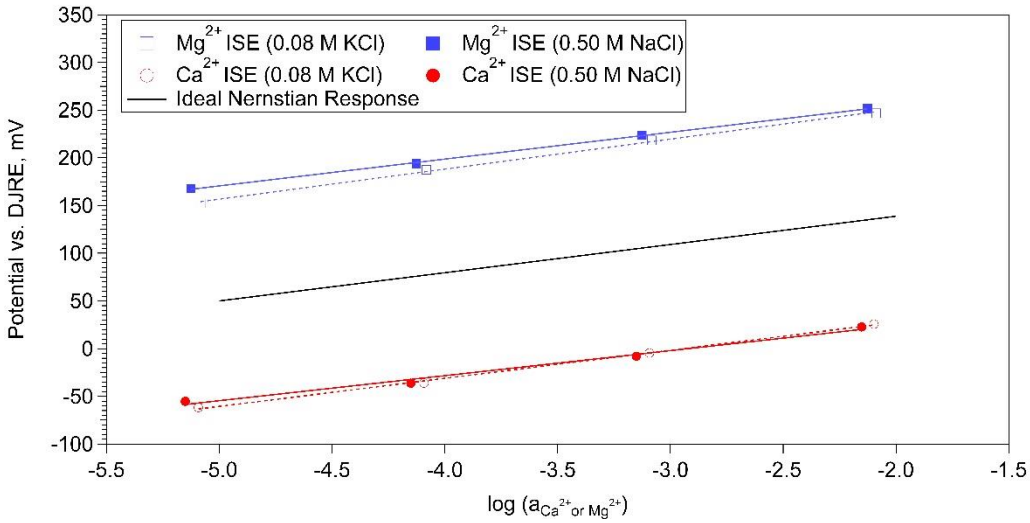

Figure 5.7. Calibration of Ca^{2+} and Mg^{2+} SM-SC-ISEs in various background solutions compared with an idealized Nernstian response. Ca^{2+} SM-SC-ISE response in a background solution of 0.08 M KCl (○) and 0.50 M NaCl (●) and Mg^{2+} SM-SC-ISE response in 0.08 M KCl (□) and 0.50 M NaCl (■).

In order to ease the fabrication process, the back, non-sensing membrane was replaced by silver epoxy (EPO-TEK EJ2189-LV). ISE characteristics did not suffer, and the epoxy ensured a connection between the Ag internal reference element and the porous carbon. For differentiation purposes, these ISEs will be further discussed as silver epoxy solid-contact ISEs (SE-SC-ISEs). Nitrate ISEs were fabricated in this manner in a CHEMSENS-type (non-threaded) housing (~4 mm OD). The carbon soaking solution consisted of 5.5 wt% tridodecylmethyl ammonium nitrate (TDMAN) and 94.5 wt% *o*-NPOE, while the corresponding ISM was fabricated using 5.9 wt% TDMAN, 30.5 wt% PVC and 63.6 wt% *o*-NPOE, all dissolved in THF. Calibration of such ISEs can be found in Figure 5.8. Five NO_3^- SE-SC-ISEs were calibrated against a double junction reference electrode with an outer filling solution of 1.0 M LiAc. Each electrode was normalized against the starting potential, and then an average of the potential change against the reference

was plotted. The calibration slope was near-Nernstian with a value of -58.6 mV/decade. The electrochemical cell was:

Ag|AgCl | 3 M KCl | 1.0 M LiAc || Sample | ISM | porous carbon,

TDMAN + o-NPOE | ISM | AgCl|Ag

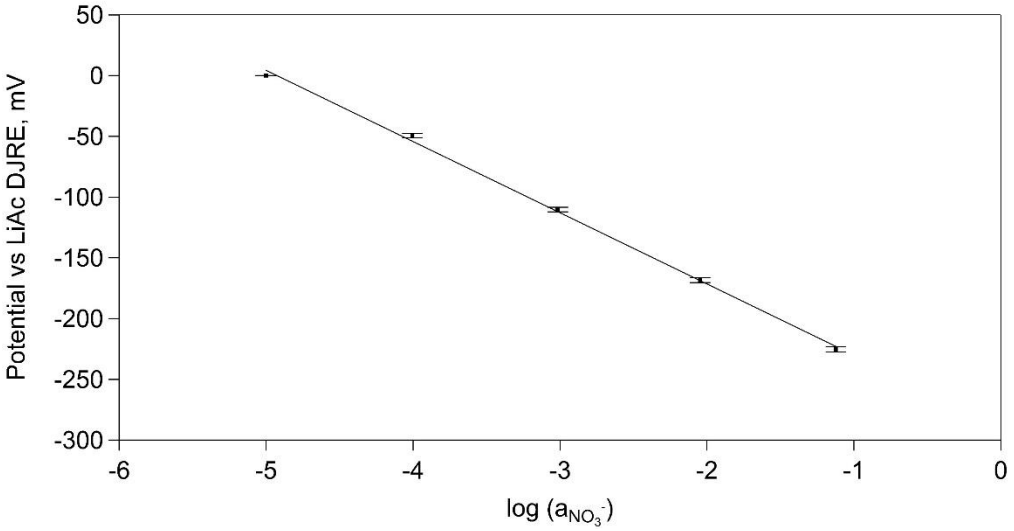

Figure 5.8. Nitrate SE-SC-ISE calibration. Each point is an average of 5 individual NO_3^- ISEs that were normalized. The error bars represent ± 1σ for the average of the change in normalized potential. The calibration slope was -58.6 mV/decade with an r^2 value of 0.9985.

5.3. Overall Conclusions

The evolution of the electrode housing configurations ultimately yielded a design of an ISE with an O.D. of 4 mm. Overall, the ISEs were successfully miniaturized from the ~6.5 mm WCL electrodes, therefore decreasing the overall ISE surface area by ~40%. The stability and sensitivity of the final ISE design were not hindered by such a miniaturization, although several iterations of electrodes were hypothesized, fabricated and tested, which ultimately led to miniaturized ISEs with similar characteristics to those used on Phoenix with a lifetime > 50 days whilst in constant contact with solution. The use of porous carbon resulted in a SC-ISE

configuration similar to previously fabricated and commercially purchased electrodes. Our final design, utilizing silver epoxy (SE), provided a simpler fabrication compared with the SM configuration, while ensuring a proper electrical connection is maintained. SE-SC-ISEs were also shown for monovalent and divalent cations as well as the anion nitrate, showing their wide-spread use for multiple ions. This type of ISE should be utilized for remote, continuous investigations of terrestrial and extraterrestrial environments due to its previously discussed stability, sensitivity and lifetime.

Future work will be to incorporate SE-SC-ISEs into the CHEMSENS SAU and test them with the proposed electronics. This final test will complete the goals outlined from the CHEMSENS project, which increased the number of possible ISEs from ~12 to >30 by miniaturizing the ISEs themselves. The increased redundancy of ISEs will result in the capability to develop algorithms to increase selectivity and detection while also increasing the accuracy and precision of the measurement. A further focus should be now placed on the development of a solid-contact reference electrodes, similar to that presented in (*93*). The successful implementation of a miniaturized solid-contact reference electrode with the above discussed SE-SC-ISEs would provide a powerful analytical instrument for terrestrial and extraterrestrial analyses.

6. Effect of Soil Leaching Parameters

6.1. Motivation to Investigate Sample Preparation Procedures Using Ion Chromatography

Discussed previously, the core of Analytical Chemistry is: sample acquisition, sample preparation and sample analysis. It is easy to gloss over the first two and focus on the analysis, but an argument can be made that the acquisition and preparation are more important than the analysis itself. The reason for this argument is that the analysis depends on how the sample is acquired and prepared. Although the Phoenix WCL analyses took place using ISEs, terrestrial soil samples are usually analyzed by IC after leaching to determine their soluble chemistry. To the best of our knowledge, there has not been an in depth study into the effect of leaching parameters on the soluble ionic concentrations in soils when using IC. Even with the popularity of IC in the field of soil chemistry, there is still no defined method for sample preparation. Many studies vary in the leaching characteristics or fail to elaborate in detail the preparatory steps taken (*64*, *94–103*). In order to successfully compare results taken from multiple sources, it is extremely important to understand how changing these parameters can affect the results presented. This is especially important when developing instrumentation and techniques for *in-situ* analyses since the sample acquisition and preparation will be automated.

When performing the first *in-situ* wet chemical analysis on another planet, the WCL cells aboard the 2007 Phoenix Mars Scout Lander analyzed 1 cc (approximately 1 g) of Martian soil by adding it to 25 mL of a leaching solution comprised of dissolved ionic species in DI water (*23*, *24*). The presence of an ionic

leaching solution was to perform a two-point calibration of the ISEs before analysis of the sample. When reporting results, the amount of each species present in the calibration solution was subtracted to yield the amount of each component in Martian regolith. The values of each species were dependent on the equilibrium with the carbonate system and the presence of various minerals present in the soil. For instance, certain amounts of calcium, magnesium, sulfate all relate to the amount of gypsum, magnesite, and calcite in the soil. Preparation is also an important when there is a limited amount of sample, as is the case with meteorite analyses (*62*).

Soils from the Antarctic Dry Valleys (ADV) have been studied in detail. Most recently, Stroble *et al.* investigated soils from both stable upland zones (SUZ) and coastal thaw Zones (CTZ) to determine a soil analogue to the Martian soil as characterized by Phoenix (*62*). The leaching of the Antarctic soils was performed as follows: 1 g of Antarctic soil was leached with 25 mL of 18.2 MΩ-cm^{-1} deionized water for 23 hrs at room temperature. The analysis of the ADV soils was then performed by IC and compared with other IC, ISE and simulant analyses. The main reason for the selection of the 25:1 ratio was to compare the results to those of the Phoenix mission.

6.2. Experimental Conditions

6.2.1. Soil Sample

To ensure homogeneity across the experiments a mixed soil sample was formulated with various Antarctic Dry Valley (ADV) soils. A mix of Taylor Valley (TV) soils

from pit #2 ranging in pit depths from 5-22 cm were combined. The actual amounts of each pit can be found in Table 6.1. Further information regarding the location of the samples can be found elsewhere (*82*). This mixture was sieved to remove any particulates > 2 mm and homogenized with a mortar and pestle. The TV soil mixture was stored in a sterile Nasco Whirl-Pak sample collection bag.

Table 6.1. Composition of the master soil sample comprised of pit #2 in Taylor Valley, Antarctica.

Soil Sample	Pit Depth, cm	Amount Added, g
ANTV 0707	1-9	20
ANTV 0708	9-12	45
ANTV 0709	12-17	136
ANTV 0710	17-20	193
ANTV 0711	20-24	119
Total		513

6.2.2. Soil Leaching Parameters

All samples were leached at ambient laboratory temperature (24±3ºC) in a Fisherbrand vial (11, 15 or 29 mL) and agitated on a LabQuake (Barnstead/Thermolyne Corporation) for the entirety of the leaching time. The leachate was directly transferred into a fresh, sterile syringe and filtered using a 0.2 μm filter (Thermo Scientific Nalgene Syringe Filter) upon completion of the desired leaching time. The filtered sample was collected in a new vial corresponding to the amount of water used for leaching. Leaching parameters to be varied were the ratio of soil to leaching solvent and the amount of time the sample was to be leached. The ratios of leaching solution to soil sample were 1:1 (as 5 g of water: 5 g soil), 5:1, 10:1 and 25:1. Leaching times were varied at 1 hr, 10 hr and

24 hr. The filtered leachates were analyzed by IC within hours after completion of leach time. The filtered leachates were diluted directly in the IC sample vial to ensure that all species were within detection limits of the instrument. Leaching ratio samples were performed in triplicate.

6.2.3. IC Protocol and Analysis

Soluble ionic species were analyzed simultaneously using a pair of Dionex ICS-2000 Reagent Free^{TM} IC systems and a Dionex AS40 Automated Sampler. Cationic separations were carried out using a Dionex Ion-pac CS12A analytical column (250 × 4 mm I.D.), a CG12A guard column (50 × 4 mm I.D.), a Cation Self-Generating Suppressor 300 (4 mm) with a suppression current of 59 mA, and 20 mM methanesulfonic acid at a flow rate of 1.0 mL/min. Anionic separations were carried out using a Dionex Ion-pac AS18 analytical column (250 × 4 mm I.D.), a AG18 guard column (50 × 4 mm I.D.), a Antion Self-Generating Suppressor 300 (4 mm) with a suppression current of 100-150 mA, and 33 mM potassium hydroxide acid at a flow rate of 1.0 mL/min. The suppressor current was changed to lower the background conductivity as the suppressor aged. Upon the replacement of the suppressor in May 2013, the suggested suppressor current of 100 mA was utilized. Sample peaks were integrated using Chromeleon 6.8 and peak areas were used for determination of concentration. Unless otherwise noted, all samples taken from the filtered leachates were run separately 5 times, yielding 15 data points for each ionic species at a given leaching ratio and time. Any removed points were done so by performing a Q-test on the 15 data points.

Calibrations were performed using the Dionex Six Cation-II Standard (Li^+, Na^+, NH_4^+, K^+, Mg^{2+}, and Ca^{2+}) and the Fluka Multi-element Ion Chromatography Standard Solutions I & II (F^-, Cl^-, NO_3^-, Br^-, SO_4^{2-}, and PO_4^{3-}) with the corresponding concentrations shown in Table 6.2. All standards, leaching solutions and subsequent leachate dilutions used 18.2 MΩ-cm^{-1} deionized water (BarnsteadNanopure, Massachusetts, USA). All data was extracted from the Chromeleon software and imported into Microsoft Excel. Peak area and standard concentrations were used to fabricate calibration curves for each ionic species. Using this information, the amount of each ionic species could be deduced from the corresponding calibration curve. All figures were constructed in Igor Pro 6.22A after the initial Excel analysis.

Table 6.2. IC calibration standards utilized for the determination of ionic species in soil samples.

Cation	Cation Stnd 1, ppm	Cation Stnd 2, ppm	Cation Stnd 3, ppm	Cation Stnd 4, ppm
Li^+	0.0025	0.05	0.50	2.50
Na^+	0.0100	0.20	2.00	10.0
NH_4^+	0.0125	0.25	2.50	12.5
K^+	0.0250	0.50	5.00	25.0
Mg^{2+}	0.0125	0.25	2.50	12.5
Ca^{2+}	0.0250	0.50	5.00	25.0
Anion	Anion Stnd 1, ppm	Anion Stnd 2, ppm	Anion Stnd 3, ppm	Anion Stnd 4, ppm
F^-	0.10	1.00	10.0	20.0
Cl^-	0.10	1.00	10.0	20.0
SO_4^{2-}	0.05	0.10	1.00	5.00
Br^-	0.10	1.00	10.0	20.0
NO_3^-	0.05	0.10	1.00	5.00
PO_4^{3-}	0.05	0.10	1.00	5.00

6.3. Effect of Leach Time and Ratio

The effect of the leach time and ratio was investigated upon the decision to miniaturize the CHEMSENS SAU compared with Phoenix WCL. The Phoenix WCL could accommodate 25 mL of leaching solution and 1 g of soil while the proposed CHEMSENS SAU will accommodate 8 mL of leaching solution and 1 g of soil. The question arose whether the Phoenix soil would yield similar results if analyzed by CHEMSENS. An extensive literature search determined that no set protocol for the leaching of soil samples existed. Although other groups have investigated the leaching effect of other species, a lack of such studies for common inorganic cations and anions led to this work. Limited studies have been conducted investigating the effect of temperature on inorganic cations and anions (*104*), therefore the focus of this work will be placed on the leach time and leach ratio.

The selection of leaching parameters included in this study was chosen based on the previous Martian analyses and the proposed SAU designs for CHEMSENS. As described in Chapter 4, the first proposed SAUs after the track design was selected were to accommodate 5 and 10 mL of leaching solution. Therefore, when comparing leaching ratios, one gram of soil will be leached by 5 and 10 mL, as well as 25 mL (representing the Phoenix WCL analyses) and the lower extreme of 1:1. In order to perform an analysis by the IC in triplicate a minimum of 1.2 mL of sample is required. Therefore, instead of using 1 g of soil and 1 g of leaching solution for the 1:1, 5 grams of soil and 5 grams of leaching solution were employed. Further investigations into the effect of using ratios of 1:1, 2:2, 3:3 and 4:4 will not be pursued here, although future work should include this

study. Leach times were varied based on several times found in the literature where 1 hour, 10 hours, and 24 hours were ultimately selected. Two types of data will be presented here: (1) quantitative analyses of the various parameters for common inorganic cations and anions, as well as (2) qualitative analyses to visualize the trends when varying the leach time and ratio. A summary of all samples analyzed can be found in Table 6.3.

Table 6.3. Summary of soil samples analyzed at room temperature (~24°C). All samples were placed on a LabQuake for agitation during their corresponding leach time. For dial dilution, a total of 400 µL was mixed in the IC sample tube.

Sample Number	Soil, g	Water, g	Leach Time, Start	Leach Time, End	Vial Dilution
1	1.0030	5.0171	6/27/2012 13:23	6/27/2012 14:23	1:4
2	0.9970	4.9937	6/27/2012 13:33	6/27/2012 14:33	1:4
3	0.9985	5.0313	6/27/2012 13:43	6/27/2012 14:43	1:4
4	1.0006	10.0297	7/4/2012 10:52	7/4/2012 11:52	1:10
5	1.0137	10.0633	7/4/2012 10:58	7/4/2012 11:58	1:10
6	1.0265	10.0532	7/4/2012 11:04	7/4/2012 12:04	1:10
7	1.0198	25.0768	7/5/2012 15:05	7/5/2012 16:05	1:4
8	1.0130	25.0756	7/5/2012 15:12	7/5/2012 16:12	1:4
9	0.9977	25.0522	7/5/2012 15:19	7/5/2012 16:19	1:4
10	5.0090	5.0200	7/9/2012 15:05	7/9/2012 16:05	1:100
11	5.0076	5.0273	7/9/2012 15:07	7/9/2012 16:07	1:100
12	5.0222	5.0220	7/9/2012 15:09	7/9/2012 16:09	1:100
13	1.0013	5.0153	8/15/2012 15:24	8/16/2012 15:24	1:20
14	1.0092	5.0236	8/15/2012 15:29	8/16/2012 15:29	1:20
15	1.0083	5.0016	8/15/2012 15:33	8/16/2012 15:33	1:20
16	1.0051	10.0042	8/20/2012 11:22	8/21/2012 11:22	1:10
17	0.9990	9.9915	8/20/2012 11:26	8/21/2012 11:26	1:10
18	0.9990	10.0317	8/20/2012 11:31	8/21/2012 11:31	1:10
19	0.9995	25.0284	8/26/2012 10:47	8/27/2012 10:47	1:4
20	1.0001	25.0244	8/26/2012 10:50	8/27/2012 10:50	1:4
21	1.0011	25.0131	8/26/2012 10:53	8/27/2012 10:53	1:4
22	0.9996	10.0409	8/26/2012 10:57	8/27/2012 10:57	1:10
23	4.9974	5.0002	8/27/2012 14:36	8/28/2012 15:06	1:100
24	5.0052	4.9930	8/27/2012 14:39	8/28/2012 15:09	1:100
25	5.0074	5.0729	8/27/2012 14:43	8/28/2012 15:13	1:100
26	0.9978	5.0028	1/22/2013 14:27	1/23/2013 0:27	1:20
27	1.0062	5.0068	1/22/2013 14:33	1/23/2013 0:33	1:20
28	1.0074	5.0044	1/22/2013 14:39	1/23/2013 0:39	1:20
29	N/A	4.9922	1/22/2013 14:46	1/23/2013 0:46	N/A
30	1.0013	10.0022	1/25/2013 10:22	1/25/2013 20:22	1:10

Sample Number	Soil, g	Water, g	Leach Time, Start	Leach Time, End	Vial Dilution
31	0.9996	10.0230	1/25/2013 10:30	1/25/2013 20:30	1:10
32	0.9979	10.0106	1/25/2013 10:33	1/25/2013 20:33	1:10
33	N/A	10.0143	1/25/2013 10:36	1/25/2013 20:36	N/A
34	0.9963	25.0002	1/27/2013 23:24	1/28/2013 9:24	1:4
35	1.0046	25.0060	1/27/2013 23:29	1/28/2013 9:29	1:4
36	0.9980	25.0075	1/27/2013 23:35	1/28/2013 9:35	1:4
37	N/A	24.9937	1/27/2013 23:39	1/28/2013 9:39	N/A
38	5.0034	4.9994	1/28/2013 23:19	1/29/2013 9:19	1:100
39	5.0059	5.0196	1/28/2013 23:23	1/29/2013 9:23	1:100
40	5.0006	5.0177	1/28/2013 23:27	1/29/2013 9:27	1:100
41	N/A	5.0011	1/28/2013 23:30	1/29/2013 9:30	N/A
42	1.0029	10.0087	2/11/2013 13:33	2/11/2013 14:33	1:10
43	0.9997	9.9998	2/11/2013 13:38	2/11/2013 14:38	1:10
44	1.0035	10.0017	2/11/2013 13:43	2/11/2013 14:43	1:10
45	N/A	9.9953	2/11/2013 13:44	2/11/2013 14:44	N/A
46	1.0017	5.0105	2/13/2013 15:43	2/14/2013 15:43	1:20
47	1.0002	5.0117	2/13/2013 15:47	2/14/2013 15:51	1:20
48	0.9971	5.0133	2/13/2013 15:51	2/14/2013 15:55	1:20
49	N/A	4.9920	2/13/2013 15:52	2/14/2013 15:56	N/A
50	0.9958	25.0125	2/20/2013 15:03	2/21/2013 15:03	1:4
51	0.9997	25.0300	2/20/2013 15:07	2/21/2013 15:07	1:4
52	0.9974	25.0450	2/20/2013 15:11	2/21/2013 15:11	1:4
53	N/A	25.0366	2/20/2013 15:14	2/21/2013 15:14	N/A
54	1.0085	10.0151	2/20/2013 15:18	2/21/2013 15:18	1:10
55	0.9988	10.0398	2/20/2013 15:22	2/21/2013 15:22	1:10
56	1.0038	10.0115	2/20/2013 15:25	2/21/2013 15:25	1:10
57	N/A	9.9927	2/20/2013 15:27	2/21/2013 15:27	N/A
58	1.0007	10.0152	6/15/2013 9:53	6/15/2013 19:53	1:10
59	0.9994	10.0317	6/15/2013 9:57	6/15/2013 19:57	1:10
60	1.0000	10.0087	6/15/2013 9:59	6/15/2013 19:59	1:10
61	N/A	10.0039	6/15/2013 10:01	6/15/2013 20:01	N/A
62	1.0002	5.0072	6/15/2013 10:09	6/15/2013 20:09	1:20
63	1.0011	5.0133	6/15/2013 10:13	6/15/2013 20:13	1:20
64	1.0015	5.0018	6/15/2013 10:15	6/15/2013 20:15	1:20
65	N/A	5.0073	6/15/2013 10:17	6/15/2013 20:17	N/A

6.3.1. Cations

The inorganic cations selected to monitor whilst varying leaching parameters were similar to the ions found by Phoenix and also present in the ANTV (Antarctic Taylor Valley) soils. For this reason, Li^+, Na^+, NH_4^+, K^+, Mg^{2+} and Ca^{2+} were selected. Lithium was calibrated although no quantifiable amount was present in

the ANTV soils after dilutions. After initial tests, there was no appreciable Ba^{2+} present in the ANTV soil therefore it was excluded from this study. Heavy metals, such as $Fe^{3/2+}$, were also excluded due to the potential poisoning of the stationary phase. Chromatograms of the cationic species in the standard and an ANTV soil sample are shown in Figure 6.1. The elution order was: Li^+, Na^+, NH_4^+, K^+, Mg^{2+} and Ca^{2+}.

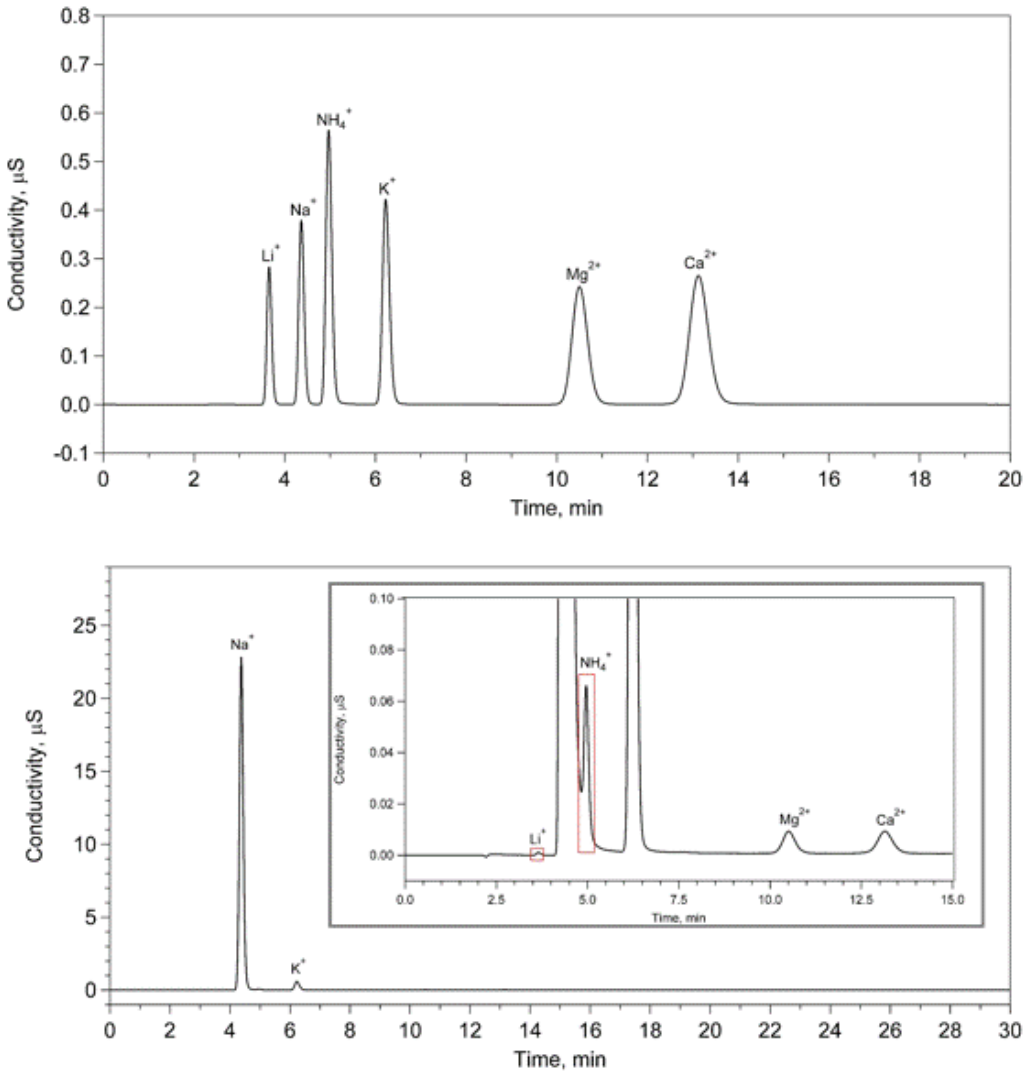

Figure 6.1. Chromatograms of cation standard 2 (top) and ANTV sample 58 (bottom). Inset in sample chromatogram is the zoomed in baseline to view various peaks.

The most prevalent cation present was Na^+. This was expected since TV is present in the CTZ, where the majority of ionic species are present due to sea spray. All other species were approximately an order of magnitude less, with K^+ being the next highest cation followed by NH_4^+ and Ca^{2+} and Mg^{2+}. Figure 6.2 shows the investigation of leach ratio for various amounts of leaching solution for 1 hour. The concentrations are presented as the amount leached from soil in parts per million (ppm) after accounting for dilution. The general trend shown is that as the leach ratio is increased from 5:5 to 25:1, there is an increased amount of cationic species. The exception to this trend is Mg^{2+} and Ca^{2+}. For the 1 hour investigation, it appears that all Ca^{2+} samples are the same, within error, while Mg^{2+} decreases after the ratio is increased from 5:1 to 10:1. The same trend is seen, more prevalent, in Figures 6.3 and 6.4 where the leach ratio was varied while leaching for 10 hours and 24 hours, respectively. As seen in Figure 6.1, due to the amount of Na^+ present, the amount of NH_4^+ is affected. Therefore, discrepancies exist across the amounts of NH_4^+. The values used to formulate Figures 6.2 – 6.4 are presented in Table 6.4.

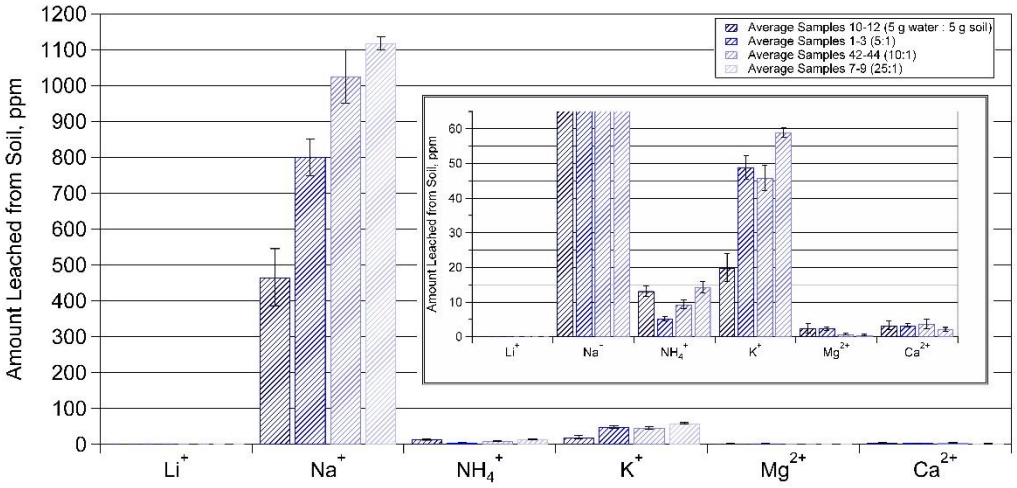

Figure 6.2. Investigation of the effect of varying the leaching ratio with leaching for 1 hour. Inset: zoomed in plot to quantify the amounts of NH_4^+, K^+, Mg^{2+} and Ca^{2+}. The error bars represent ±1 σ while each bar is the mean value of 15 samples.

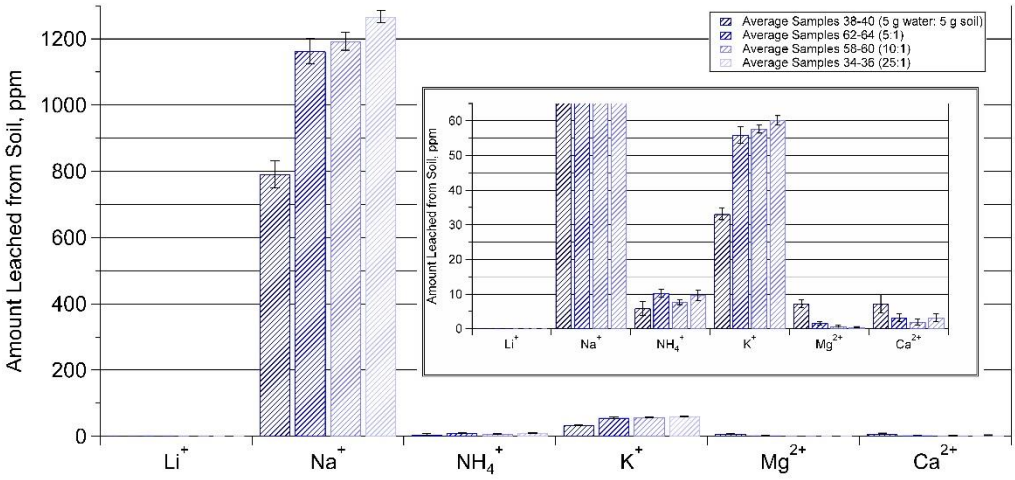

Figure 6.3. Investigation of the effect of varying the leaching ratio with leaching for 10 hours. Inset: zoomed in plot to quantify the amounts of NH_4^+, K^+, Mg^{2+} and Ca^{2+}. The error bars represent ±1 σ while each bar is the mean value of 15 samples.

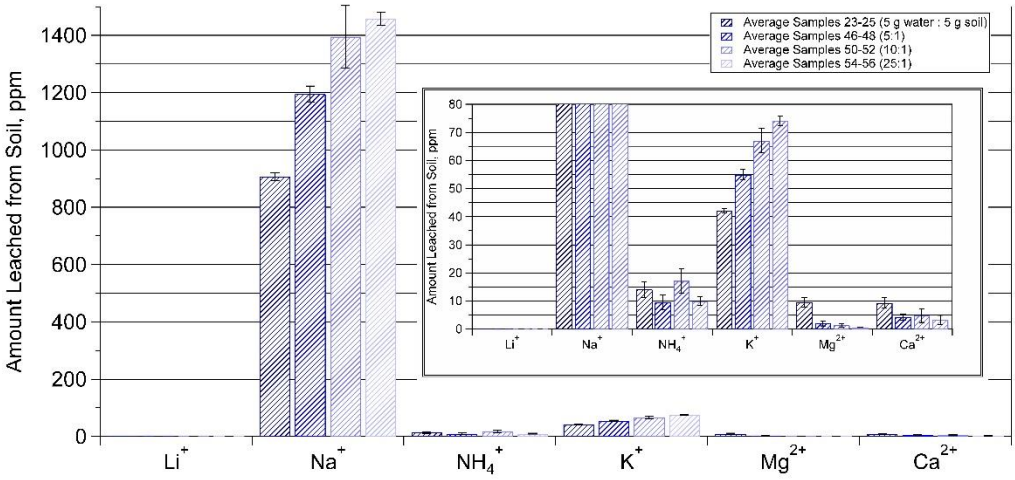

Figure 6.4. Investigation of the effect of varying the leaching ratio with leaching for 24 hours. Inset: zoomed in plot to quantify the amounts of NH_4^+, K^+, Mg^{2+} and Ca^{2+}. The error bars represent ±1 σ while each bar is the mean value of 15 samples.

Table 6.4. Mean concentrations of cationic species for various samples used to formulate Figures 6.2 – 6.4. Leach ratio is given as g water:g soil.

Leach Parameters		Concentrations, ppm				
Time, hr	Ratio	Na^+	NH_4^+	K^+	Mg^{2+}	Ca^{2+}
1	5:5	466 ± 79.4	13.2 ± 1.60	20.0 ± 4.06	2.41 ± 1.31	3.29 ± 1.26
1	5:1	800 ± 51.2	5.27 ± 0.57	48.8 ± 3.36	2.41 ± 0.49	3.26 ± 0.52
1	10:1	1025 ± 74.1	9.38 ± 1.32	45.9 ± 3.73	0.80 ± 0.26	3.67 ± 1.41
1	25:1	1118 ± 19.0	14.3 ± 1.75	58.9 ± 1.33	0.52 ± 0.16	2.10 ± 0.60
10	5:5	791 ± 40.0	5.87 ± 2.04	33.1 ± 1.64	7.24 ± 1.11	7.28 ± 2.59
10	5:1	1163 ± 38.7	10.3 ± 1.16	56.0 ± 2.36	1.65 ± 0.47	3.17 ± 1.06
10	10:1	1192 ± 26.5	7.65 ± 0.67	57.7 ± 1.24	0.79 ± 0.29	1.99 ± 0.94
10	25:1	1267 ± 18.7	9.66 ± 1.50	60.1 ± 1.34	0.52 ± 0.14	3.18 ± 1.16
24	5:5	906 ± 13.4	14.1 ± 2.75	42.1 ± 0.68	9.57 ± 1.75	9.34 ± 1.81
24	5:1	1195 ± 28.4	9.45 ± 2.60	55.0 ± 1.94	2.00 ± 0.87	4.28 ± 1.20
24	10:1	1395 ± 108	17.2 ± 4.27	67.0 ± 4.32	1.35 ± 0.52	4.77 ± 2.37
24	25:1	1458 ± 23.8	9.93 ± 1.58	74.1 ± 1.68	0.64 ± 0.09	3.29 ± 1.60

To further investigate the trend of changing both the leaching ratio and time as well as understand the decreases in Ca^{2+} and Mg^{2+}, contour plots were fabricated in Igor Pro. Each contour plot is a visual representation of the effect on concentration of the corresponding ion while varying the leach time (y-axis) and ratio (x-axis, plotted as a whole number). Each plot contains a color scale where the lowest concentration values are shown as red and the highest concentration values are shown as purple, increasing in the order of:

Red < Orange < Yellow < Green < Blue < Purple

Figures 6.5 – 6.9 show such contour plots for Na^+, NH_4^+, K^+, Mg^{2+} and Ca^{2+}, respectively.

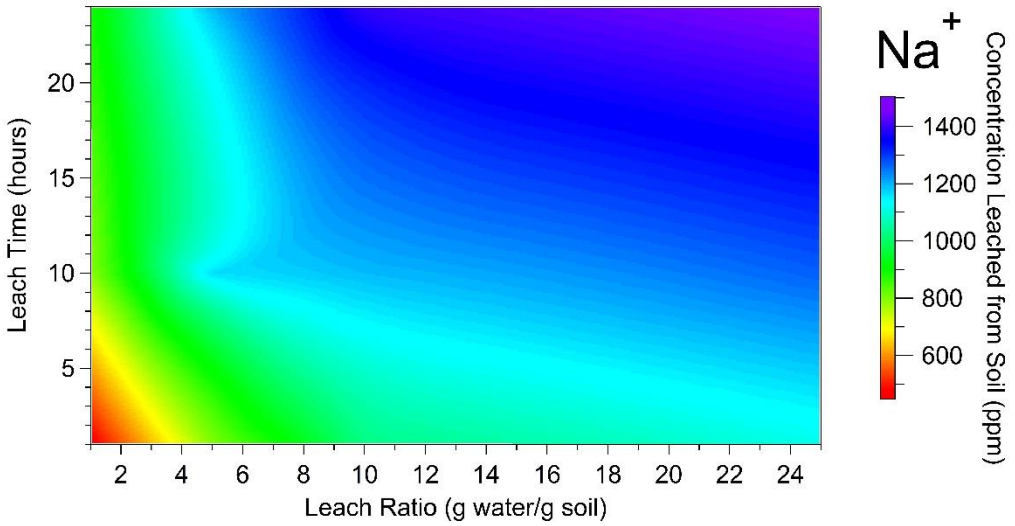

Figure 6.5. Contour plot showing how varying leach time and ratio effects the concentration of Na^+ in ANTV soils.

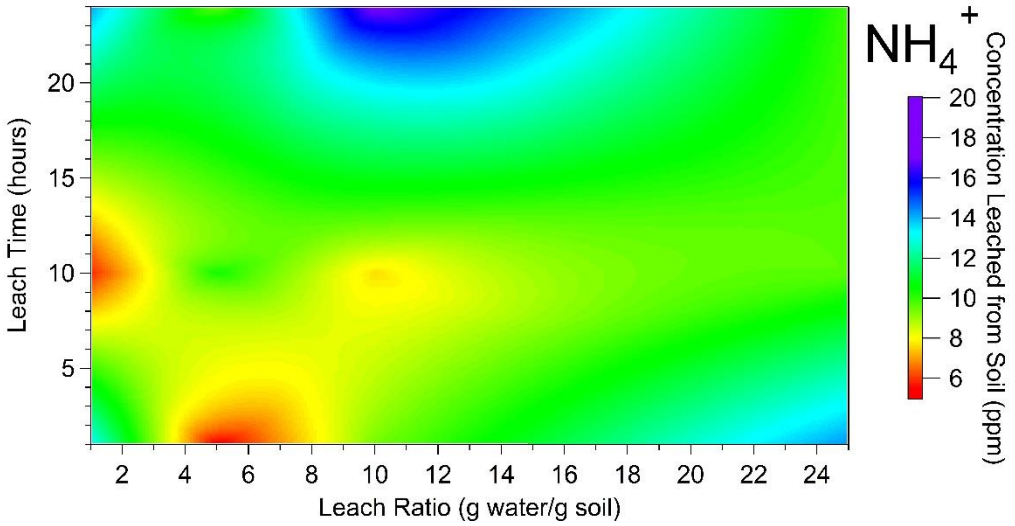

Figure 6.6. Contour plot showing how varying leach time and ratio effects the concentration of NH_4^+ in ANTV soils.

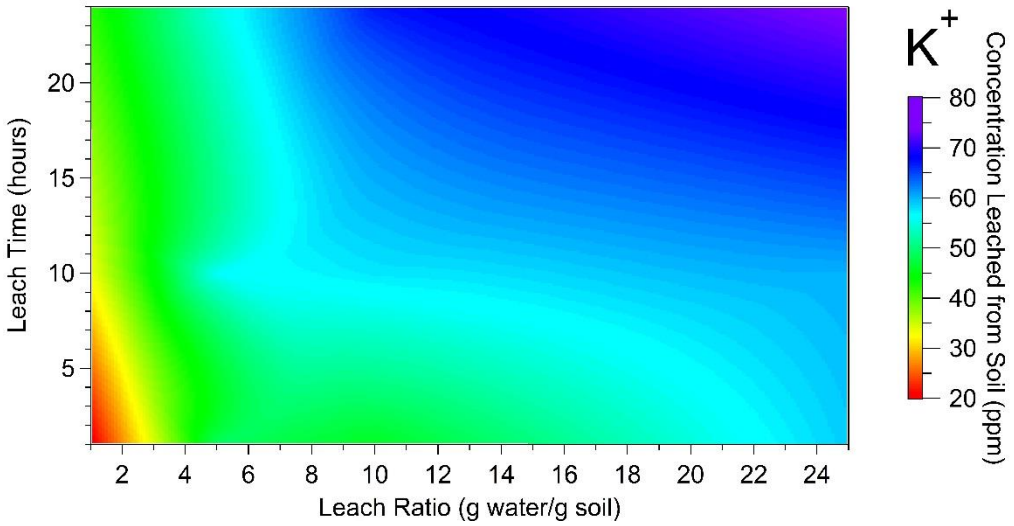

Figure 6.7. Contour plot showing how varying leach time and ratio effects the concentration of K^+ in ANTV soils.

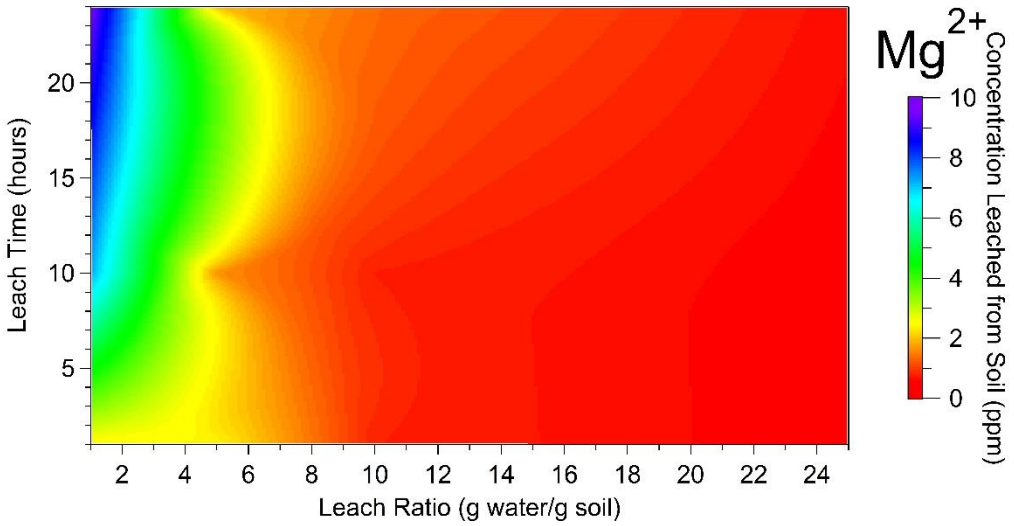

Figure 6.8. Contour plot showing how varying leach time and ratio effects the concentration of Mg^{2+} in ANTV soils.

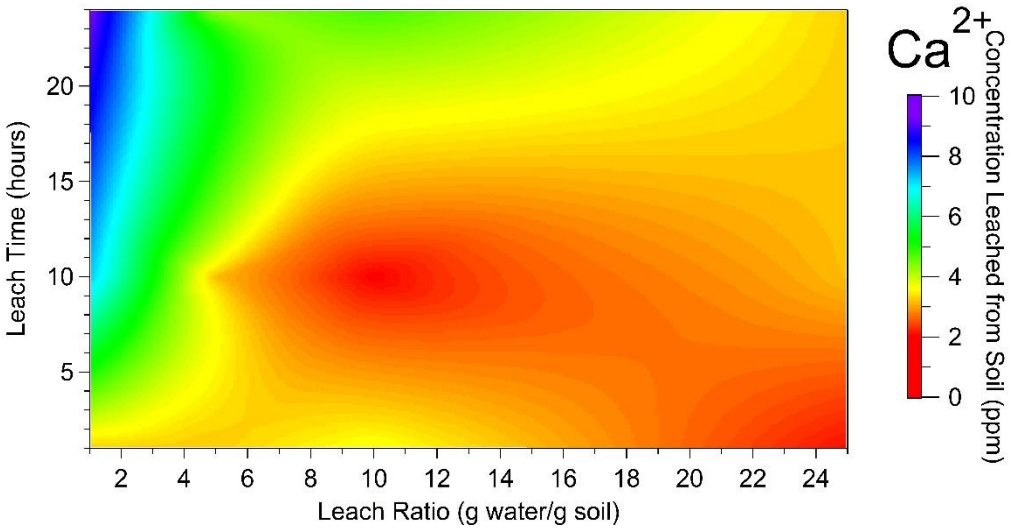

Figure 6.9. Contour plot showing how varying leach time and ratio effects the concentration of Ca^{2+} in ANTV soils.

The general trend of increasing cationic species as the leaching ratio and time are increased is optimized in Figures 6.5 and 6.7, corresponding to Na^+ and K^+. A line that could be drawn between (1,1) and (25,24) would almost be linear. As stated previously, the detection of NH_4^+ suffered from the high amounts of soluble Na^+ present in the solution, and if one truly wants to investigate the effect of leaching parameters on NH_4^+, further studies would have to be performed by either removing the Na^+ from the system or finding another soil archetype that is high in NH_4^+ and low in Na^+.

An opposite trend was experienced by Mg^{2+} and Ca^{2+} as exhibited in Figures 6.8 and 6.9. Initially, at a leach ratio of 1, and at varying leach times, the amount of both divalent cations increased. Upon the increase of the ratio to 5:1, decreases in each cation existed. This was also the case from ratios of 10:1 and 25:1, more prevalently for Mg^{2+}. The low values, after accounting for dilution, resulted in ranges from 0-10 ppm for both cations. The overall low amounts of Mg^{2+} and Ca^{2+}

present yielded a hypothesis that as the amount of leaching solution increased, in this case 18.2 MΩ nanopure water, the impurities present, such as carbonate, along with carbonate-bearing minerals present in the soil resulted in an overall decrease in the amount of these species at higher leaching volumes.

6.3.2. Anions

The anionic species selected to monitor whilst varying leaching parameters were also similar to the ions found by Phoenix and also present in the ANTV soils. The species settled on were F^-, Cl^-, SO_4^{2-}, Br^-, NO_3^- and PO_4^{3-}. Calibration standards for the halides and oxyanion species were combined to yield a set of calibration standards with all species. Due to the lack of I^- present, it was excluded for this study. The exclusion of ClO_4^-, an anion of great interest for Phoenix and Chapter 2, was due to the fact that ClO_4^- is highly soluble and should be soluble in the presence of any water. The experimental conditions would also have to be changed to accommodate a different column for the separation of ClO_4^-, therefore the above mentioned six anions were selected for analysis. Chromatograms for the anionic calibration standard and an ANTV soil sample are shown in Figure 6.10. The elution order was F^-, Cl^-, SO_4^{2-}, Br^-, NO_3^- and PO_4^{3-}.

As was the case with the cations, the most prevalent anionic species was due to sea spray and was Cl^-. Approximately an order of magnitude lower was SO_4^{2-} and NO_3^- followed by PO_4^{3-}. Concentrations of F^- and Br^- were lower than the rest at levels corresponding to 0-30 ppm F^- and 0-6 ppm Br^-. Figure 6.11 shows the

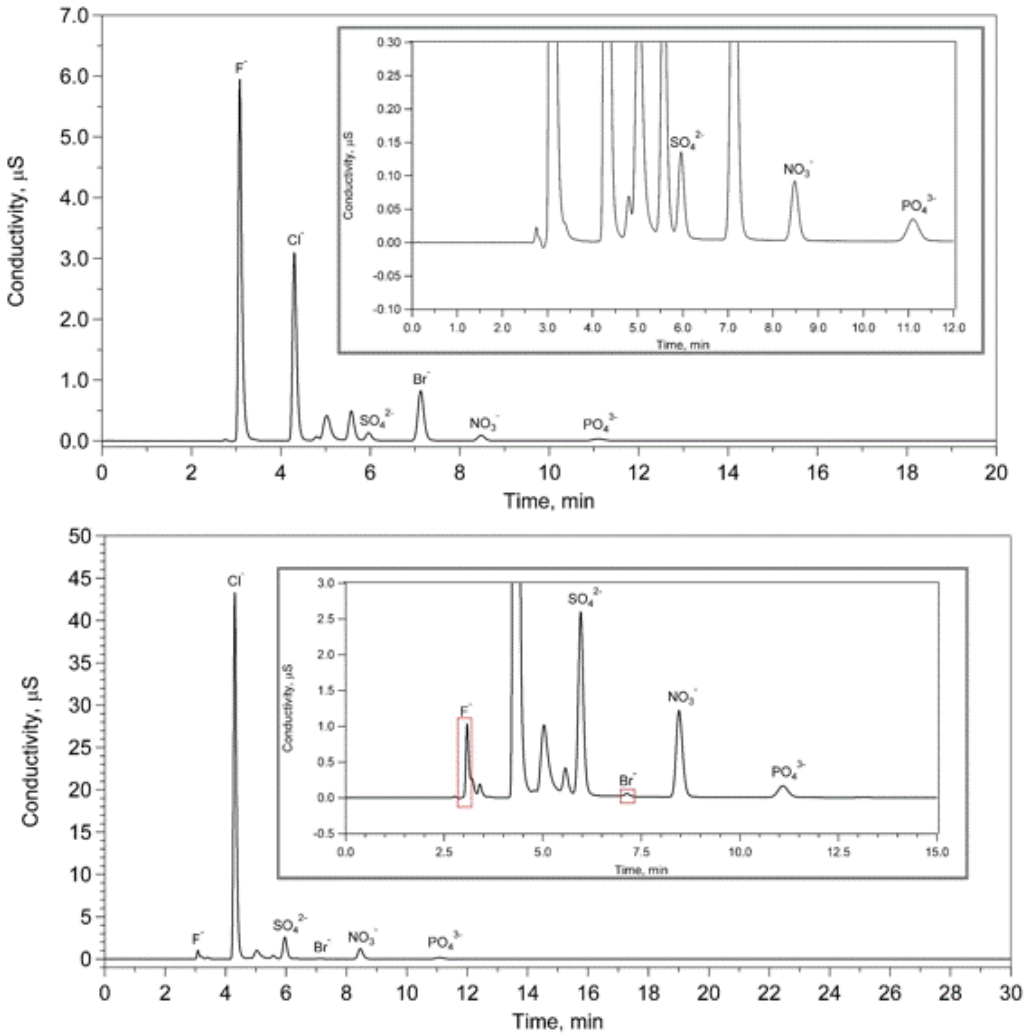

Figure 6.10. Chromatograms of anion standard 2 (top) and ANTV sample 58 (bottom). Inset in both chromatograms is zoomed in baseline to view various peaks.

concentrations of the anionic species as leach ratio was varied and leach time was kept constant at a value of 1 hour. The general trend shown for the 1-hour studies was similar to the cations, where there was a general increase as the ratio was increased. This trend was also observed for the 10 hour leach time, shown in Figure 6.12. The complete opposite trend was seen in Figure 6.13, where there was a general decrease in the amount of each anionic species as the leach ratio was increased for leach times of 24 hours, with the exception of F^- and PO_4^{3-}. An

argument could be made that the values for the ratios of 5:1, 10:1 and 25:1 were all in fact within error of each other, resulting in no change between the leach ratio at 24 hours. The corresponding amounts of each anionic species used to formulate these figures can be found in Table 6.5.

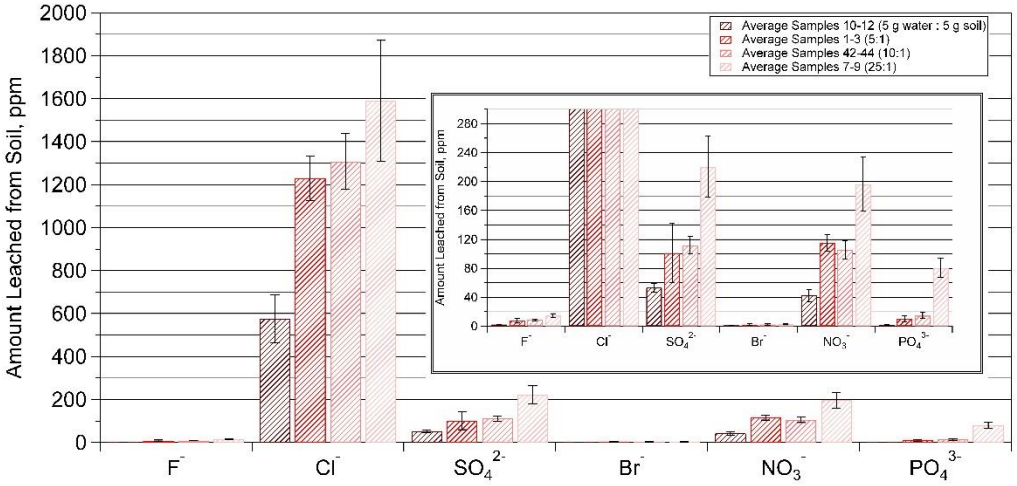

Figure 6.11. Investigation of the effect of varying the leaching ratio with leaching for 1 hour. Inset: zoomed in plot to quantify the amounts of F^-, SO_4^{2-}, NO_3^- and PO_4^{3-}. The error bars represent ±1 σ while each bar is the mean value of 15 samples.

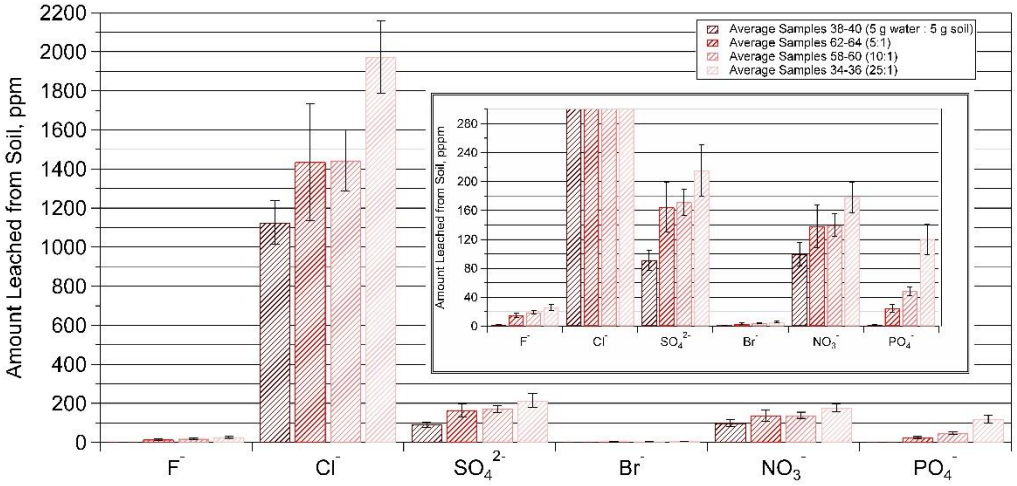

Figure 6.12. Investigation of the effect of varying the leaching ratio with leaching for 10 hours. Inset: zoomed in plot to quantify the amounts of F^-, SO_4^{2-}, NO_3^- and PO_4^{3-}. The error bars represent ±1 σ while each bar is the mean value of 15 samples.

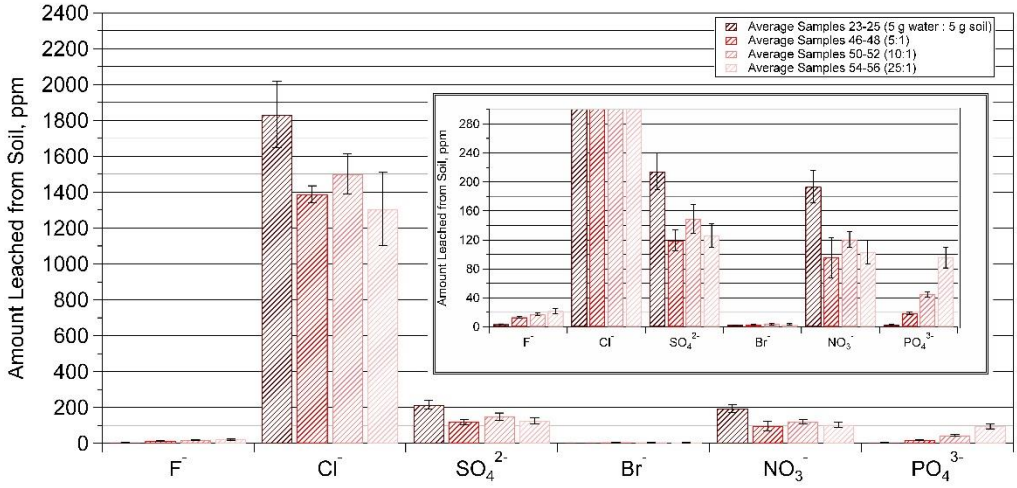

Figure 6.13. Investigation of the effect of varying the leaching ratio with leaching for 24 hours. Inset: zoomed in plot to quantify the amounts of F^-, SO_4^{2-}, NO_3^- and PO_4^{3-}. The error bars represent ±1 σ while each bar is the mean value of 15 samples.

Table 6.5. Mean concentrations of anionic species for various samples used to formulate Figures 6.11 – 6.13. Leach ratio is given as g water:g soil.

Leach Parameters		Concentration, ppm					
Time, hr	Ratio	F-	Cl-	SO42-	Br-	NO3-	PO43-
1	5:5	2.39 ± 0.35	576 ± 111	53.2 ± 5.72	1.05 ± 0.36	42.4 ± 8.11	1.86 ± 0.55
1	5:1	7.51 ± 3.28	1230 ± 103	101 ± 41.4	1.97 ± 1.19	116 ± 11.3	10.1 ± 3.79
1	10:1	8.71 ± 1.12	1308 ± 131	112 ± 12.1	2.39 ± 0.73	105 ± 12.9	14.6 ± 4.27
1	25:1	14.6 ± 2.84	1589 ± 282	221 ± 42.2	2.73 ± 0.93	197 ± 37.2	80.5 ± 13.4
10	5:5	2.32 ± 0.36	1126 ± 111	91.1 ± 13.4	1.16 ± 0.37	99.4 ± 16.7	1.50 ± 0.52
10	5:1	14.7 ± 3.22	1435 ± 299	164 ± 34.5	3.42 ± 1.08	138 ± 29.7	24.7 ± 5.55
10	10:1	19.0 ± 2.47	1444 ± 156	171 ± 18.0	3.84 ± 0.60	140 ± 15.6	48.4 ± 6.15
10	25:1	25.7 ± 4.60	1974 ± 186	215 ± 35.4	5.83 ± 1.35	178 ± 21.3	120 ± 20.8
24	5:5	3.66 ± 0.40	1832 ± 185	215 ± 25.5	2.50 ± 0.40	194 ± 22.7	3.30 ± 0.33
24	5:1	13.3 ± 0.94	1389 ± 47	119 ± 14.5	2.72 ± 0.88	95.6 ± 27.8	18.9 ± 2.11
24	10:1	17.0 ± 1.72	1501 ± 111	149 ± 20.3	3.84 ± 1.04	121 ± 10.9	44.9 ± 3.68
24	25:1	21.9 ± 3.93	1306 ± 206	126 ± 16.2	3.42 ± 0.76	103 ± 16.4	95.8 ± 14.4

Contour plots were also fabricated to qualitatively visualize the trends in the data as described for the cations. Figures 6.14 – 6.19 show such plots for F^-, Cl^-, SO_4^{2-}, Br^-, NO_3^- and PO_4^{3-}, respectively. In most cases, for each anionic species, the lowest amounts present occur when the sample is leached at a ratio of 1 for

periods of 1 hour. As the leach time increased, the overall amount for F^-, Br^- and PO_4^{3-} showed little to no change, while as the time increased at a ratio of 1, the most prevalent anions Cl^-, SO_4^{2-} and NO_3^- all experienced increases. For all anionic species, as the leach ratio increased, the amount of the corresponding species also increased.

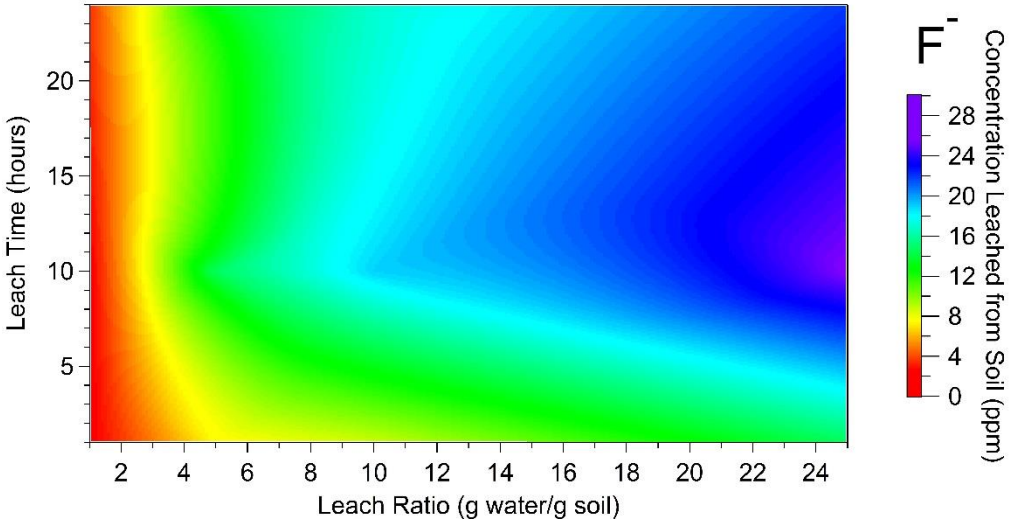

Figure 6.14. Contour plot showing how varying leach time and ratio effects the concentration of F^- in ANTV soils.

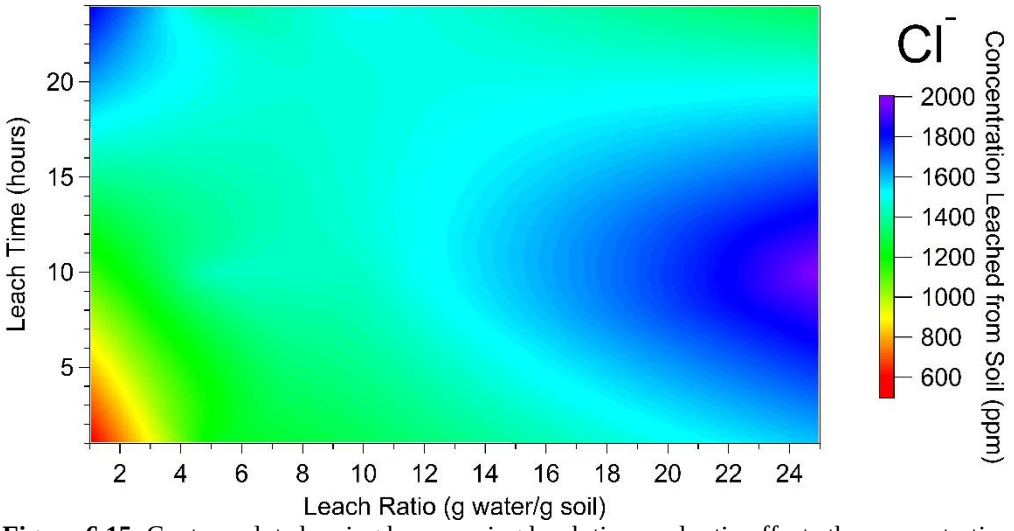

Figure 6.15. Contour plot showing how varying leach time and ratio effects the concentration of Cl^- in ANTV soils.

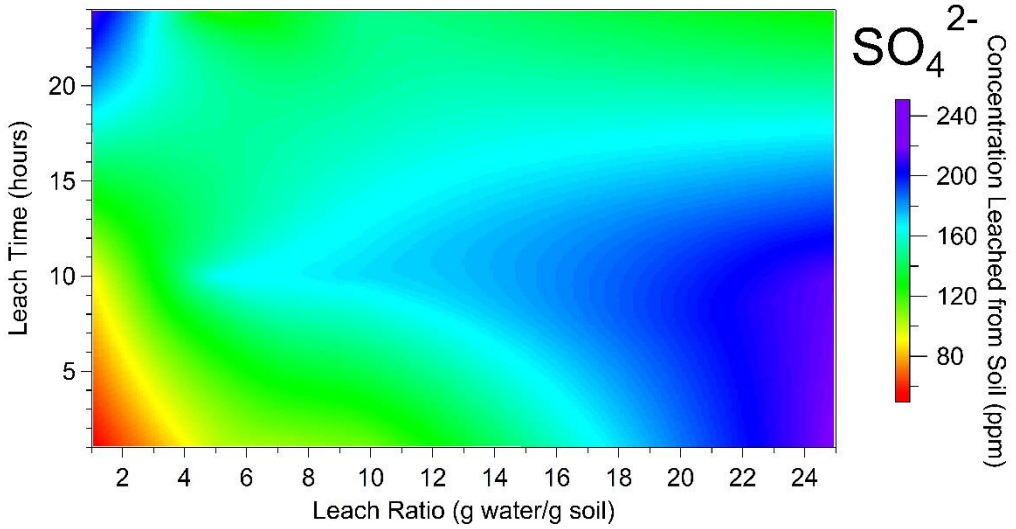

Figure 6.16. Contour plot showing how varying leach time and ratio effects the concentration of SO_4^{2-} in ANTV soils.

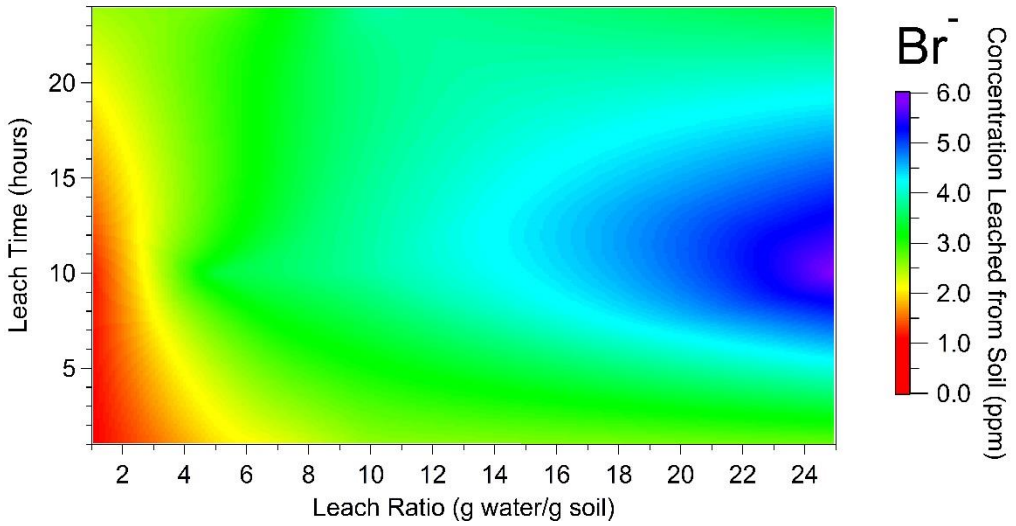

Figure 6.17. Contour plot showing how varying leach time and ratio effects the concentration of Br^- in ANTV soils.

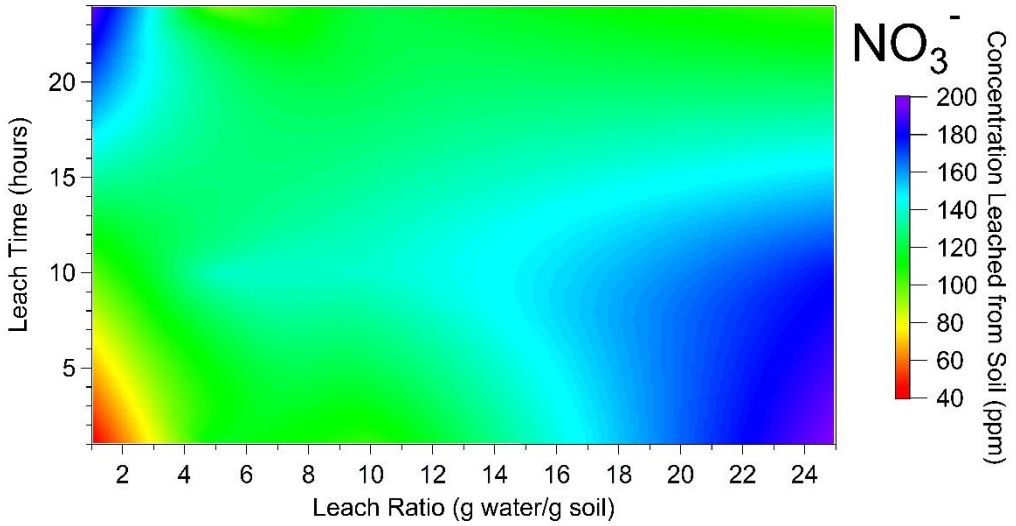

Figure 6.18. Contour plot showing how varying leach time and ratio effects the concentration of NO_3^- in ANTV soils.

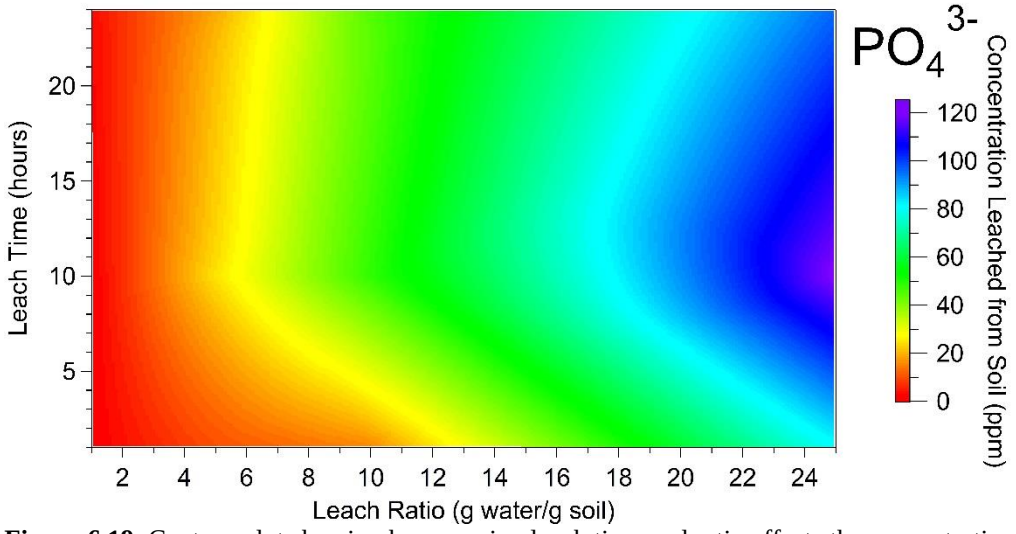

Figure 6.19. Contour plot showing how varying leach time and ratio effects the concentration of PO_4^{3-} in ANTV soils.

6.4. Conclusions and Future Work

Overall, the leaching parameters selected for sample preparation effect the concentration seen when using Antarctic soil. These effects vary from somewhat between drastic to slight, but exist nonetheless. In terms of cations, the greatest

effects are seen upon increasing the leach ratio from 1:1 to 25:1, while slight increases in concentrations occur as the leach time is increased. This trend is also true for Mg^{2+} and Ca^{2+}, although the effect is negative instead of positive. As stated, the hypothesis for this phenomena is that as an increased amount of leaching solution is added and the time increased, the divalent cations complex with soluble carbonates present in the 18.2 MΩ nanopure water and carbonate bearing minerals present in the soil. Therefore, if Mg^{2+} and Ca^{2+} analyses are of the highest priority the leaching parameters should contain a low ratio of leaching solution to soil and be leached from > 15 hours. It should also be noted that this model assumes low overall amounts of Mg^{2+} and Ca^{2+}. Further studies should investigate these trends using soil samples that contain approximately an order of magnitude greater soluble concentrations, if available.

The presence of Na^{+} and K^{+} in the Antarctic soil as the highest soluble cationic species, while no surprise, leads to the conclusion that the ideal leaching parameters are approximately a leach ratio of 10:1 for 10 hours. This conclusion is based on the above data that suggests the soluble amounts of the most prevalent cations do not increase significantly after these studies. This also allows the user to have the shortest possible leach time and get the most ideal results from the leach analysis.

A similar analysis of the anion results confirms a similar effect as stated for the cationic species. The greatest effect is seen as the leach ratio, as well as the leach time both increase. Due to the higher overall amounts of anions present, no effects similar to Mg^{2+} or Ca^{2+} are present. Due to the amounts of anionic species

present in the Antarctic soil, the optimal leach parameters would be a leach time of 10 hours with a leach ratio of 25:1. This differs from the cationic species optimal parameters, although this leach ratio for cationic species of 25:1 would result in a slightly higher amount of soluble species. Since soil samples are leached for cations and anions at the same time, the ideal parameters for the soil analysis would lie between leach ratios of 10:1 and 25:1 for 10 hours. The preparation step could be tailored, depending on which ionic species are of the highest importance. Future work should be performed to fill in the contour plots above, which would provide an increased understanding of the effects of leaching parameters.

The use of an 8:1 leaching ratio for CHEMSENS will provide a near ideal analysis of the soil based on the above studies. The analysis will be continuous, therefore the chemistry will change over time. To test this model, the analysis should occur, either continuously or by performing spot-checks, for 10 hours. If one assumes that that an immediate analysis of the soil by ISEs is similar to the trends associated with 1 hour leach studies, then a hypothetical re-analysis of the soil analyzed by Phoenix by the CHEMSENS instrument would result in approximately similar amounts of soluble ionic species, with most likely slight decreases in Na^+, K^+, Cl^- and possibly great discrepancies with Mg^{2+}, Ca^{2+}, SO_4^{2-}, and NO_3^- (if analyzed). The surface of Mars is constantly changing due to winds and the movement of dust, but if a rover with a CHEMSENS type instrument were to travel to the North Martian Pole, it would be interesting to see this hypothesis tested.

Conclusions

An analysis of the Phoenix results in combination with the production of a simulant led to the confirmation and quantification of the soluble sulfate in the Phoenix samples equivalent to ~1.3(±0.5) wt%. These analyses also updated the concentrations of the soluble ionic species present in the Phoenix soil from previous reports. A further investigation into the calcium ISE response from the WCL analyses also provided insight into the composition of the perchlorate on the surface of Mars. Calcium electrodes were fabricated to determine the behavior most similar to that produced for the Phoenix WCL analyses. These studies concluded that the most probable composition of the perchlorate is a ratio of 60% $Ca(ClO_4)_2$:40% $Mg(ClO_4)_2$, consistent with the respective carbonate ratio. The presence of $Ca(ClO_4)_2$ implies that the Phoenix landing site was much drier than previously thought, and might not have seen liquid water since the formation of the Heimdall crater where Phoenix landed.

The RCAL instrument was successfully interfaced with a rover and the operational sequence was fully performed. A new instrument, CHEMSENS, that built upon the successes of WCL and RCAL was designed and fabricated. The final design incorporated a more laboratory-based analysis protocol including the ability to weigh the sample, calibrate with liquid solutions and mix with a stir plate. The design also shrunk the overall volume of the leaching solution cavity from 25 mL to ~8 mL. Each SAU also increased the number of overall sensors from 23 to over 50. Included in this number was an increase from 15 ISEs to over 40. One SAU wall was also reserved for other electrochemical sensors. The electrodes were

successfully miniaturized after several designs were fabricated and tested. The final design, utilizing silver epoxy and porous carbon, produced ISEs that were stable and sensitive with extended lifetime in constant contact with a solution.

An analysis of the soil leaching parameters led to the conclusion that depending on the protocol followed, the concentration values can vary. The optimal conditions for the determination of soluble cations was a leach time of 10 hours at a ratio of 25:1 (leach solution:soil). The optimal conditions for the determination of soluble anions was a leach time of 10 hours at a ratio of 10:1. Performing a concurrent analysis, as is usually done, should be performed for 10 hours with a leach ratio between 10:1 and 25:1 depending on the species of highest importance. Due to the low amounts of Ca^{2+} and Mg^{2+} present in the Antarctic soil, the effects were opposite of the general trends of increasing concentrations as the leach time and ratio were increased. This was hypothesized to be due to the presence of carbonate in the leach solution and minerals present in the soil.

Overall, an instrument was designed and fabricated to perform *in-situ* analyses in remote terrestrial or extraterrestrial environments using ISEs. Confirmation of simulant results and leaching parameter effects was performed by IC. The CHEMSENS instrument should further be tested upon integration of ISEs in the SAU and with the proposed electronics. The next step of this research will be to perform laboratory and field-based studies for the analysis of environmental samples to further characterize its analytical capabilities.

References

1. F. W. Taylor, *The Scientific Exploration of Mars* (Cambridge University Press, Cambridge, 2010).

2. H. P. Klein, J. Lederberg, A. Rich, Biological Experiments: The Viking Mars Lander, *Icarus* **16**, 139–146 (1972).

3. H. P. Klein *et al.*, The Viking Mission search for life on Mars, *Nature* **262**, 24–27 (1976).

4. H. P. Klein, The Viking Biological Experiments on Mars, *Icarus* **34**, 666–674 (1978).

5. M. P. Golombek, Overview of the Mars Pathfinder Mission and Assessment of Landing Site Predictions, *Science* **278**, 1743–1748 (1997).

6. P. H. Smith, Results from the Mars Pathfinder Camera, *Science* **278**, 1758–1765 (1997).

7. H. Wanke, G. Dreibus, R. Rieder, I. Ryabchikov, Chemical composition of rocks and soils at the pathfinder site, *Space Sci. Rev.* **96**, 317–330 (2001).

8. M. D. Smith *et al.*, First Atmospheric Science Results from the Mars Exploration Rovers Mini-TES., *Science* **306**, 1750–3 (2004).

9. R. E. Arvidson *et al.*, Overview of the Spirit Mars Exploration Rover Mission to Gusev Crater: Landing site to Backstay Rock in the Columbia Hills, *J. Geophys. Res.* **111**, E02S01 (2006).

10. B. Wouters *et al.*, Capillary ion chromatography at high pressure and temperature., *Anal. Chem.* (2012), doi:10.1021/ac301598j.

11. B. C. Clark *et al.*, Chemistry and mineralogy of outcrops at Meridiani Planum, *Earth Planet. Sci. Lett.* **240**, 73–94 (2005).

12. R. Rieder *et al.*, Chemistry of rocks and soils at Meridiani Planum from the Alpha Particle X-ray Spectrometer., *Science* **306**, 1746–9 (2004).

13. NASA, Mars Exploration (available at http://science.nasa.gov/about-us/smd-programs/mars-exploration/).

14. J. R. Guinn, M. D. Garcia, K. Talley, Mission design of the Phoenix Mars Scout mission, *J. Geophys. Res.* **113**, E00A26 (2008).

15. P. H. Smith *et al.*, Introduction to special section on the Phoenix Mission: Landing Site Characterization Experiments, Mission Overviews, and Expected Science, *J. Geophys. Res.* **113**, E00A18 (2008).

16. H. U. Keller *et al.*, Phoenix Robotic Arm Camera, *J. Geophys. Res.* **113**, E00A17 (2008).

17. K. Leer *et al.*, Magnetic properties experiments and the Surface Stereo Imager calibration target onboard the Mars Phoenix 2007 Lander: Design, calibration, and science goals, *J. Geophys. Res.* **113**, E00A16 (2008).

18. M. T. Lemmon *et al.*, in *39th Lunar and Planetary Science Conference*, (2008).

19. P. A. Taylor *et al.*, Temperature, pressure, and wind instrumentation in the Phoenix meteorological package, *J. Geophys. Res.* **113**, E00A10 (2008).

20. H. P. Gunnlaugsson *et al.*, Telltale wind indicator for the Mars Phoenix lander, *J. Geophys. Res.* **113**, E00A04 (2008).

21. J. H. Hoffman, R. C. Chaney, H. Hammack, Phoenix Mars Mission--the thermal evolved gas analyzer., *J. Am. Soc. Mass Spectrom.* **19**, 1377–83 (2008).

22. M. H. Hecht *et al.*, Microscopy capabilities of the Microscopy, Electrochemistry, and Conductivity Analyzer, *J. Geophys. Res.* **113**, E00A22 (2008).

23. S. P. Kounaves *et al.*, The MECA Wet Chemistry Laboratory on the 2007 Phoenix Mars Scout Lander, *J. Geophys. Res.* **114**, E00A19 (2009).

24. S. P. Kounaves *et al.*, Wet Chemistry experiments on the 2007 Phoenix Mars Scout Lander mission: Data analysis and results, *J. Geophys. Res.* **115**, E00E10 (2010).

25. M. H. Hecht *et al.*, Detection of perchlorate and the soluble chemistry of martian soil at the Phoenix lander site., *Science* **325**, 64–7 (2009).

26. W. V. Boynton *et al.*, Evidence for Calcium Carbonate at the Mars Phoenix Landing Site, *Science* **325**, 61–4 (2009).

27. P. H. Smith *et al.*, H2O at the Phoenix landing site., *Science* **325**, 58–61 (2009).

28. S. P. Kounaves *et al.*, Soluble sulfate in the martian soil at the Phoenix landing site, *Geophys. Res. Lett.* **37**, L09201 (2010).

29. C. R. Stoker *et al.*, Habitability of the Phoenix landing site, *J. Geophys. Res.* **115**, 1–24 (2010).

30. R. C. Quinn, J. D. Chittenden, S. P. Kounaves, M. H. Hecht, The oxidation-reduction potential of aqueous soil solutions at the Mars Phoenix landing site, *Geophys. Res. Lett.* **38**, L14202 (2011).

31. J. Wang, *Analytical Electrochemistry* (Wiley-VCH, New York, ed. 2nd, 2000).

32. J. Bobacka, A. Ivaska, A. Lewenstam, Potentiometric ion sensors., *Chem. Rev.* **108**, 329–51 (2008).

33. J. Bobacka, M. McCarrick, A. Ivaskat, All solid-state Poly(viny1 chloride) Membrane Ion-selective Electrodes With Poly(3- octylthiophene) Solid Internal Contact, *Analyst* **119**, 1985–1991 (1994).

34. J. Bobacka, Potential Stability of All-Solid-State Ion-Selective Electrodes Using Conducting Polymers as Ion-to-Electron Transducers., *Anal. Chem.* **71**, 4932–7 (1999).

35. P. Sjoberg, J. Bobacka, A. Lewenstam, All-Solid-State Chloride-Selective Electrode Based on Poly (3-octylthiophene) and Tridodecylmethylammonium Chloride, *Electroanalysis* **11**, 821–824 (1999).

36. A. Michalska, K. Maksymiuk, Conducting polymer membranes for low activity potentiometric ion sensing., *Talanta* **63**, 109–17 (2004).

37. R. E. Gyurcsányi, N. Rangisetty, S. Clifton, B. D. Pendley, E. Lindner, Microfabricated ISEs: critical comparison of inherently conducting polymer and hydrogel based inner contacts., *Talanta* **63**, 89–99 (2004).

38. T. Lindfors, H. Aarnio, A. Ivaska, Potassium-Selective Electrodes with Stable and Geometrically Well-Defined Internal Solid Contact Based on Nanoparticles of Polyaniline and Plasticized Poly (vinyl chloride) salt (ES) form of PANI has exceptionally good pH stability . form even at pH 1, *Anal. Chem.* **79**, 8571–8577 (2007).

39. A. Rzewuska *et al.*, Composite Polyacrylate-Poly(3,4-ethylenedioxythiophene) Membranes for Improved All-Solid-State Ion-Selective Sensors, *Anal. Chem.* **80**, 321–327 (2008).

40. T. Lindfors, Light sensitivity and potential stability of electrically conducting polymers commonly used in solid contact ion-selective electrodes, *J. Solid State Electr.* **13**, 77–89 (2008).

41. A. Michalska, M. Wojciechowski, E. Bulska, K. Maksymiuk, Experimental study on stability of different solid contact arrangements of ion-selective electrodes., *Talanta* **82**, 151–7 (2010).

42. M. Vamvakaki, N. A. Chaniotakis, Solid-contact ion-selective electrode with stable internal electrode, *Anal. Chim. Acta* **320**, 53–61 (1996).

43. K. McElhoney, G. D. O'Neil, N. A. Chaniotakis, S. P. Kounaves, Stability and Lifetime of Potassium Solid-Contact Ion Selective Electrodes for Continuous and Autonomous Measurements, *Electroanalysis* **24**, 2071–2078 (2012).

44. C.-Z. Lai, M. A. Fierke, A. Stein, P. Bühlmann, Ion-selective electrodes with three-dimensionally ordered macroporous carbon as the solid contact., *Anal. Chem.* **79**, 4621–6 (2007).

45. G. A. Crespo, S. Macho, F. X. Rius, Ion-selective electrodes using carbon nanotubes as ion-to-electron transducers., *Anal. Chem.* **80**, 1316–22 (2008).

46. M. Fouskaki, N. Chaniotakis, Fullerene-based electrochemical buffer layer for ion-selective electrodes., *Analyst* **133**, 1072–5 (2008).

47. G. A. Crespo, S. Macho, J. Bobacka, F. X. Rius, Transduction Mechanism of Carbon Nanotubes in Solid-Contact Ion-Selective Electrodes, *Anal. Chem.* **81**, 676–681 (2009).

48. Z. Mousavi, T. Han, C. Kvarnstrom, J. Bobacka, A. Ivaskat, in *ECS Transactions*, (2009), pp. 19–26.

49. M. A. Fierke, C.-Z. Lai, P. Bühlmann, A. Stein, Effects of architecture and surface chemistry of three-dimensionally ordered macroporous carbon solid contacts on performance of ion-selective electrodes., *Anal. Chem.* **82**, 680–8 (2010).

50. NICO2000, Technical Specifications for the Potassium Ion-Selective Electrode (ELIT 8031), 1–5.

51. E. Bakker, P. Bühlmann, E. Pretsch, Carrier-Based Ion-Selective Electrodes and Bulk Optodes. 1. General Characteristics., *Chem. Rev.* **97**, 3083–3132 (1997).

52. Y. Umezawa, P. Buhlmann, K. Umezawa, K. Tohda, S. Amemiya, Potentiometric Selectivity Coefficients of Ion-Selective Electrodes, *Pure Appl. Chem.* **72**, 1851–1856 (2000).

53. J. R. Sandifer, Ed., *Ion-Transfer Kinetics: Principles and Applications* (VCH, New York, NY, 1995).

54. H. Small, T. S. Stevens, W. C. Bauman, Novel ion exchange chromatographic method using conductimetric detection, *Anal. Chem.* **47**, 1801–1809 (1975).

55. J. E. Girard, Ion Chromatography with Coulometric Detection for the Determination of Inorganic Ions, *Anal. Chem.* **51**, 836–839 (1979).

56. N. Chem, C. Anderson, Ion Chromatography : A New Technique for Clinical Chemistry, *Clin. Chem.* **22**, 1424–1426 (1976).

57. D. C. Harris, *Quantitative Chemical Analysis* (W.H. Freeman and Company, ed. 7, 2007), p. 663.

58. J. S. Fritz, D. T. Gjerde, *Ion Chromatography* (Wiley-VCH, ed. 4th, 2009).

59. R. A. Wharton, C. P. McKay, R. L. Mancinelli, G. M. Simmons, Early martian environments: the Antarctic and other terrestrial analogs, *Adv. Space Res.* **9**, 147–53 (1989).

60. S. J. Wentworth, E. K. Gibson, M. A. Velbel, D. S. McKay, Antarctic Dry Valleys and indigenous weathering in Mars meteorites: Implications for water and life on Mars, *Icarus* **174**, 383–395 (2005).

61. D. D. Wynn-Williams, H. G. M. Edwards, Proximal Analysis of Regolith Habitats and Protective Biomolecules in Situ by Laser Raman Spectroscopy: Overview of Terrestrial Antarctic Habitats and Mars Analogs, *Icarus* **144**, 486–503 (2000).

62. S. T. Stroble, K. M. McElhoney, S. P. Kounaves, Comparison of the Phoenix Mars Lander WCL soil analyses with Antarctic Dry Valley soils, Mars meteorite EETA79001 sawdust, and a Mars simulant, *Icarus* **225**, 933–939 (2013).

63. D. C. Catling *et al.*, Atmospheric origins of perchlorate on Mars and in the Atacama, *J. Geophys. Res.* **115**, E00E11 (2010).

64. B. Sutter, J. B. Dalton, S. A. Ewing, R. Amundson, C. P. McKay, Terrestrial analogs for interpretation of infrared spectra from the Martian surface and subsurface: Sulfate, nitrate, carbonate, and phyllosilicate-bearing Atacama Desert soils, *J. Geophys. Res.* **112**, G04S10 (2007).

65. A. G. Fairén *et al.*, Astrobiology through the ages of Mars: the study of terrestrial analogues to understand the habitability of Mars, *Astrobiology* **10**, 821–43 (2010).

66. M. E. Rovers, V. Marineris, M. Sinus, C. Hills, Mars on Earth : soil analogue es for future Mars missions, *Astron. Geophys.* **49**, 2.20–2.23 (2008).

67. B. C. Clark, Geochemical components in Martian soil, *Geochim. Cosmochim. Acta* **57**, 4575–4581 (1993).

68. M. I. Richardson, M. A. Mischna, Long-term evolution of transient liquid water on Mars, *J. Geophys. Res.* **110**, E03003 (2005).

69. G. D. Clow, Generation of Liquid Water on Mars through the Melting of a Dusty Snowpack, *Icarus* , 95–127 (1987).

70. P. R. Christensen *et al.*, Mineralogy at Meridiani Planum from the Mini-TES Experiment on the Opportunity Rover., *Science* **306**, 1733–9 (2004).

71. W. D. Grant, Life at low water activity., *Philos. Trans. R. Soc. London, Ser. B.* **359**, 1249–66 (2004).

72. R. A. Kerr, Pesky Perchlorate All Over Mars, *Science* **340**, 138 (2013).

73. S. P. Kounaves *et al.*, Identification of the perchlorate parent salts at the Phoenix Mars landing site and possible implications, *Icarus* , Submitted February (2013).

74. N. O. Rennó *et al.*, Possible physical and thermodynamical evidence for liquid water at the Phoenix landing site, *J. Geophys. Res.* **114**, 1–11 (2009).

75. B. Sutter *et al.*, The detection of carbonate in the martian soil at the Phoenix Landing site: A laboratory investigation and comparison with the Thermal and Evolved Gas Analyzer (TEGA) data, *Icarus* **218**, 290–296 (2012).

76. T. L. Heet, R. E. Arvidson, S. C. Cull, M. T. Mellon, K. D. Seelos, Geomorphic and geologic settings of the Phoenix Lander mission landing site, *J. Geophys. Res.* **114**, E00E04 (2009).

77. V. F. Chevrier, J. Hanley, T. S. Altheide, Stability of perchlorate hydrates and their liquid solutions at the Phoenix landing site, Mars, *Geophys. Res. Lett.* **36**, L10202 (2009).

78. G. M. Marion, D. C. Catling, K. J. Zahnle, M. W. Claire, Modeling aqueous perchlorate chemistries with applications to Mars, *Icarus* **207**, 675–685 (2010).

79. I. B. Campbell, G. G. C. Claridge, *Antarctica: Soils, Weathering Processes and Environment* (Elsevier, Amsterdam, 19887).

80. H. Y. Mcsween, E. Jarosewich, Petrogenesis of the Elephant Moraine A79001 meteorite : Multiple magma pulses on the shergottite parent body Mean grain sizes Initial sampie pfocessing was done at the Meteotite cu- was sawed , four thin sections, *Geochim. Cosmochim. Acta* **47**, 1501–1513 (1983).

81. A. J. T. Jull, D. J. Donahue, Terrestrial 14C age of the Antarctic shergottite , EETA 79001, *Geochim. Cosmochim. Acta* **52**, 1309–1311 (1988).

82. S. P. Kounaves *et al.*, Discovery of natural perchlorate in the Antarctic Dry Valleys and its global implications., *Environ. Sci. Technol.* **44**, 2360–4 (2010).

83. S. R. Lukow, thesis, Tufts University (2005).

84. R. W. Cattrall, H. Freiser, Coated Wire Ion Selective Electrodes, *Anal. Chem.* **43**, 1905–1906 (1970).

85. H. James, G. Carmack, H. Freiser, Coated Wire Ion Selective Electrodes, *Anal. Chem.* **44**, 856–857 (1972).

86. R. W. Cattrall, S. Tribuzio, H. Freiser, Potassium ion responsive coated wire electrode based on valinomycin, *Anal. Chem.* **46**, 2223–4 (1974).

87. L. Cunningham, H. Freiser, Coated-wire ion-selective electrodes, *Anal. Chim. Acta* **180**, 271–279 (1986).

88. P. Bühlmann, E. Pretsch, E. Bakker, Carrier-Based Ion-Selective Electrodes and Bulk Optodes. 2. Ionophores for Potentiometric and Optical Sensors., *Chem. Rev.* **98**, 1593–1688 (1998).

89. R. Xu, D. M. Bloor, Preparation and Properties of Coated-Wire Ion-Selective Electrodes for Anionic and Cationic Surfactants, *Langmuir* , 9555–9558 (2000).

90. NASA Jet Propulsion Laboratory, California Institute of Technology, SRR: Sample-Return Rover (available at http://www-robotics.jpl.nasa.gov/systems/system.cfm?System=6).

91. T. Lindfors , F. Sundfors, L. Höfler , R. E. Gyurcsányi , The Water Uptake of Plasticized Poly(vinyl chloride) Solid-Contact Calcium-Selective Electrodes, *Electroanalysis* **23**, 2156–2163 (2011).

92. D. B. Rorabacher, Statistical Treatment for Rejection of Deviant Values : Critical Values of Dixon ' s " Q " Parameter and Related Subrange Ratios at the 95 % Confidence Level, *Anal. Chem.* **63**, 139–146 (1991).

93. G. D. O'Neil, R. Buiculescu, S. P. Kounaves, N. A. Chaniotakis, Carbon-Nanofiber-Based Nanocomposite Membrane as a Highly Stable Solid-State Junction for Reference Electrodes, *Anal. Chem.* **83**, 5749–5753 (2011).

94. U. S. S. L. Staff, *Diagnosis and Improvement of Saline and Alkali Soil* (1954), p. 160.

95. E. K. Gibson, S. J. Wentworth, D. S. McKay, Chemical weathering and diagenesis of a cold desert soil from Wright Valley, Antarctica: An analog of Martian weathering processes, *J. Geophys. Res.* **88**, A912 (1983).

96. J. G. Bockheim, Properties and Classification of Cold Desert Soils from Antarctica, *Soil Sci. Soc. Am. J.* **61**, 224–231 (1997).

97. I. A. Berger, R. U. Cooke, The Origin and Distribution of Salts on Alluvial Fans in The Atacama Desert, Northern Chile, *Earth Surf. Proc. Land.* **22**, 581–600 (1997).

98. J. G. Bockheim, Landform and Soil Development in the McMurdo Dry Valleys, Antarctica: A Regional Synthesis, *Arct. Antarct. Alp. Res.* **34**, 308–317 (2002).

99. H. Bao, Multiple oxygen and sulfur isotopic analyses on water-soluble sulfate in bulk atmospheric deposition from the southwestern United States, *J. Geophys. Res.* **108**, 4430 (2003).

100. H. Bao, K. A. Jenkins, M. Khachaturyan, G. C. Díaz, Different sulfate sources and their post-depositional migration in Atacama soils, *Earth Planet. Sci. Lett.* **224**, 577–587 (2004).

101. S. A. Ewing *et al.*, A threshold in soil formation at Earth's arid–hyperarid transition, *Geochim. Cosmochim. Acta* **70**, 5293–5322 (2006).

102. H. Bao, D. R. Marchant, Quantifying sulfate components and their variations in soils of the McMurdo Dry Valleys, Antarctica, *J. Geophys. Res.* **111**, D16301 (2006).

103. K. Al-Barrak, D. L. Rowell, The solubility of gypsum in calcareous soils, *Geoderma* **136**, 830–837 (2006).

104. P. Hatsis, C. a Lucy, Effect of temperature on retention and selectivity in ion chromatography of anions., *J. Chromatogr. A* **920**, 3–11 (2001).